

Master Thesis

Tensile Test of Tissue-Engineered Tendon Constructs Using a Dynamic Load Frame

carried out for the purpose of obtaining the degree of Diplom-Ingenieurin (Dipl.-Ing. in oder DI),

submitted at TU Wien

Faculty of Mechanical and Industrial Engineering

by

Jennifer Leach

Mat.Nr.: 12112940

under the supervision of

Univ.Prof.Dipl.-Ing.Dr.Philipp Thurner Projektass.in(FWF) Ekaterina Oleinik, MSc Univ.Ass.Dipl.-Ing. Felix Groß

Institute of Lightweight Design and Structural Biomechanics, E317



I confirm, that the printing of this thesis requires the approval of the examination board.

Affidavit

I declare in lieu of oath, that I wrote this thesis and carried out the associated research myself, using only literature cited in this volume. If text passages from sources are used literally, they are marked as such.

I confirm that this work is original and has not been submitted elsewhere for any examination, nor is it currently under consideration for a thesis elsewhere.

I acknowledge that the submitted work will be checked electronically-technically using suitable and state-of-the-art means (plagiarism detection software). On the one hand, this ensures that the submitted work was prepared according to the high-quality standards within the applicable rules to ensure good scientific practice "Code of Conduct" at the TU Wien. On the other hand, a comparison with other student theses avoids violations of my personal copyright.

Acknowledgements

I want to thank my advisors, Ekaterina Oleinik and Felix Groß, for their assistance and trans-continental support. I'd also like to extend my gratitude to Univ. Prof. Dipl.-Ing. Dr. Philipp Thurner for welcoming me into his lab.

To the galpals in Vienna, I couldn't have completed the master's degree, let alone the thesis, without your love, support, and encouragement.

To the group of friends I lovingly call the misfits, you all kept me sane and provided a space for venting and stress relief; your support means the world.

To LeeAnn, I don't have a way with words like you do but thank you. Ice coffees, breakfast sandwiches, and you and your goats were the best part of moving to Connecticut.

I want to thank my family for their tremendous support and love over the past year. Thank you to my mother for letting me visit so often, and thank you to my husband for continually pushing me to complete this work. Lastly, I must thank little Remy his upcoming arrival in April has been the biggest encouragement needed to finish this thesis.

Abstract

Fibrin is a biopolymer with properties ideal for supporting cell seeding and mimicking native tissue environments, and it has gained significant interest in musculoskeletal tissue engineering, which has recently also concerned tendon repair. This work investigates the mechanical properties of fibrin ring constructs produced for tissue engineering applications, focusing on developing a testing protocol and experimental setup to study how cyclic and stress relaxation loading affects cell-free and cell-ring-shaped constructs and aims to provide a comprehensive understanding of the stresses the constructs experience during mechanical testing and also during mechanical stimulation in the MagneTissue bioreactor. Previous studies apply displacements and strains to the ring constructs while in the MagneTissue bioreactor; however, previous works fail to address the stress the rings experience while in the bioreactor. A protocol is developed using a dynamic load frame equipped with adapters similar to the ones used in a specific bioreactor. The testing is conducted in a water bath containing phosphate-buffered saline (PBS) to ensure the rings are hydrated. The cyclic and stress relaxation loading mimics the loading applied to the ring constructs in the bioreactor, which are loaded to 10% or 20% strain, depending on the experiment. The experimental findings show that for both cyclic loading and stress relaxation, constructs subjected to 20% strain experienced higher maximum stress values than those at 10% strain. Statistical analysis indicated significant differences in maximum stress between the 20% strain 2-cell and cell-free groups, suggesting that the presence of cells influences the mechanical response of fibrin constructs. Significant differences were also noted between the 10% and 20% pooled data for the maximum and minimum stress values. This clearly supports the idea that the strain level impacts the stress the constructs experience and, in constructs without cells, leads to permanent deformation of the constructs. While this setup replicates and mimics the mechanical environment within the bioreactor, it provides an understanding of the stresses experienced by the constructs without having to perform multiple day-long experiments.

Contents

LB	St OI I	rigures		IV
Lis	st of	Tables		xii
Lis	st of A	Abbrevi	iations and Symbols	xvii
1.	Intro	oductio	n	1
	1.1.	Motiva	ation	. 1
	1.2.	Aim o	f the Thesis	3
	1.3.	Struct	ure of the Thesis	4
2.	Back	kground	I	5
	2.1.	Bioma	terial Scaffolds	5
		2.1.1.	Introduction to the Function of Scaffolds	5
		2.1.2.	Scaffolding Approaches in Tissue Engineering	6
	2.2.	Fibrin	ogen, Fibrin, and Fibrin Scaffolds	10
		2.2.1.	Fibrinogen and Fibrin Structure	10
		2.2.2.	Fibrin Scaffolds	12
	2.3.	Hydro	gels	13
	2.4.	Tissue	Bioreactors	14
	2.5.	Mecha	unical Testing	16
		2.5.1.	Tensile Testing	16
		2.5.2.	Viscoelasticity and Stress Relaxation Testing	17
3.	Met	hodolog	gy	23
	3.1.	Sampl	e Preparation	23
		3.1.1.	Tendon-Derived Progenitor Cells Isolation	23
		3.1.2.	Cell Culture	24
		3.1.3.	Cell-Free Rings Preparation	24
		3.1.4.	Cell-Seeded Rings Preparation	26
		3.1.5.	Ring-Shaped Geometry and Stress Calculations	26
	3.2.	Mecha	nical Preparation and Testing	28
		3.2.1.	Tensile Tension Adaptor and Alignment Piece	28
		3.2.2.	Water Bath	31

		3.2.3.	Testing Setup	31
		3.2.4.	Experimental Protocol	32
		3.2.5.	Data Processing	43
		3.2.6.	Cyclic Loading Data Processing	43
		3.2.7.	Stress Relaxation Data Processing	52
		3.2.8.	Instantaneous and Equilibrium Moduli	57
		3.2.9.	Statistical Analysis	57
4.	Resu	ılts		58
	4.1.	10% aı	nd 20% Cyclic Loading Results	58
	4.2.	10% aı	nd 20% Stress Relaxation Results	64
	4.3.	Cyclic	and Stress Relaxation Comparison	69
		4.3.1.	10% Strain	69
		4.3.2.	20% Strain	75
		4.3.3.	Instantaneous and Equilibrium Moduli	80
		4.3.4.	Prony Series Modelling	87
	4.4.	Post T	Cesting Qualitative View of Constructs	89
5.	Disc	ussion		92
	5.1.	Advan	cements and Prospective Developments	96
	5.2.	Limita	tions	97
6.	Cond	elusion		98
Α.	P-Va	alues fro	om Statistical Testing	100
	A.1.	Cyclic	Testing P-Values	100
	A.2.	Relaxa	ation Testing P-Values	101
	A.3.	Cyclic	and Stress Relaxation Comparison	103
		A.3.1.	10% Strain	103
		A.3.2.	20% Strain	103
Re	feren	ces		112

List of Figures

1.1.	Outline of mechanical testing performed	4
2.1.	Schematic diagram of fibringen and fibrin structure, namely the conversion	
	of fibrin from fibrinogen due to the presence of thrombin [15]	11
2.2.	From Mosesson, schematic diagram of fibrin assembly highlighting bilateral and lateral branch junctions. Two color schemes represent the fibrin molecules [14]	11
2.3.	From Ekaterina Oleinik, M.Sc., a PhD student in the Institute of Lightweight Design and Structural Biomechanics. Thrombin and fibrinogen are mixed with the addition of tendon-derived progenitor cells (TDPCs) to create rings. The rings are mounted on a spool-hook system within the Magne-Tissue bioreactor, where the spool is stationary, and the hook moves	
	with magnets	15
2.4.	Adapted from Gdoutos' Mechanical Testing of Materials, a typical cylin-	
	drical testing sample is shown. Note that the gage length is marked $[23]$	17
2.5.	Yield strength, ultimate strength on a stress-strain curve $[25]$	17
2.6.	A general stress relaxation experiment, where the strain is held constant	
	at ε_0 , and the resulting time-dependent stress is recorded [27]	19
2.7.	The physical elements of a Maxwell model, consisting of a spring and dashpot in series [34]	20
2.8.	Generalized Maxwell model, consisting of Maxwell units (in which a unit is a spring and dashpot connected in series) connected in parallel with an isolated spring to represent the equilibrium modulus, from "Mechanical	
	characterization of hydrogels" by Mohammad Islam and Michelle Oyen [19].	21
3.1.	(a) Silicon molds, 500 μ L volume, (b) Fibrin rings in silicon molds in the incubator, (c) Fibrin rings polymerized in the silicon molds	25
3.2.	Fibrin rings in a petri dish with PBS while waiting to be tested	25
3.3.	(a) and (b) Not to scale and are CAD Rendition of the fibrin ring. (c) shows the L_i dimension and the diameter, d, of one of the strands	27
	y / /	

5.4.	section cut of the ring to view the cross-section of one strand, this mustrates	
	the cross-sectional area (CSA), scaled to 20:1	27
3.5.	Schematic of the testing setup, the S2M load cell connects to the upper	
	portion of the Thelkin load frame. The lower adaptor connects to the	
	bottom of the Thelkin load frame	29
3.6.	(a) Custome-made tube for the MagneTissue bioreactor, which contains	
	the spool-hook system that the fibrin rings are attached to [11], (b) The	
	adaptors contain a half-spool to allow the fibrin ring to sit comfortably	29
3.7.	Not to scale. CAD rendition of the alignment piece, top view, front view,	
	side view, and front/side view shown	30
3.8.	Not to scale. CAD rendition of water bath, front, and front/side view shown	31
3.9.	(a) Water bath setup, (b) Closeup of the testing setup without the water	
	bath	32
3.10.	The upper and lower adaptor pieces are in the process of alignment	33
3.12.	(a) Initial calibration, (b) Zoomed-in photo of the initial calibration (in	
	blue, 10.00mm reference dimension) to see the initial measurement of the	
	marker (in red, 7.113mm), (c) Example of measuring a strand, (d) Zoomed-	
	in photo of measuring the marker again (as it is under the PBS solution)	
	and one of the strands to get the diameter of the strand)	36
3.13.	The heavyweight cardstock piece is placed on the lower adapter. The upper	
	adapter is lowered until the spool-side face contacts the measurement block	
	(cardstock). This sets the starting distance and can be saved in the software	
	as the zero position. This ensures that the length of the ring, when placed	
	on the spools, is 3 cm	38
3.14.	Figure from Ekaterina Oleinik, M.Sc., a PhD student in the Institute of	
	Lightweight Design and Structural Biomechanics. One of the protocols	
	where initially 10% strain is applied for 6 hours per day at 0.5 Hz, then 3%	
	strain at $0.5~\mathrm{Hz}$ for $18~\mathrm{hours}$ per day. After each resting phase, the cyclic	
	load for the 6 hour phase increases by 2%, up to 20% by day 7	40
3.15.	Displacement profile for the 20% Strain, Cyclic Test. Over one second, the	
	machine head displaces 6 mm, holds for two seconds, and then, over one	
	second, goes to 0 mm displacement	41

3.16. Displacement profile for the 10% Strain, Stress Relaxation Test. Over one second, the machine head displaces to 3 mm, which stays there for the test	
duration	42
3.17. Raw data from the first trial of the 2-cell group, 20% strain from the cyclic loading test. Due to the load cell operating near its lower limit and the soft, low-stiffness nature of the rings, force oscillations are generated whenever the machine head moves up or down, resembling the behavior of an underdamped system	44
3.18. Raw data from the first trial of the 2-cell group, 20% strain, from the cyclic loading test, and the positional data from the head of the loading frame. At any given plateau region, there is the characteristic behavior of an underdamped system, where the waveform oscillates around some value with decreasing amplitude over time. The largest spikes in the data occur whenever the machine head moves up or down	45
3.19. Upper and lower plateau data, with maroon representing only the upper plateau data and light blue representing only the lower plateau segments. In this view, there is a band of data for the lower plateau and an upper band for the upper plateau. The next steps in data processing involve smoothing the noisy data to isolate the realistic values	46
3.20. The upper and lower graphs display the same data, with differences in time scale (x-axis) and magnitude of stress (y-axis). The solid blue line represents the raw data from the first trial of the 2-cell group at 20% strain from the cyclic loading test. The yellow scatter indicates the upper and lower plateau data segments before processing with the moving median and mean. The maroon scatter represents the smoothed upper plateau data, while the light blue scatter represents the smoothed lower plateau data. The lower graph shows the oscillation of the raw data around the smoothed upper and lower plateau segments, where average values of the lower plateau data have been adjusted to 0 N, and the upper and lower	
plateau data have been shifted accordingly	48

3.21. Stitched upper and lower plateau data from the processed results of the first trial from the 2-cell group at 20% strain from the cyclic loading test. This figure eliminates any gaps between the plateaus in the upper and lower regions to present a continuous data line. All data have been adjusted such that the light blue lower plateau data line averages zero	49
3.22. Upper plateau data after normalization (orange line). The data comes from the first trial from the 2-cell group at 20% strain from the cyclic loading test. The black line is the 3-term Prony series model (R^2 =0.99921). After 600 seconds, the final normalized stress value is 0.8563 [-]. This value can also be expressed as the final stress being 85.63% of the initial stress. The three-time constant (τ) values are: $\tau_1 = 72.7s$, $\tau_2 = 1000.0s$, and $\tau_3 = 5207.6s$	50
3.23. Raw data from the first trial of the cell-free group, stress relaxation test at 10% strain. As with the cyclic loading, on the initial one-second ramp-up to the holding strain level, there are large oscillations in the data before the amplitude rapidly decreases. The stress relaxation test runs for 300 seconds	52
3.24. Zoomed-in view of the raw data from the first trial of the cell-free group, 10% strain from the stress relaxation test. This figure shows the waveform oscillating around decreasing stress values	53
3.25. The blue line represents the raw data from the first trial of the cell-free group at 10% strain from the stress relaxation test. The orange line represents the smoothed data after it passed through a lowpass filter with a cutoff of 0.001 Hz and subsequent smoothing through a moving median and average.	55

3.5	26. The orange line is the normalization of the data from the first trial from the cell-free group at 10% from the stress relaxation test. The black line is the	
	3-term Prony series model that fits the normalized data with an R^2 value of 0.98662. After 300 seconds, the final normalized stress value is 0.84 [-]. This value can be expressed as the final stress being 84.0% of the initial stress. The three-time constant (τ) values are: $\tau_1 = 64s$, $\tau_2 = 251s$ and $\tau_3 = 2050s$. Like with the cyclic loading testing, the τ_3 value is excluded from analysis because the data is only from 0 seconds to 300 seconds, but τ_3 is included for model convergence purposes	56
4.	1. Results of cyclic loading tests. Data is shown as the mean \pm SD. The 9-cell, 20% strain and cell-free, 10% strain groups have N=2 samples. The remaining groups have N=3 samples each. The 9-cell, 20% strain group experiences the greatest stress, followed by the 2-cell, 20% strain, and cell-free, 20% strain groups. Statistical analysis found that the maximum values for the 20% strain, 2-cell vs. the cell-free, are distinct (p-value \leq 0.1)	58
4.5	2. Two asterisks (**) refer to a P-value between 0.01 and 0.001. 10% 2-cell and cell-free data (N=5) was pooled together. 20% 2-cell and cell-free data (N=6) was pooled together. The maximum and the minimum pooled comparisons had p-values less than 0.001	60
4.3	3. Normalized cyclic loading test results, data shown as mean ± SD. The 9-cell, 20% strain and the cell-free, 10% strain groups have N=2 samples. The remaining groups have N=3 samples each. By the end of the test, the cell-free, 10% group retained the highest percentage of the initial stress, whereas the cell-free, 20% group had the lowest. When pooling together all the 10% strain data into one group and the 20% 2-cell and cell-free into a group (excluding the 9-cell), the 10% strain data retained a higher final percentage of the initial stress, compared to the 20% strain group (p-value=0.0644). The 2-cell group at 20% strain and the 2-cell group at 10%	
4.4	strain had similar final percentages of the initial stress (p-value > 0.9999). 4. Normalized cyclic pooled minimum value results. The 10% group had N=5	61
	-	

4.5.	Stress relaxation curves. Five groups are represented here. Data is shown as	
	mean \pm SD, N=3 for each group. The 9-cell, 20% strain group experiences	
	the greatest stress (p-value=0.10 when compared to the 20% strain 2-cell	
	group), followed by the 20% 2-cell and cell-free groups (p-value=0.70, the	
	20% 2-cell and the $20%$ cell-free groups do not statistically differ). The 2-	
	cell, 10% strain group had slightly higher initial stress than its counterpart,	
	the cell-free, 10% strain group (p-value=0.0523)	64
4.6.	Two asterisks (**) refer to a p-value between 0.01 and 0.001. 10% 2-cell	
	and cell-free data (N=6) was pooled together. 20% 2-cell and cell-free data	
	(N=6) was pooled together. The maximum pooled comparison had a p-	
	value of 0.0022, and the minimum pooled comparisons had a p-value less	
	than 0.001	66
4.7.	Normalized stress relaxation test results. There are five groups of data,	
	with each group showing the normalized mean of the individual samples	
	that comprise it. All groups have N=3 samples each. By the end of the	
	test, 10% strain groups (2-cell and cell-free) retained the highest percentage	
	of the initial stress, compared to the 20% strain groups (2-cell and cell-free)	
	(p-value=0.0391)	67
4.8.	Normalized relaxation pooled minimum value results. Both groups had	
	N=6 samples, and the results of a Welch's t-test found a p-value of 0.0391.	
	One asterisk (*) refers to a p-value between 0.1 and 0.01	68
4.9.	Stress data from the cyclic loading and stress relaxation tests conducted	
	at 10% strain. The stress relaxation mean curves have their initial stress	
	aligned with the corresponding cyclic data to account for zeroing issues in	
	the test setup. Data is shown as the mean with \pm SD. Each group consists	
	of N=3 samples, except for the 10% strain cell-free group from the cyclic	
	loading test, which has N=2 samples	70
4.10.	(a) 10% maximum value comparison, (b) 10% minimum value compari-	
	son (time after $t=300s$). No significant differences were found for either	
	comparison. Cyclic data had N=5 samples, and relaxation data had N=6 $$	
	samples	72

4.11. Normalized stress data from the cyclic loading and stress relaxation test	
conducted at 10% strain. Regardless of the loading type, the constructs at 10% strain have similar normalized stresses at 300s (p-value=0.8410)	73
4.12. Normalized pooled 10% cyclic and relaxation comparison. Cyclic data had	10
N=5 samples, and relaxation data had N=6 samples. Min refers to the	
	74
4.13. This figure displays the stress data from the cyclic loading and stress relaxation testing conducted at 20% strain. The stress relaxation mean curves have their initial stress aligned with the corresponding cyclic curves to account for zeroing issues in the test setup. Data is shown as mean (solid	
line) \pm SD (shaded areas). Each group consists of N=3 samples, except	
for the 20% strain 9-cell group from the cyclic loading test, which has N=2 samples	75
4.14. (a) 20% maximum value comparison, (b) 20% minimum value comparison (time after t=300s). Cyclic data had N=8 samples, and relaxation data	77
4.15. Normalized stress results from the cyclic loading and stress relaxation testing conducted at 20% strain. After 300s, the loading type (cyclic pooled vs. stress relaxation pooled) does have a significant impact on the normalized	78
4.16. Normalized pooled 20% cyclic and relaxation comparison. Cyclic data had N=8 samples, and relaxation data had N=9 samples. Min refers to the	79
4.17. Boxplots of the instantaneous moduli (σ_0/ε_0) for the 10% and 20% strain groups. Data is shown as median (red line) with minimum (lower whisker) to maximum (upper whisker) values.	82
4.18. Boxplots of the pooled instantaneous moduli for the 10% and 20% strain groups. Data is shown as a median (line) with minimum to maximum values. One asterisk (*) refers to a P-value between 0.01 and 0.1, two asterisks (**) refer to a P-value between 0.01 and 0.001, and four asterisks	
(****) refer to a p-value less than 0.0001 .	84

4.19.	This figure illustrates the equilibrium moduli for the 10% and 20% strain	
	groups. Data is shown as median (red line) with minimum (lower whisker)	
	to maximum (upper whisker) values. For some plots, the whiskers are	
	missing or only single-sided	85
4.20.	Boxplots of the pooled equilibrium moduli for the 10% and 20% strain	
	groups. Data is shown as a median (line) with minimum to maximum val-	
	ues. Two asterisks (**) refer to a P-value between 0.01 and 0.001, three	
	asterisks (***) refer to a p-value between 0.0001 and 0.001, and four aster-	
	isks (****) refer to a p-value less than 0.0001	86
4.21.	Depicted here are the Prony series models for cyclic loading and relaxation	
	testing conducted at 10% strain	88
4.22.	Illustrated here are the Prony series models for the cyclic and loading re-	
	laxation testing conducted at 20% strain	90
4.23.	Photo of a fibrin ring after testing at 20% strain with cyclic loading. The	
	ring contains cells cultured for two days.	91
5.1.	(a) Rings containing cells (b) Cell-free rings	93
5.2.	qPCR analysis of collagen I (col1a) and collagen III (col3) expression by	
	calculation of the ratio of these genes to GAPDH: floating - floating control,	
	gravity – gravity control, CL – cyclic loading, SL – static loading. Data are	
	shown as median with standard deviation (SD), n=4. Statistical analysis	
	was done with a nonparametric Kruskal - Wallis test followed by Dunn's	
	post-hoc test using GraphPad Prism 8.2.1. Values were considered statisti-	
	cally significant for p<0.05. Figure from Ekaterina Oleinik, M.Sc., a PhD	
	student in the Institute of Lightweight Design and Structural Biomechanics.	94

List of Tables

4.1.	Mean maximum and minimum stress values for each group from the cyclic	
	loading testing. Statistical testing results are summarized in (Tables A.1	
	and A.2)	59
4.2.	Final normalized stress values for each group from the cyclic loading testing.	63
4.3.	Mean maximum and minimum stress values from the relaxation loading	
	testing. The stress relaxation mean curves have their initial stress aligned	
	with the corresponding cyclic data to account for zeroing issues in the test	
	setup, which is why the maximum values are the same as in Table $4.1.$	65
4.4.	Final normalized stress values for each group from the relaxation loading	
	testing	69
4.5.	Mean maximum and stress values at $t=300s$ from the cyclic and relaxation	
	loading testing at 10% strain. The stress relaxation mean curves have	
	their initial stress aligned with the corresponding cyclic data to account	
	for zeroing issues in the test setup, which is why the maximum values are	
	the same for corresponding groups	71
4.6.	Normalized stress values at $t=300s$ for each group from the cyclic and	
	relaxation loading testing at 10% strain	74
4.7.	Mean maximum and stress values at t=300s from the cyclic and relaxation	
	loading testing at 20% strain. The stress relaxation mean curves have	
	their initial stress aligned with the corresponding cyclic data to account	
	for zeroing issues in the test setup, which is why the maximum values are	
	the same for corresponding groups	76
4.8.	Normalized stress values at $t=300s$ for each group from the cyclic and	
	relaxation loading testing at 20% strain	80
4.9.	This table depicts each group's mean instantaneous (σ_0/ε_0) and equilib-	
	rium modulus $(\sigma_{\infty}/\varepsilon_0)$	81
4.10.	This Table depicts the mean Prony series time constants τ_1 and τ_2 and R^2	
	value for the 10% strain, cyclic and relaxation groups, 2-cell and cell-free.	87
4.11.	This Table depicts the mean Prony series time constants τ_1 and τ_2 and R^2	
	value for the 20% strain, cyclic and relaxation groups, 2-cell and cell-free.	89

A.1.	Table of p-values from statistical testing performed between the $maximum$ values of the respective groups. With the significance level set to 0.10, all p-values are less than or equal to 0.10, indicating significant differences between the groups. 20% strain 9-cell and 10% strain cell-free are excluded due to $N=2$ sample size. A * denotes the data set is normally distributed. When two normally distributed data sets are compared, a t-test with Welch's correction is used; otherwise, the statistical method is a Mann-Whitney U test	. 100
A.2.	Table of p-values from statistical testing performed between the minimum values of the respective groups. With the significance level set to 0.10, all p-values are less than or equal to 0.10, indicating significant differences between the groups. 20% strain 9-cell and 10% strain cell-free are excluded due to N=2 sample size. A * denotes the data set is normally distributed. When two normally distributed data sets are compared, a t-test with Welch's correction is used; otherwise, the statistical method is a Mann-Whitney U test.	. 100
A.3.	Table of p-values from statistical testing performed between the final normalized values of the respective groups. With the significance level set to 0.10, all groups except the 20% 2-cell compared to the 10% 2-cell have p-values less than or equal to 0.10. 20% strain 9-cell and 10% strain cell-free are excluded due to N=2 sample size. A * denotes the data set is normally distributed. When two normally distributed data sets are compared, a t-test with Welch's correction is used; otherwise, the statistical method is a Mann-Whitney U test	. 101
A.4.	Table of p-values from statistical testing performed between the maximum stress values of the groups. With the significance level set to 0.10, all groups except the 20% 2-cell compared to the 20% cell-free have p-values less than or equal to 0.10. A * denotes the data set is normally distributed. When two normally distributed data sets are compared, a t-test with Welch's correction is used; otherwise, the statistical method is a Mann-Whitney U test.	. 101

A.5.	Table of p-values from statistical testing performed between the minimum stress values of the groups. With the significance level set to 0.10, all groups except the 10% cell-free compared to the 10% 2-cell, the 20% cell-free compared to the 20% 2-cell, and the 20% 9-cell compared to the 20% 2-cell have p-values less than or equal to 0.10. A * denotes the data set is normally distributed. A t-test with Welch's correction is used when comparing two normally distributed data sets.	. 102
A.6.	Table of p-values from statistical testing performed between the final normalized stress values of the groups. With the significance level set to 0.10, all p-values except are greater than 0.10 except for 10% 2-cell compared to 20% cell-free, 10% cell-free compared to 20% cell-free, and 10% cell-free compared to 20% 9-cell. A * denotes the data set is normally distributed. When two normally distributed data sets are compared, a t-test with Welch's correction is used; otherwise, the statistical method is a Mann-Whitney U test	. 102
A.7.	Table of p-values from statistical testing performed between the maximum stress values of the 10% cyclic and relaxation groups. All groups had N=3 samples except for the 10% cyclic cell-free (and therefore excluded from direct comparison). With the significance level set to 0.10, all p-values are greater than 0.10 except for the 10% relax 2-cell compared to the 10% relax cell-free group. A * denotes the data set is normally distributed. A t-test with Welch's correction is used when comparing two normally distributed data sets.	. 103
A.8.	Table of p-values from statistical testing performed between the stress values at 300s of the 10% cyclic and relaxation groups. All groups had N=3 samples except for the 10% cyclic cell-free (and therefore excluded from direct comparison). With the significance level set to 0.10, all p-values are greater than 0.10. A * denotes the data set is normally distributed. A t-test with Welch's correction is used when comparing two	

A.9.	Table of p-values from statistical testing performed between the normal -	
	ized stress values at $300s$ of the 10% cyclic and relaxation groups. All	
	groups had N=3 samples except for the 10% cyclic cell-free (and therefore	
	excluded from direct comparison). With the significance level set to 0.10,	
	all p-values are greater than 0.10. A * denotes the data set is normally	
	distributed. When two normally distributed data sets are compared, a	
	t-test with Welch's correction is used; otherwise, the statistical method is	
	a Mann-Whitney U test.	. 104
A.10.	. Table of p-values from statistical testing performed between the maxi-	
	mum stress values of the 20% cyclic and relaxation groups. All groups	
	had N=3 samples except for the 20% cyclic 9-cell (and therefore excluded	
	from direct comparison). The significance level is set to 0.10. A * denotes	
	the data set is normally distributed. When two normally distributed data	
	sets are compared, a t-test with Welch's correction is used; otherwise, the	
	statistical method is a Mann-Whitney U test	. 105
A.11.	. Table of p-values from statistical testing performed between the stress	
	values at 300s of the 20% cyclic and relaxation groups. The significance	
	level is set to 0.10. A * denotes the data set is normally distributed.	
	A t-test with Welch's correction is used when comparing two normally	
	distributed data sets	. 106
A.12.	. Table of p-values from statistical testing performed between the normal -	
	ized stress values at 300s of the 20% cyclic and relaxation groups.	
	The significance level is set to 0.10. A * denotes the data set is normally	
	distributed. When two normally distributed data sets are compared, a	
	t-test with Welch's correction is used; otherwise, the statistical method is	
	a Mann-Whitney U test.	. 107
A.13.	. Table of p-values from statistical testing performed between the instan-	
	taneous moduli values of the 10% and 20% cyclic and relaxation groups.	
	The significance level is set to 0.10. A * denotes the data set is normally	
	distributed. When two normally distributed data sets are compared, a	
	t-test with Welch's correction is used; otherwise, the statistical method is	
	a Mann-Whitney U test.	. 108

	4. Table of p-values from statistical testing performed between the equilib-	A.14.
	rium moduli values of the 10% and 20% cyclic and relaxation groups.	
	The significance level is set to 0.10. A * denotes the data set is normally	
	distributed. When two normally distributed data sets are compared, a	
	t-test with Welch's correction is used; otherwise, the statistical method is	
109	a Mann-Whitney U test.	
	5. Table of p-values from statistical testing performed between the $ au_1$ values	A.15.
	of the 10% and 20% cyclic and relaxation groups. The significance level	
	is set to 0.10. A * denotes the data set is normally distributed. A t-test	
	with Welch's correction is used when comparing two normally distributed	
110	data sets.	
	6. Table of p-values from statistical testing performed between the $ au_2$ values	A.16.
	of the 10% and 20% cyclic and relaxation groups. The significance level	
	is set to 0.10. A * denotes the data set is normally distributed. When	
	two normally distributed data sets are compared, a t-test with Welch's	
	correction is used; otherwise, the statistical method is a Mann-Whitney	
111	U test.	

List of Abbreviations and Symbols

PLGA poly(lactic-co-glycolic acid)

ECM extracellular matrix

FPA fibrinopeptide A

FPB fibrinopeptide B

Fbg fibrinogen

Thr thrombin

Fbg20 20 mg/mL of fibrinogen

PBS phosphate-buffered saline

Thr0.625 0.625 IU of thrombin

 $CaCl_2$ calcium chloride

SLA stereolithography

CSA cross-sectional area

col1a collagen I

col3 collagen III

IU international unit

TDPCs tendon-derived progenitor cells

v/v volume/volume

TDPCs tendon-derived progenitor cells

Introduction

1.1. Motivation

Within the United States, 33 million musculoskeletal injuries have been reported annually, with 50% of those involving tendon and ligament injuries [1]. Hand injuries alone account for up to 20% of all treated injuries in an emergency department, with traumatic hand injuries ranging from minor soft tissue injuries and fractures to complex injuries requiring nerve, tendon, or artery repair. Within this spectrum, 54.8% of patients with a minor laceration and 92.5% with a deep injury through a minor laceration reported tendon injuries [2]. Furthermore, it is estimated that tendon injuries account for 30% to 50% of all sports-related injuries. Of tendon injuries related to sports, these are primarily dominated by issues with the Achilles tendon, where it is reported that the Achilles is involved in as much as half of all sports-related injuries [3] [4]. Regarding the Achilles tendon, roughly 25% of athletes with Achilles tendon overuse injuries require surgery [5]. Not only are tendon injuries so prevalent in sports but also the aging population, where rotator cuff disorders are one of the most common causes of shoulder disability, with rotator cuff tears being present in approximately 50% of individuals in their 80s [4]. It is evident that tendon issues and injuries are not confined to a specific group or population; anyone can experience tendinopathy at some point in their lifetime.

In the cases of these tendon injuries, especially in the cases of rotator cuff tears, clinical intervention is required, mainly due to the complex anatomy and hypovascularization of the surrounding tissues [6]. When the tears are too large to heal independently due to low cellularity and vascularity, tendon implantation becomes the repair strategy [7]. Regarding utilizing grafts for tendon implantation, biomechanical strength and graft stability, post-repair, were increased using mechanical fixation methods [6]. Now, emerging research looks to using tissue-engineering options based on scaffolds, where cells can be seeded within, and the scaffolds may contain or be embedded with growth factors 7.

Biopolymers used as scaffolds are nothing new in tissue engineering studies; the biocompatible and biodegradable polymer poly(lactic-co-glycolic acid) (PLGA) has been used for decades due to its mechanical tunability and other properties [8] [9]. However, fibrin 1. Introduction

TU Bibliothek, Die approbierte gedruckte Originalversion dieser Diplomarbeit ist an der TU Wien Bibliothek verfügbar wien vour knowledge hub. The approved original version of this thesis is available in print at TU Wien Bibliothek.

is another vital polymer broadly utilized in medicine and materials science. Fibrin is a protein hydrogel resulting from fibringen [8]. Both fibrin and fibringen have been well-defined in their role within blood clotting, cellular and matrix interactions, and the inflammatory response. Fibrin gels are an ideal candidate for scaffolding due to their high seeding efficiencies, cell distribution, and adhesive properties. Fibrin can also be produced from a patient's blood, eliminating most risks regarding foreign body reactions or infection [10].

Fibrin hydrogels have recently gained significant interest in the application of tissue engineering due to their close mimicry of the natural mechanical properties of skeletal muscle tissue. Their suitability to support cell seeding in high density with a uniform distribution and binding of various growth factors makes fibrin an ideal candidate for applications in tissue engineering [11]. The incidence of musculoskeletal injuries requiring surgical treatments like tendon implantations would support the belief that studies into bioengineered tendon tissue are worthwhile for their application to the replacement or restoration of such damaged tissues. Tissue repair is an emerging interest because musculoskeletal injuries are common and sometimes require surgical intervention. Fibrin hydrogels used in scaffold-based tissue engineering exhibit inherent biocompatibility, tuneable properties, and an ability to mimic native tissue environments. Fibrin hydrogels used for musculoskeletal tissue engineering could offer new approaches for restoring or replacing injured tissues.

This thesis aims to present a comprehensive protocol for studying the mechanical properties of fibrin constructs. The mechanical environment in which cells reside is vital for the viability of cells and for tissue engineering success. The focus here is on fibrin, which is used in a bioreactor and has loads applied to the construct and, thus, to the enclosed cells. The shape of the constructs to be considered is that of rings; this shape was preferred because of the availability of existing supplies for their fabrication. One of the significant influences on this thesis is the work by Heher et al., which established the protocol for fabricating fibrin rings adopted in this work. The work by Heher et al. used a MagneTissue bioreactor system to cyclically load ring constructs to a predetermined strain level [11]. The MagneTissue bioreactor was designed to overcome the limitations of other bioreactors: the extent and type of strain cannot be controlled in other bioreactors, despite research showing that defined mechanical stimuli are critical for the development

of biomimetic skeletal muscle constructs [11]. However, the stresses applied to the ring constructs while subjected to various training protocols in the MagneTissue bioreactor are unknown. This work aims to further understand these constructs' mechanical properties and determine the stresses on the fibrin constructs vs. time, especially as one experiment within the Magne Tissue bioreactor may take seven days or longer to complete [11].

1.2. Aim of the Thesis

This thesis focused on three main aspects related to the study of fibrin ring constructs: the (1) development and manufacturing of the experimental setup for mechanical testing, the (2) creation of a test protocol, and the (3) mechanical testing of different groups of fibrin rings, cell-free and rings with cells to validate the setup and obtain first results. Cyclic loading and stress relaxation tests were performed at two strain levels for cell-free and cell-ring-shaped constructs.

First, developing and manufacturing a setup to create the freestanding ring-shaped fibrin matrices was described and presented in detail in Chapter 3. This setup ensured the consistent and reproducible fabrication of fibrin rings for testing. Secondly, the dynamic load frame SDL-S-001 mini (Thelkin GmbH, Winterthur, Switzerland) required custommade adaptors. Chapter 3 described the design and manufacturing of these adaptors. Finally, a bath was necessary to test the constructs in wet conditions. There was an existing design for a bath available; this needed updating to suit the specific requirements of this thesis.

A detailed test protocol was developed in Chapter 3 for the mechanical properties of the fibrin rings using a dynamic load frame. Detailed procedures were given for mounting and unmounting the fibrin ring constructs onto the test stand, initiating the test setup, identifying the starting point for testing, and outlining test profiles. Limitations of the test setup were also discussed. The stress relaxation and cyclic loading tests protocol at two different strain levels, 10% and 20%, was detailed in Chapter 3.

Finally, mechanical tests were conducted on the fibrin rings. This testing was done to understand the events within the bioreactor and the magnitude of stresses that cells experience in such constructs. Fig. 1.1 summarizes the eight tests conducted.

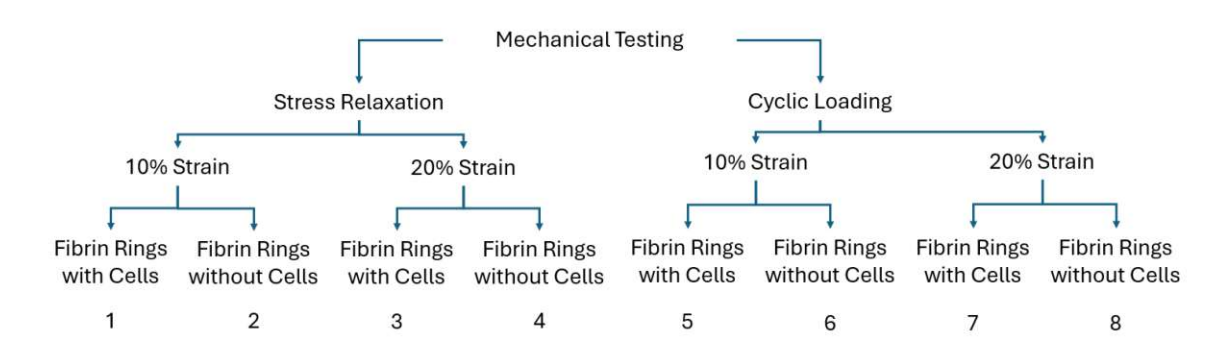


Figure 1.1.: Outline of mechanical testing performed.

Therefore, the results presented in this thesis provided initial data on the relaxation and cyclic loading tests performed at two different strain levels for each group of the fibrin constructs. These tests illustrated the process and the stresses experienced within the bioreactor. The mechanical behavior of the fibrin rings was investigated further by calculating the relaxation time constants.

1.3. Structure of the Thesis

Chapter 2 entails a thorough background on fibrin and fibrin scaffolds and the theory underlying the testing methods: stress, strain, stress relaxation, and cyclic loading. In addition, it also covers an overview of hydrogels as well as bioreactors. Chapter 3, Methodology, outlines the materials and methods this thesis uses, with more detailed information concerning the fabrication of the fibrin rings. Chapter 3 also describes designing and manufacturing the dynamic load frame adaptors, the water bath, and test protocols. Chapter 4, Results, presents the data on mechanical testing of the fibrin rings tested using the dynamic load frame. Discussion of any data in relation to existing literature, interpretations, and limitations concerning the data can be found in Chapter 5, Discussion. Finally, Chapter 6, Conclusion, summarizes the thesis and proposes future experiments and developments.

2.1. Biomaterial Scaffolds

Tissue engineering, comprising cells, growth signals, and scaffolds, is an emerging sector that looks to restore damaged tissues. This background section details one of the cornerstones of tissue engineering, scaffolds, with a particular focus on fibrin hydrogels. It will provide background information regarding the role of scaffolds, their definition and function within tissue engineering and biomaterials, and the fabrication of these scaffolds.

2.1.1. Introduction to the Function of Scaffolds

In the field of tissue engineering, there are three main pillars: cells, growth-stimulating signals, and scaffolds. The combination may also be referred to as the "tissue engineering triad," in which these are crucial elements of engineered tissues [12]. The third, scaffolds, are of particular importance to this work.

To understand scaffolds in tissue engineering applications, one must grasp what the scaffolds are mimicking. Most normal cells within human tissues are "anchorage-dependent," meaning that these cells require an extracellular matrix (ECM). Therefore, at a minimum, scaffolds are there to mimic the ECM by providing structural support for cell attachment and tissue development. The ECM can be has five main functions [12]:

- 1. Provide structural support for cells to attach and proliferate,
- 2. Provide or enhance the mechanical properties of tissues,
- 3. Provide bioactive cues that allow for cells to respond to their microenvironment,
- 4. Provide a reservoir of growth factors and increases their actions,
- 5. Provide a physical environment that is flexible enough to allow for remodeling in response to the body's needs.

Likewise, the scaffolds need to have the following analogous functions [12]:

1. Provide structural support for cells that are derived externally to attach, proliferate, and differentiate in vitro and in vivo,

- 2. Provide shape and mechanical stability to tissue defects and provide rigidity and stiffness to engineered tissues,
- 3. Provide a medium for cells to interact and facilitate proliferation and differentiation,
- 4. Provide a delivery vehicle and reservoir for externally derived growth factors,
- 5. Provide a medium for promoting vascularization and new tissue formation during remodeling.

2.1.2. Scaffolding Approaches in Tissue Engineering

In the last two decades, four major scaffolding approaches have emerged for tissue engineering applications. These are [12]:

- 1. Pre-made porous scaffolds for cell seeding,
- 2. Decellularlized ECM from allogenic (ECM derived from individuals of the same species) or xenogenic (ECM derived from a member of another species) tissues for cell seeding,
- 3. Cell sheets with self-secreted ECM,
- 4. Cell encapsulation in a self-assembled hydrogel matrix.

The following sections go into more detail regarding each of these approaches.

Pre-Made Porous Scaffolds

One of the most commonly used scaffold fabrication methods is utilizing pre-made porous scaffolds made from biodegradable materials and seeded with cells. There are two main categories for making porous scaffolds based on their sources: natural and synthetic biomaterials. In the case of naturally occurring biomaterials (collagen, gelatin, silk [13]), these are obtained from natural sources, as the name suggests. Once acquired, natural biomaterials are processed into porous scaffolds. The natural biomaterials can be in their native form, such as an ECM from allografts or xenografts, or they may be smaller blocks built up into larger units [12].

The advantage of natural biomaterials is that they usually have superb biocompatibility on a cellular level, allowing cells to attach and grow with high viability. The disadvantage

is that natural materials are limited in physical and mechanical stability and thus lack suitability for particular load-bearing applications. Another issue is that natural biomaterials derived from allogenic or xenogenic sources may cause an antigenic response in hosts [12].

In the case of synthetic biomaterials, these can be further classified into inorganic (for example, bioglass) or organic (for example, synthetic polymer) biomaterials. The advantage of utilizing synthetic biomaterials is that the fabricators have better control over the physical and mechanical properties. In short, these properties can be tailored and tuned to suit specific tissue needs. However, biocompatibility becomes the central issue in this case, as cells may have difficulties in attachment, proliferation, and differentiation on such materials [12].

Whether or not natural or synthetic biomaterials are used, pre-made porous scaffolds have several advantages. For example, this approach is the most diversified choice for biomaterials, ranging from ceramics to hydrogels. Additionally, the pre-made porous scaffold approach can incorporate precise designs of architecture and microstructure. The physiochemical properties of the scaffolds can be engineered to mimic the properties of native ECM in target tissues. That said, there are disadvantages. For example, post-fabrication cell seeding has issues as it is time-consuming and can result in heterogeneous distribution due to limited penetration of the cells to the scaffold. The inhomogeneous distribution of cells in the scaffolds can lead to heterogeneous properties and ECM amounts in the engineered tissues [12].

Decellularlized ECM from Allogenic or Xenogenic Sources

The most nature-mimicking scaffolds are acellular ECM derived from allogenic or xenogenic tissues. All allogenic or xenogenic cellular antigens are removed from tissues in this scaffolding approach, but the ECM components are preserved. As such, the sources for immunogenicity upon implantation are removed (the antigens). The ECM components are conserved among species, so they are well tolerated immunologically. The decellularized ECM can be used for homologous functions when it is used to replace an analogous structural tissue that has been damaged. Furthermore, the decellularized ECM may also be utilized in non-homologous functions, such in the case where it is used for a purpose

that is different from which it fulfills in its native state, or it is used in the location of the body where a structural function does not usually occur. For example, Chan and Leong state in their article, "Scaffolding in tissue engineering: general approaches and tissue-specific considerations," that amnion membrane has been used for peripheral nerve regeneration [12].

The significant advantage of this method is that it is physiologically close to nature when it comes to the mechanical and biological properties of the decellularized ECM if used in homologous ways. The natural ECM has excellent biocompatibility, and the growth factors preserved in the decellularized matrix may further facilitate cell growth and remodeling. However, similar to the case of pre-made porous scaffolds, cell seeding in decellularized ECM may also lead to inhomogeneous distribution, and if there is incomplete removal of the cellular components, the "decellularized" ECM may elicit an immune reaction upon implantation [12].

Cell Sheets with Self-Secreted ECM

Cell sheet engineering operates on the premise that layers of confluent cells are stacked atop one another to create denser matrices. Cell sheet engineering uses an approach where cells secrete their own ECM upon confluence and are harvested without using enzymatic methods. The cells are cultured on a thermo-responsive polymer until they have reached confluence. At that point, the confluent cell sheet is detached by thermally regulating the hydrophobicity of the polymer coatings. Consequently, cell sheet engineering approaches are ideal for epithelium, endothelium, and cell-dense tissues, as the formation of cell sheets requires cells to grow into confluence at high density so that cells can form tight junctions with each other and secrete ECM [12].

An advantage of this approach is that the laminated layers result in rapid neovascularization. The disadvantage of this approach is that due to the thickness of the layer, it is difficult to build up large or thick construct tissues, and so constructing ECM rich tissues and hypocellular tissues is unlikely as the amount of ECM secreted is limited. Tissues with rich ECM for load-bearing purposes are unlikely to be fabricated by this approach [12].



Cell Encapsulation in Self-Assembled Hydrogel Matrix

Cell encapsulation is the process by which living cells are trapped within the confines of a semi-permeable membrane or a homogeneous solid mass. Typically, hydrogels are the biomaterial of choice for encapsulation. The hydrogels are formed by covalent or ionic crosslinking of water-soluble polymers. The predominant use for encapsulation has been for immunoisolation during allogenic or xenogenic cell transplantation, with the most well-known application being xenogenic pancreatic cell transplantation for diabetes [12].

In order for the immunoisolation to work, the key feature for these types of biomaterials is that the encapsulating material needs to be crosslinked or processed in a way so that it becomes impenetrable to cells and also impermeable to large molecules such as antibodies and cellular antigens while remaining permeable to nutrients such as oxygen and glucose. For the xenogenic pancreatic cell application, the encapsulated cells need to be able to secrete therapeutic biomolecules through the hydrogel. Regarding semi-permeable membranes, the encapsulated cells need to be able to maintain viability and functionality despite the limited solid anchorage support. Whereas in the case of a homogeneous solid mass, the entrapped cells interact with the biomaterials, and therefore, the biomaterials should have good biocompatibility to enable cellular attachment and proliferation [12].

However, the most commonly used encapsulating materials are alginate and agarose. Nevertheless, these materials have limited ability to support cell attachment and differentiation, resulting in low cell viability and growth. Another example is collagen, but collagen must be supplemented to improve cell viability [12].

Cell encapsulation has advantages; this approach can be as simple as a one-step procedure, provide homogeneous cell distribution in the hydrogel, and have excellent cell viability. In addition, this approach allows for an injectable application where polymerization can be initiated after injection, which leads to the "setting" of hydrogel after injected into defective tissues. Due to the injectable feature of this scaffold, this approach is sometimes referred to as injectable scaffolding or in situ tissue. This approach's disadvantages typically come from poor mechanical properties, so these scaffolds are rarely used for tissues with load-bearing functions [12]. However, this work utilizes cell encapsulation in a selfassembly hydrogel. Fibrin hydrogels are chosen as this work seeks to expand on the work by Heher et al., which used fibrin [11].

2.2. Fibringen, Fibrin, and Fibrin Scaffolds

This section details fibringen and fibrin, which are important to this work. These proteins are essential as building blocks in tissue engineering applications and, as mentioned previously, as scaffolds. This section describes the molecular structure of fibringen and its conversion into fibrin. Subsequently, the focus will shift toward using fibrin as a scaffold material for tissue engineering. It will highlight fibrin's unique biomechanical properties and modification strategies to tailor its suitability for various tissue regeneration applications. This section provides a comprehensive foundation for discussing fibrin scaffolds in tissue engineering.

2.2.1. Fibringen and Fibrin Structure

Fibringen molecules are two sets of polypeptide chains, linked by disulfide bridges: $A\alpha$ and B β and γ -chains [10] [14]. Fibringen serves as a precursor for fibrin, where the enzyme thrombin cleaves fibrinopeptide A (FPA) from the $A\alpha$ -chains. This cleavage initiates the polymerization process of fibrin.

The precursor fibringen and its derivative fibrin exhibit shared functions in various aspects, as Mosesson noted, "blood clotting, [...], cellular and matrix interactions, the inflammatory response, wound healing, and neoplasia." Furthermore, he states that the governing of these functions are derived from interactive sites on fibringen and fibrin, and in many cases, are inaccessible in fibringen and only emerge due to fibrin formation or fibringen interactions with surfaces [14].

The three polypeptide chains forming fibringen, which are joined together by disulfide bridges, form an elongated structure roughly 45 nm in length. The fibringen molecules contain two outer D domains with a coiled-coil segment connected to a central E domain. In total, fibringen contains 1482 residues, with the majority being found on the A α chain, with 610, followed by the B β -chain, containing 461, leaving 411 residues on the



major γ -chain, γA . Fig. 2.1 illustrates the fibringen and fibrin molecules schematically [14].

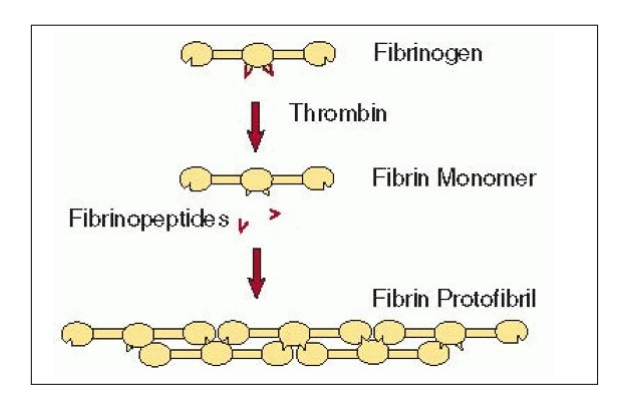


Figure 2.1.: Schematic diagram of fibringen and fibrin structure, namely the conversion of fibrin from fibringen due to the presence of thrombin [15].

Thrombin exposes a polymerization site, E_A by cleaving an N-terminal FPA sequence on the $A\alpha$ -chain, which kicks off fibrin assembly. The polymerization site, E_A , creates an association with a complementary-binding pocket in the D domain, which begins to align fibrin molecules into double-stranded twisting fibrils by overlapping and staggering the molecules in an end-to-middle domain arrangement. Multi-stranded fibers are created by undergoing lateral associations. From here, two types of "branch junctions" form the basis of fibrin networks: bilateral branch and equilateral branch junctions. Fig. 2.2 illustrates schematically fibrin assembly into multi-fibril formation [14].

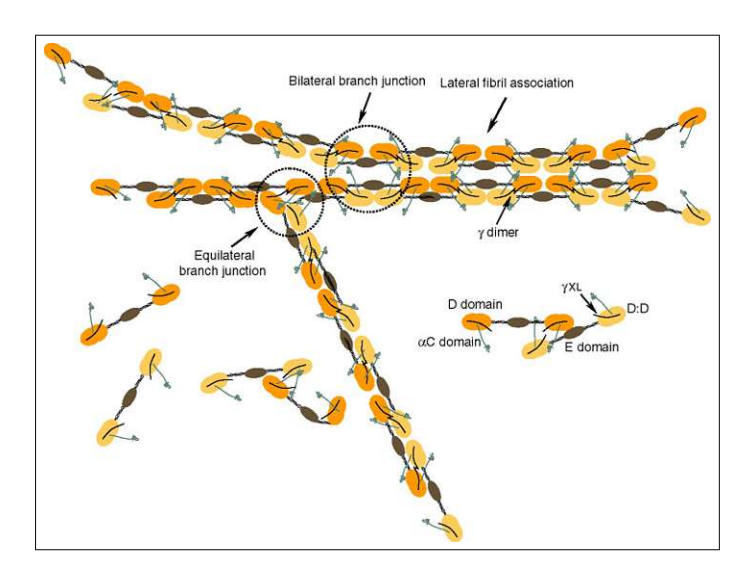


Figure 2.2.: From Mosesson, schematic diagram of fibrin assembly highlighting bilateral and lateral branch junctions. Two color schemes represent the fibrin molecules [14].

Bilateral junctions occur when a double-stranded fibril converges laterally with another, resulting in a four-stranded fibril. By continuing the lateral convergence with more fibrils, multi-stranded fibril structures can be expanded upon. Equilateral junctions are formed among three fibrin molecules by convergent interactions. This results in three doublestranded fibrils. Compared to bilateral junctions, equilateral junctions appear to form more frequently when fibrinopeptide cleavage is slow, resulting in networks that are more branched and less porous of a matrix [14].

Cleaving at FPA is not the only option for thrombin. Similar to the cleavage of FPA, there is another site where thrombin cleaves: fibrinopeptide B (FPB). However, the release of FPB is slower when compared to that of FPA, and releasing FPB exposes a different polymerization site, E_B . E_B associates with a complementary binding site on the β -chain segment of the D domain. While there are two different sites for polymerization, the resulting fibril structure is the same [14].

2.2.2. Fibrin Scaffolds

In wound healing, fibrin acts as a scaffold to block blood loss and promote cellular interactions. In particular, the presence of cells affects fibrin clots. With the addition of platelets, the fibrin network forms thinner fibers where the platelets aggregate [16].

The fibrin network can assemble into sheets or films, where the films may have antimicrobial functions. Regarding fibrin's biomechanical properties, it has been shown to exhibit over 330% extensibility as it is a stretchy, rubber-like material with viscoelastic properties. The mechanical properties of clots originate from the fact that fibrin has a hierarchical structure, where fiber properties such as orientation, stretching, bending, and buckling matter [17].

Creating a fibrin hydrogel is relatively simple; at their core, they are made from purified allogenic fibringen and purified thrombin, both of which can be purchased commercially. There are some disadvantages regarding the use of fibrin hydrogels as scaffolds. Namely, the gel experiences shrinkage during the formation of flat sheets, exhibits low mechanical stiffness, and often degrades before tissue-engineered structures can be formed. However, these disadvantages can be overcome; for example, the gel shrinkage can be mitigated by



incorporating a fixing agent into the fibrin gel. In addition, low mechanical stiffness can be mitigated or improved by combining the fibrin hydrogel with other materials to form a composite scaffold. Combining materials allows the fabricator to set the mechanical strength to suit their needs. Lastly, several approaches can be employed to reduce fibrin hydrogel degradation. These include optimizing the pH levels, using denatured 3-D fibrin matrices, and using calcium ions (Ca²⁺) [10]. As a result, the fibrin network structure is highly tunable.

The fibrin network can be modified by adapting the fibringen-to-thrombin ratio, adding bioactive factors, introducing composites, and including binding agents. Increasing the fibringen-to-thrombin ratio concentration results in smaller pore sizes within the matrix, and thus, the matrix becomes less permeable to large solutes and infiltration of cells. On the other hand, the higher concentration of thrombin results in the polymerization of a highly branched fibrin network with thin fibers. Lower thrombin concentrations see a low degree of fiber branching and a high degree of porosity but with thicker fibrin fibers in the network. Fine-tuning beyond changing the ratio of fibrinogen-to-thrombin can be achieved by adding salt or calcium; increasing the calcium sees an increase in the size of the fibers but at the expense of overall stiffness [16].

As mentioned, fibrin is a viscoelastic material that exhibits both viscous and elastic characteristics when deformed. When stress is applied to a viscous material, it resists the shear flow and strains with time. Rather than an elastic material, fibrin exhibits nonlinear elastic characteristics, in that fibrin will stretch easily at small strains, but at larger strains, it significantly stiffens. These mechanical properties are affected by the tuning of the fibringen-to-thrombin concentration, which affects the fibrin polymerization as mentioned previously [16].

2.3. Hydrogels

Hydrogels consist of a network of crosslinked hydrophilic polymers. As the name suggests, they are a semi-sold material (gel-like) that contains large amounts of liquid due to the hydrophilic polymers and small amounts of solid [18]. The strong hydrophilicity of the polymer chains allows for hydrogels to retain large amounts of water within the

intermolecular space. The swelling behavior depends on the composition and the amount of cross-linking [19]. As mentioned, fibrin is a hydrogel. Hydrogels are attractive scaffold materials due to their ability to uniformly entrap cells spatially and allow for high cell density when compacted. Fibrin, in particular, is an excellent hydrogel over synthetic due to its higher density of cell adhesion sites [20]. Furthermore, they are incredibly versatile as they can respond to and undergo physiochemical changes due to external stimuli such as pH, light, temperature, and more. Lastly, they have the ability, in some cases, to revert to their original state when the external stimuli (trigger) is removed [18].

The mechanical behavior of hydrogels relates to their material chemistry and morphology at different length scales. The deformation of a hydrogel involves mechanisms such as viscoelasticity and nonlinear elasticity. The viscoelastic relaxation behavior is a response to the fluctuations of the polymer chain under strain. When under tension, hydrogels take up water, whereas compression causes hydrogels to lose water. The asymmetry in response to tension-compression introduces complexity in understanding the time- and strain-dependence related to water flow. When performing testing on hydrogels, it's important to be mindful of the type of testing being conducted, as the test setup, conditions, and preparation of the samples all affect the results [19].

Mechanical testing of hydrogels often involves small load cells (10-100N) and large crosshead displacements due to the fact that they are soft materials but can sustain large deformations – in many cases, more than 100% of their initial length. Hydrogels often need testing in a water environment to prevent water loss during the experiment; water loss affects the gel structure and the test results. In load relaxation testing, hydrogels involve viscoelastic mechanisms, where it can be observed that the linear viscoelastic models are made up of springs and dashpots [19]. This will be discussed in a later section (2.5.2).

2.4. Tissue Bioreactors

A bioreactor is a device with a chamber that provides mechanical stimulus to influence biological processes. The purpose of a bioreactor is to create a tissue-specific physiological environment to allow for tissue maturation by providing biochemical and physical regulatory signals to cells, which allow for them to undergo differentiation or to produce ECM



[21]. Bioreactors may act as incubators and allow for the controlling of gasses, nutrients, and signaling molecules [22]. Bioreactor systems mechanically stimulate cell-seeded scaffolds; in the case of skeletal muscle, bioreactors of this nature promote alignment in addition to muscle maturation. According to Heher, "the fixation of the scaffold between two points creates predictable lines of isometric strain as the cells pull against the posts" [11]. The scaffold anchoring approach is popular; for example, the MagneTissue bioreactor utilized by Heher et al. allows for the adjustable cyclic or static mechanical stimulation of cells via a magnetic force, where cells are embedded in a fibrin ring matrix and anchored on two ends [11]. Fig. 2.3 outlines the ring casting for the fibrin rings (with the addition of TDPCs) used in the MagneTissue bioreactor, mounting, and the MagneTissue bioreactor itself. As previously mentioned, this work aims to understand these constructs' mechanical properties, especially as the experiments within the MagneTissue bioreactor may take seven days or longer to complete.

2.5. Mechanical Testing

This segment provides an overview of the foundational knowledge and theoretical framework of the various mechanical tests conducted within this work.

2.5.1. Tensile Testing

In tensile testing, or in this case of this work, linear ramp testing, specimens are pulled at a constant rate with an axial force until the specimen fails. From this test, the concept of engineering stress arises and is defined as [23]:

$$\sigma = \frac{P}{A_i} \tag{2.1}$$

where P is the load and A_i is the initial cross-sectional area. σ has the units of Pascal, Pa, measured as Newtons per meter squared (N/m^2) . It is important to note that as the specimen is stretched, the initial area, A_i will decrease; thus, the true stress the material experiences is described as $\bar{\sigma}$ [23]:

$$\bar{\sigma} = \frac{P}{A} \tag{2.2}$$

It is a subtle difference, but because the cross-sectional area, A, is less than the initial area, A_i , the true stress experienced at that point will be greater than the engineering stress $(\bar{\sigma} > \sigma)$ [23].

Typically, on specimens, a section will be marked with a gage length as seen in Fig. 2.4 [23].

The main purpose of the gage length is so that when the specimen fails, it will fail within this region while avoiding any effects in the shoulder region (where the specimen is gripped). The specimen must be gripped to be held at the maximum load without slipping or failure in that shoulder section, and any effects from bending are minimized. The initial gage length is denoted by L_i , and throughout tensile testing, a new measurement of L is made so that ΔL can be found. Thus, the engineering strain, ε is [23]:

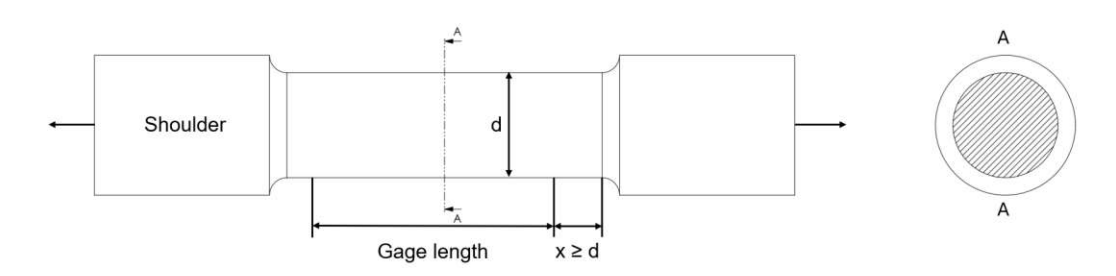


Figure 2.4.: Adapted from Gdoutos' Mechanical Testing of Materials, a typical cylindrical testing sample is shown. Note that the gage length is marked [23].

$$\varepsilon = \frac{L - L_i}{L_i} = \frac{\Delta L}{L_i} \tag{2.3}$$

The strain has no units; it is a dimensionless quantity [23].

Understanding engineering stress and strain is necessary as it gives a geometry-normalized picture of how a material resists loading until it fails. From tensile testing, several properties can be determined, such as the ultimate tensile strength, σ_{UTS} , which is the maximum stress the material experiences before failure, and the tensile yield strength, σ_Y , which is the point at which any further stress will cause the material to deform irreversibly [24]. Fig. 2.5 illustrates these material properties graphically.

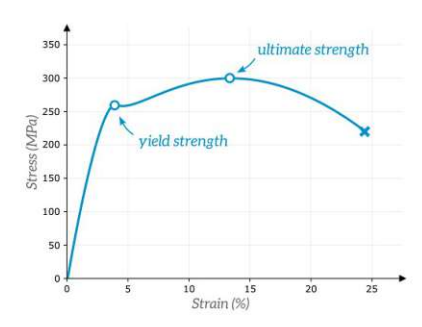


Figure 2.5.: Yield strength, ultimate strength on a stress-strain curve [25]

By knowing these properties, a comparison between materials can be made.

2.5.2. Viscoelasticity and Stress Relaxation Testing

The mechanical testing performed in this work includes stress relaxation and cyclic loading. These tests are selected because this work investigates the stresses the rings experience when in the MagneTissue bioreactor. The MagneTissue bioreactor was created to

2. Background

make skeletal muscle constructs by applying a physiologically relevant strain regime by stimulating cells embedded in a fibrin matrix [11]. However, the bioreactor setup does not allow for the measurement of forces; thus, the stresses experienced by the construct cannot be calculated. Therefore, part of the purpose of this work, as mentioned in Chapter 1.2, is to establish a protocol and conduct initial mechanical tests to understand the mechanical properties of fibrin rings, specifically during stress relaxation and cyclic loading.

This section presents the basic theory of viscoelasticity and stress relaxation. A material is said to be viscoelastic if it undergoes time-dependent deformation under load and then time-dependent recovery from deformation once unloaded [26]. Furthermore, these materials exhibit a combination of elastic and viscous responses - hence viscoelasticity [27]. Polymers are the classic example of viscoelastic materials [27] with a multitude of studies done to define their characteristics [28][29][30]. However, there are examples of materials relevant to this work that exhibit viscoelasticity, namely, biological tissues such as ligaments [26][31][32] and tendons [32] [33]. The common characteristics that viscoelastic materials exhibit are creep and relaxation where creep is defined as a change in strain over time when constant stress is applied to the material, and relaxation is the change in stress over time when a constant strain is applied to the material [26]. Stress relaxation is particularly relevant to this work, as this study examines the change in stress over time in fibrin rings held at a constant strain.

Linear Viscoelastic Theory

The foundation of linear viscoelasticity can be summarized by Boltzmann's superposition principle: "Each loading step makes an independent contribution to the final state." In this section, only small deformations and load cases that contain only one non-zero stress component (uniaxial loading) are considered [27].

The Boltzmann superposition integral is defined as [26][31]:

$$\sigma(t) = \int_0^t E(t - \tau) \frac{d\varepsilon(\tau)}{d\tau} d\tau \tag{2.4}$$

where $\sigma(t)$ is the stress, E(t) is the relaxation function dependent on time, $\varepsilon(t)$ is the strain, and τ is the variable of integration. Note, in linearly viscoelastic materials, the

relaxation modulus, E(t), depends only on time and is independent of strain [26][31]. E(t) can be obtained experimentally; a constant strain is applied, and the resulting timedependent stress in relaxation is recorded, as seen in Fig. 2.6. Linearity is verified by tests at several strain levels [26].

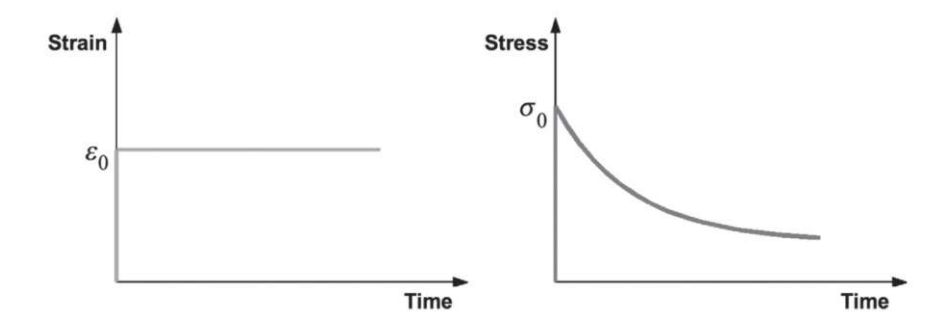


Figure 2.6.: A general stress relaxation experiment, where the strain is held constant at ε_0 , and the resulting time-dependent stress is recorded [27].

By measuring the stress response from the strain jump, the stress relaxation modulus may be defined as [27]:

$$E_r(t) = \frac{\sigma(t)}{\varepsilon_0} \tag{2.5}$$

Maxwell Model

While viscoelasticity can be nicely summarized by Boltzmann's superposition principle [27], in practice, simple phenomenological models can be applied and provide a quick way to estimate the mechanical response to loading [34]. This work utilizes fibrin, which is a polymer [16], and as a polymer, it has solid and fluid attributes [34]. As previously mentioned, viscoelastic materials like fibrin exhibit elastic and viscous responses [17]. Due to its elasticity (solid attribute), this behavior can be described with Hooke's law (Eqn. 2.6), where σ is the stress, E is the elastic modulus, and ε is the strain [34].

$$\sigma = E\varepsilon \tag{2.6}$$

Likewise, the viscous response, η , (fluid attribute) relates the stress, σ , and the strain rate, $\dot{\varepsilon}$, which can be seen in Eqn. 2.7 [34].

$$\sigma = \eta \dot{\varepsilon} \tag{2.7}$$

To simplify polymers, the elastic response (solid attribute) can be represented by a spring, and a dashpot can represent the viscous response (fluid attribute). The Maxwell model is then when a spring and a dashpot are connected in series. As the Maxwell model is a simplistic model and does not capture the molecular structure or entropy changes, it is still helpful in describing and visualizing, at a basic level, the time-dependent response [34].

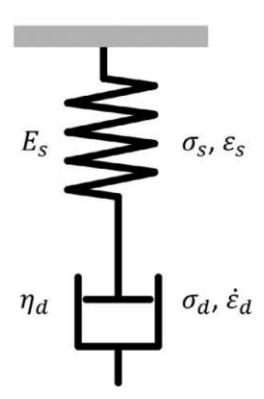


Figure 2.7.: The physical elements of a Maxwell model, consisting of a spring and dashpot in series [34].

As seen in Fig. 2.7, the physical components of the Maxwell element are shown connected in series. It is important to note that while connected in series in this way, the applied stress, σ_o is equivalent to both the spring stress, σ_s and dashpot stress, σ_d , which is shown in Eqn. 2.8 [34].

$$\sigma_o = \sigma_s = \sigma_d \tag{2.8}$$

On the other hand, the total strain of the system, ε , is the sum of the strain from the spring, ε_s , and the strain of the dashpot, ε_d , as seen in Eqn. 2.9 [34].

$$\varepsilon = \varepsilon_s + \varepsilon_d \tag{2.9}$$

Of note to this work, the stress relaxation response can be described (Eqn. 2.10) using the Maxwell element when holding the strain constant [34].

$$\sigma(t) = \sigma_o e^{-\frac{E_s}{\eta}t} \tag{2.10}$$

Eqn. 2.10 can be rewritten in terms of the relaxation modulus, $E_{\Re}(t)$, which is equal to $\sigma(t)/\varepsilon_o$. This leads to Eqn. 2.11, where E_o is the instantaneous modulus and τ_{\Re} is the relaxation time for a single spring-dashpot element [35].

$$E_{\Re}(t) = E_o e^{-\frac{t}{\tau_{\Re}}} \tag{2.11}$$

Unfortunately, one Maxwell element is not enough in order to describe polymers. Instead, multiple Maxwell elements can be connected in series to more accurately model polymers by better describing the time-dependent properties over a range of loading times. In this case, a normalized relaxation modulus function is defined based on the generalized Maxwell model [35]. A generalized Maxwell model can be seen in Fig. 2.8, where there is a linear spring and an n number of Maxwell units [19].

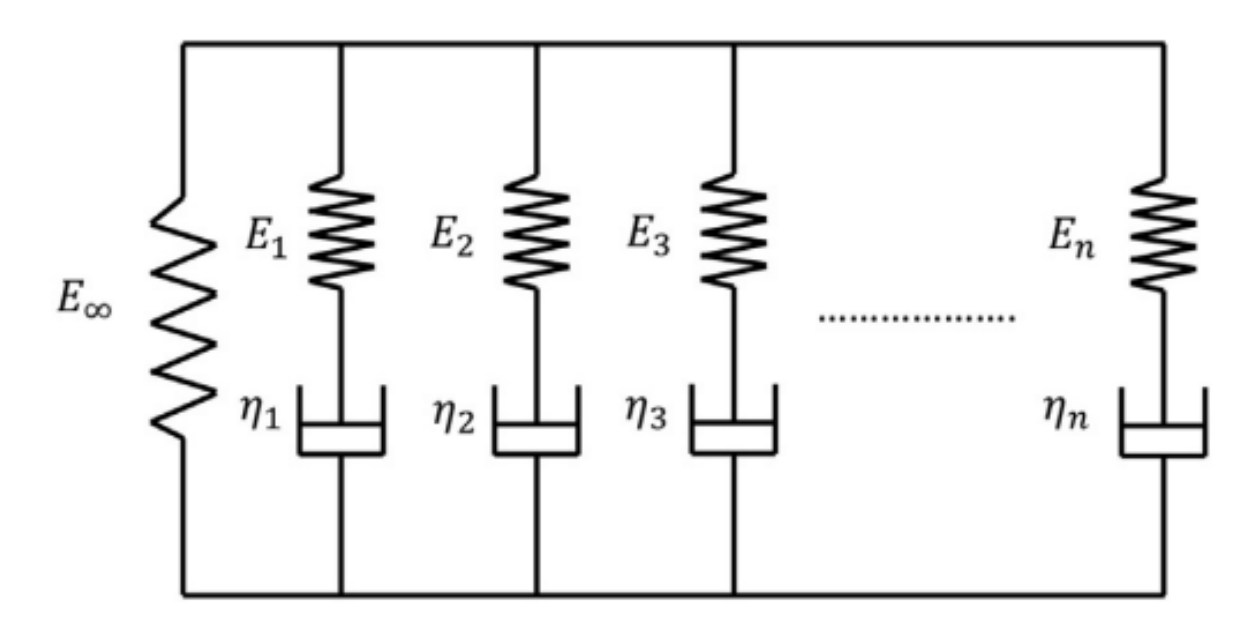


Figure 2.8.: Generalized Maxwell model, consisting of Maxwell units (in which a unit is a spring and dashpot connected in series) connected in parallel with an isolated spring to represent the equilibrium modulus, from "Mechanical characterization of hydrogels" by Mohammad Islam and Michelle Oyen [19].

The corresponding relaxation modulus $(E_{\Re}(t))$ can be defined in terms of a Prony series [19][35]:

$$E_{\Re}(t) = E_{\infty} + \sum_{i=1}^{n} E_{i} e^{-\frac{t}{\tau_{i}}}$$
(2.12)

 E_{∞} is the linear spring modulus (equilibrium modulus), E_i is the stiffness of the spring of the *ith* element and τ_i is the characteristic relaxation time of the *ith* element [19]. Eqn. 2.12 is utilized in this work. After conducting stress relaxation experiments, a Prony series curve fit is applied to the data to estimate the relaxation time constants (τ_i) .

3. Methodology

This chapter details the cell culturing, the fabrication of the fibrin rings used in the experiments, the design of the adaptors for the load frame, the ring-shaped geometry of the rings and how it affects the stress calculations, the entirety of the testing setup, and the protocol for the stress relaxation and cyclic loading tests, as well as data processing.

3.1. Sample Preparation

All samples undergo identical preparation until the cell-seeding stage, where some samples remain cell-free and some are seeded. A single batch of fibrin produces all the rings tested in this thesis. Rings containing cells are stored in complete media and removed from the incubator before testing. Although testing spans two days, all samples are tested under the same parameters.

3.1.1. Tendon-Derived Progenitor Cells Isolation

Rat TDPCs were isolated according to Gehwolf, R. et al. [36]. Briefly, Sprague Dawley 3-month-old male rats were anesthetized with isoflurane and decapitated. The Achilles tendons were aseptically dissected, cut into small pieces, and digested at 37°C overnight in a complete medium: Dulbecco's modified Eagle's medium high glucose (DMEM-HG; VWR), supplemented with 10% fetal calf serum (volume/volume (v/v)) (FCS, Hyclone), 1% penicillin/streptomycin 100X (v/v) (Capricorn Scientific) and 1% L-glutamine 100X (v/v) (VWR) containing 3 mg/ml collagenase type II (Gibco). The next day, the remaining undigested tissue fragments were gently dissociated by pipetting. Then, the solution was transferred through a 40 µm cell strainer into a 50 ml conical tube, supplemented with 10 ml of the complete medium. The cells were centrifuged at 150 g for 5 min at room temperature; the supernatant was carefully discarded, and the cell pellet was resuspended in 10 ml of complete medium and transferred to a $25~\mathrm{cm^2}$ cell culture flask. After several days in culture, the cells reached approximately 70% confluency and were passaged until the required number of cells was obtained.

Rat TDPCs were cultured in the complete medium. For expansion, cells were cultured in standard cell culture conditions (37°C, 5% CO₂) on 15 cm Petri dishes and sub-cultured at 70% confluence to avoid induction of differentiation. Medium exchange was done every second day.

3.1.3. Cell-Free Rings Preparation

Ring-shaped fibrin scaffolds were created using a Tissucol Duo kit 5.0 ml (Baxter Healthcare GmbH, Vienna, Austria). The fibringen and thrombin were mixed in a 1:1 ratio. In other words, if a working solution of 500 μ L was required, 250 μ L of fibringen was mixed with 250 μ L of thrombin.

The fibringen had a stock concentration of 78.5 mg/mL when procured from the supplier. The final concentration needed for the experiments was 20 mg/mL of fibringen (Fbg20). The fibringen was diluted with DMEM High Glucose (Sigma-Aldrich Handels GmbH, Vienna, Austria) to 40 mg/mL, as this would result in a final concentration of 20 mg/mL after mixing with thrombin.

When thrombin was procured from the supplier, it had a stock concentration of 500 international unit (IU). The final concentration used in the experiments was 0.625 IU of thrombin (Thr0.625). The thrombin was diluted with 40 mM calcium chloride (CaCl₂). Calcium increases the rate of fibrin monomer polymerization [37]. Due to the low concentration required, thrombin was diluted in several steps. From the stock concentration of 500 IU, a dilution was made to 50 IU, then to 4 IU, and finally to 1.25 IU, as the last step was to mix the thrombin (Thr) with fibringen (Fbg), it would be diluted to the required 0.625 IU.

A pipette was used to mix the Fbg20:Thr0.625 mixture gently and then quickly deposited into custom-made silicon ring molds (Fig. 3.1a). Each mold has a volume of 500 μ L, a total length of 3 cm, and a depth of 2 mm. The empty molds were placed into a petri dish. After the mixture was injected into the molds, the cover of the petri dish was placed on, and the dishes were put into an incubator set to 37°C, where they remained for 45



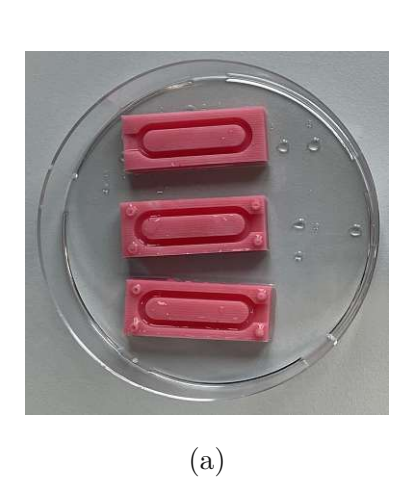






Figure 3.1.: (a) Silicon molds, 500 μ L volume, (b) Fibrin rings in silicon molds in the incubator, (c) Fibrin rings polymerized in the silicon molds.

minutes (Fig. 3.1b). Subsequently, the cell-free rings were removed from the molds and placed in a petri dish containing PBS (Sigma-Aldrich Handels GmbH, Vienna, Austria), where they remained until they were tested on the load frame (Fig. 3.2).

Due to the fast polymerization of fibringen after coming into contact with the thrombin, it is recommended to aliquot the fibringen into separate Eppendorf[®] tubes and have two pipettes available. For example, 250 μ L of the fibringen was placed separately into a 1 mL Eppendorf[®] tube. At this point, two pipettes should be standing by and ready to go. One pipette was used to add 250 μ L of thrombin to the fibringen. Immediately after adding the thrombin to the mixture, the other pipette set to 480μ L was picked up, and the mixture was carefully triturated (pipetted up and down several times) so as not to cause bubbles and to have a more homogenous mixture and then transferred into the mold. This process needed to happen quickly because polymerization and setting had already begun when the mold was filled (Fig. 3.1c).



Figure 3.2.: Fibrin rings in a petri dish with PBS while waiting to be tested.

3.1.4. Cell-Seeded Rings Preparation

TDPCs cells were encapsulated in fibrin hydrogels using the clinically approved Tissucol Duo 500 5.0 mL Fibrin Sealant (Baxter Healthcare Corp., Deerfield, USA) according to Tomasch J. et al. [38]. Briefly, fibringen was diluted from a 78.5 mg/mL stock in the DMEM High Glucose to 40 mg/mL. Thrombin stock of 500 U/mL was diluted in 40 mM CaCl₂ to a working solution of 4 U/mL and further diluted in cell suspension (in pure DMEM) to 1.25 U/mL. Like cell-free rings, thrombin+cells and fibringen were mixed in a 1:1 ratio, injected into silicon molds, and polymerized for 45 minutes at 37°C. After removing the rings from the molds, they were put in complete media containing 100 KIU of Aprotinin to avoid fibrin digestion and then placed into the incubator until testing on the load frame.

3.1.5. Ring-Shaped Geometry and Stress Calculations

The samples investigated were ring-shaped with a unique geometry due to how the rings are cast in a silicon mold. This section examines the unique geometry and its impact on stress calculations. As seen in Fig. 3.3a, one face of the fibrin ring is rounded, while the other face (Fig. 3.3b) is flat. This rounded top face is due to how the silicon molds are made, which impacts the final geometry of the sample.

When the ring is placed on the load frame, it has a nominal length of 3 cm at the starting position of the test. This dimension serves as the initial gage length, L_i , which is used in calculating the engineering strain, ε . The cross-sectional area of the sample can be likened to a semicircle sitting on a rectangle, as seen in Fig. 3.4. This geometry breakdown allows for calculating the cross-sectional area of the sample by adding the area of the rectangle and the area of the semicircle together.

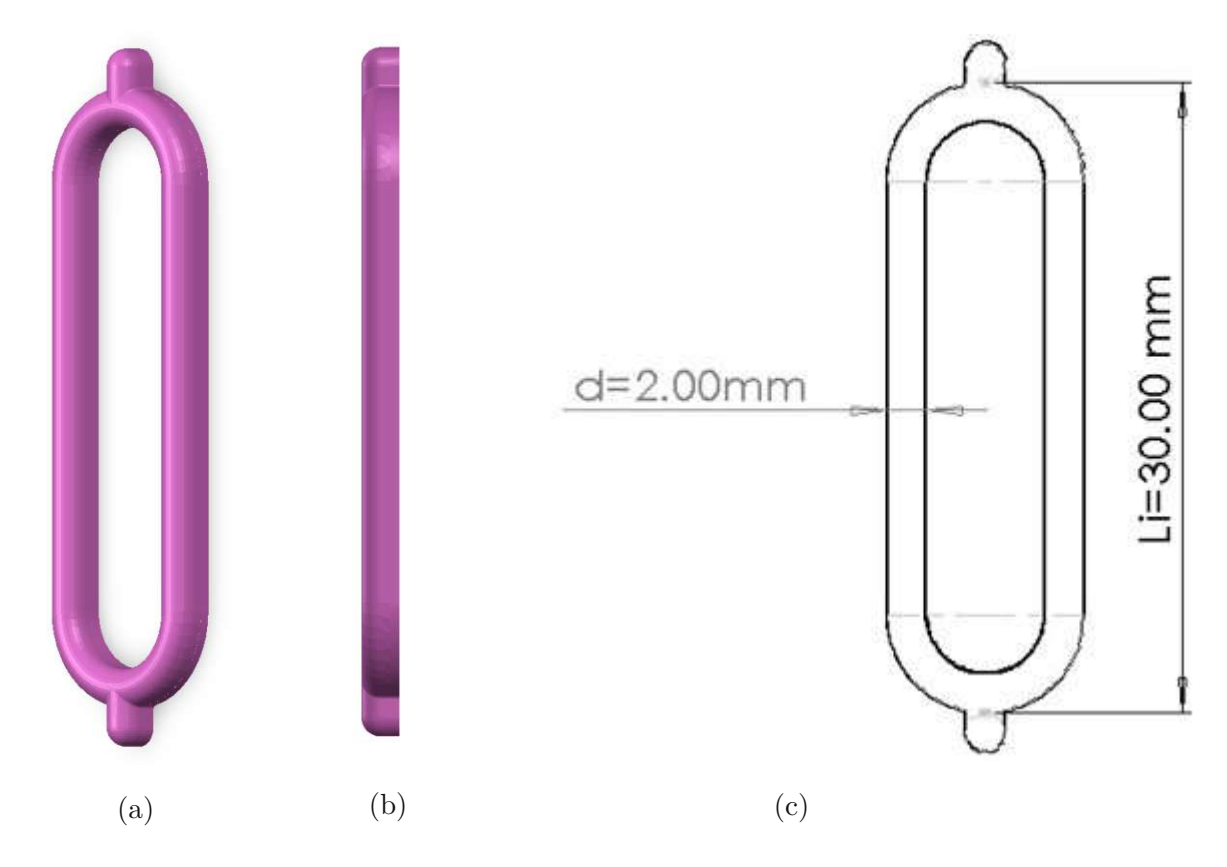


Figure 3.3.: (a) and (b) Not to scale and are CAD Rendition of the fibrin ring. (c) shows the L_i dimension and the diameter, d, of one of the strands.

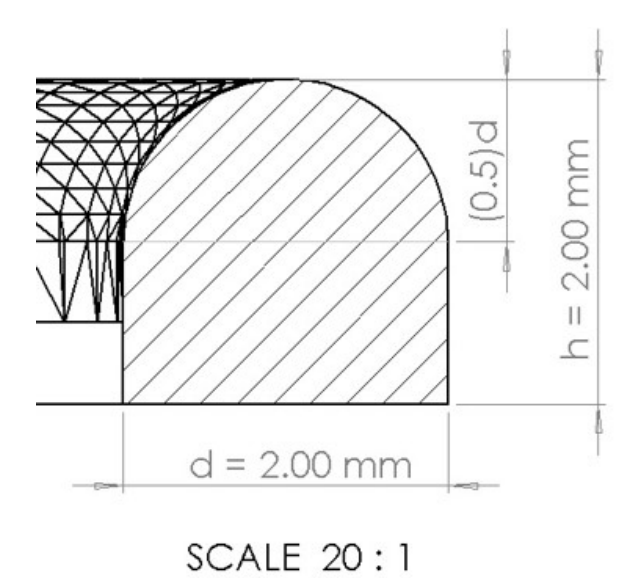


Figure 3.4.: Section cut of the ring to view the cross-section of one strand, this illustrates the CSA, scaled to 20:1

3. Methodology

The CSA of the sample can be calculated by using Eqn. 3.1.

$$CSA = \frac{1}{2} \left(\frac{\pi}{4} d^2 \right) + (h - 0.5d)d \tag{3.1}$$

where d is the circle's diameter (and the length of the rectangle), and h is the total height (or depth, depending on how one looks at it) of the ring. Fig. 3.4 illustrates the semicircle on top of the rectangle. Nominally, the diameter, d, is 2 mm, and the height, h, is 2 mm.

After casting, the rings typically retain the 2 mm height/depth; however, the diameter tends to be more variable. To account for the variability in the samples, the diameter of one of the strands is measured for each trial of every test. Details on how to measure one of the strand's diameter are given in Section 3.2.4.

The CSA calculated using Eqn. 3.1 is used to calculate the engineering stress, σ .

3.2. Mechanical Preparation and Testing

3.2.1. Tensile Tension Adaptor and Alignment Piece

A servo dynamic load frame was used to perform the tensile test experiments. The SELmini-001 (Thelkin GmbH, Winterthur, Switzerland) from Thelkin was equipped with a 10 N nominal load cell (S2M Force Transducer Hottinger Brüel & Kjaer GmbH, Darmstadt, Germany). Custom-made adaptors were developed for tensile tests to be performed on the rings. Fig. 3.5 shows a schematic of the testing setup.

The design of the adaptors leveraged the MagneTissue bioreactor half-spool design [11], which can be seen in Fig. 3.6a. Like in the bioreactor, the fibrin ring was held in place by the spool design; the ring sat on the upper adaptor and hooked underneath the lower adaptor. The main feature of these adaptors was their half-spool shape, as seen in Fig. 3.6b. This shape allowed for the fibrin ring to sit comfortably on the adaptor. The bottom adaptor remained stationary, while the upper one was displaced from the bottom. The entire testing setup can be found in Chapter 3.2.3, Testing Setup.

The design had the following requirements:



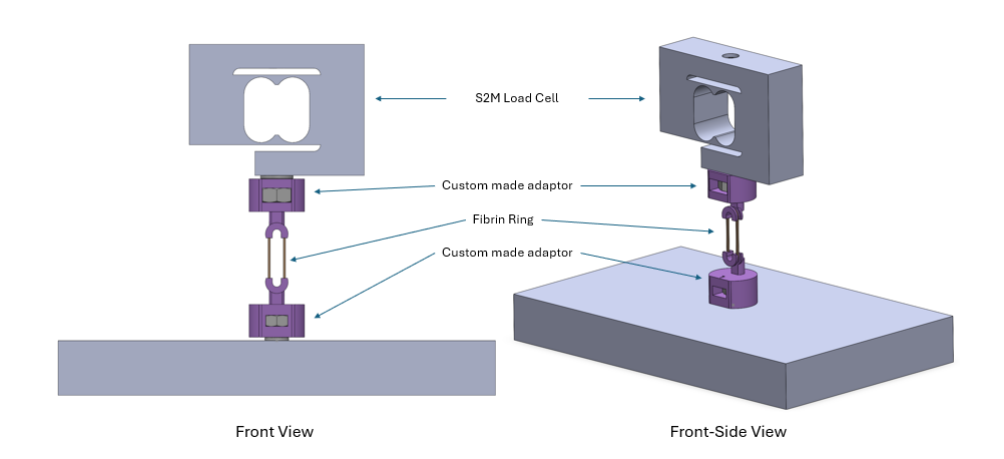


Figure 3.5.: Schematic of the testing setup, the S2M load cell connects to the upper portion of the Thelkin load frame. The lower adaptor connects to the bottom of the Thelkin load frame.

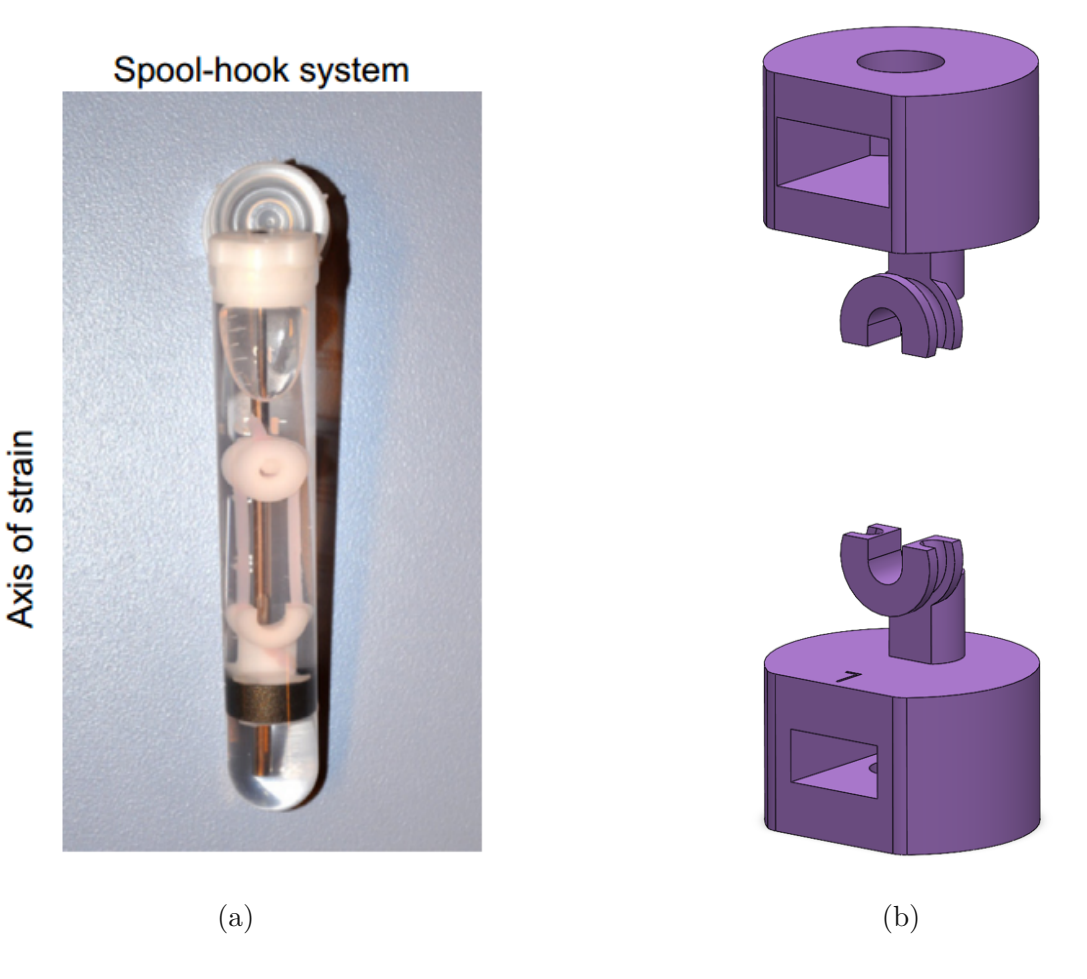


Figure 3.6.: (a) Custome-made tube for the MagneTissue bioreactor, which contains the spool-hook system that the fibrin rings are attached to [11], (b) The adaptors contain a half-spool to allow the fibrin ring to sit comfortably.

3. Methodology

- The ring must have axial alignment and concentricity to be located directly under the load path of the force transducer to minimize any moments,
- The upper adaptor must be attachable to the load cell,
- The lower adaptor must be attachable to the lower Thelkin surface,
- The adaptors must be easily removable for cleaning.

The adaptors were 3D printed on an Anycubic Photon Mono X 6ks stereolithography (SLA) printer (Anycubic, Shenzhen, China) using grey 405 nm SLA UV-curing resin (Anycubic, Shenzhen, China) by Scott Recor.

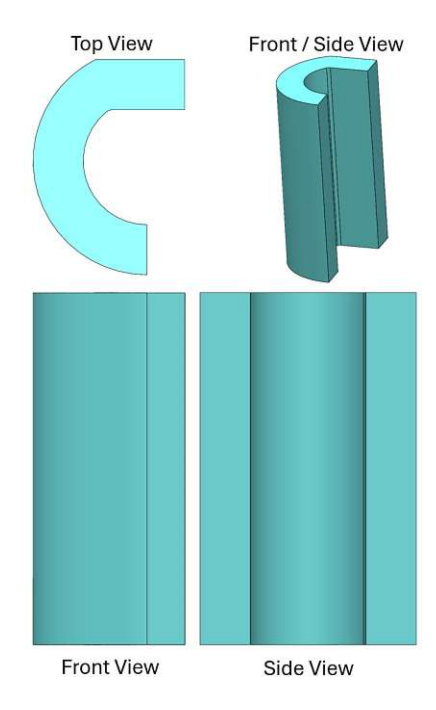


Figure 3.7.: Not to scale. CAD rendition of the alignment piece, top view, front view, side view, and front/side view shown

An alignment piece was also 3D printed on the Anycubic Photon Mono X 6ks using grey 4.5 nm SLA UV-curing resin by Scott Recor. The upper and lower adapters fit within the alignment piece (Fig. 3.7). The front flat faces of the adapter were aligned against the inner flat face of the alignment piece. This ensured the front flat faces of the half-spool adapters were not crooked and thus prevented the fibrin ring from being crooked. The plane of the front face of the half-spool was parallel to the flat front face of the adapter. All parts were printed by Scott Recor, whose help is gratefully acknowledged.

3.2.2. Water Bath

Testing was performed on the load frame using a water bath to simulate physiological (hydrated only) conditions. Fig. 3.8 shows a CAD rendition of the water bath. As seen in the front/side view, a window provided a view into the water bath. The window assisted in capturing videos and images of the contents by reducing refraction-related issues. The water bath had an inner diameter of 90 mm, a thickness of 5 mm, and a height of 65 mm.

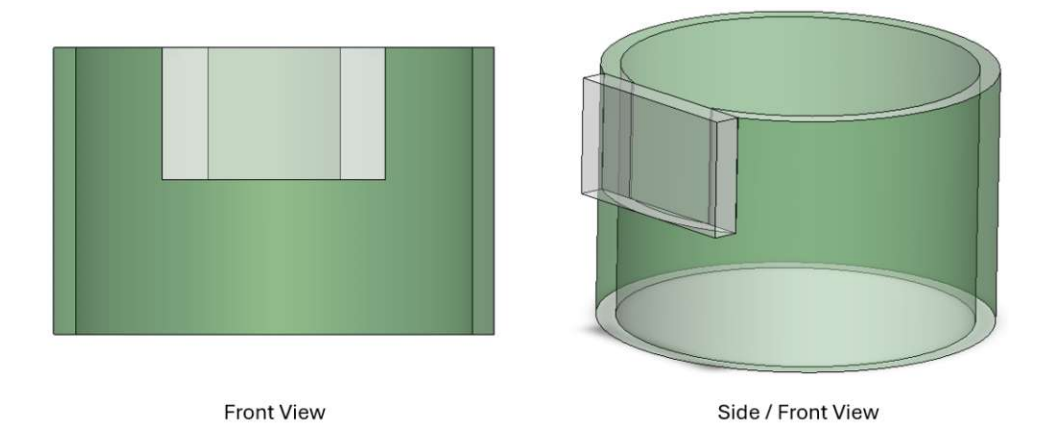
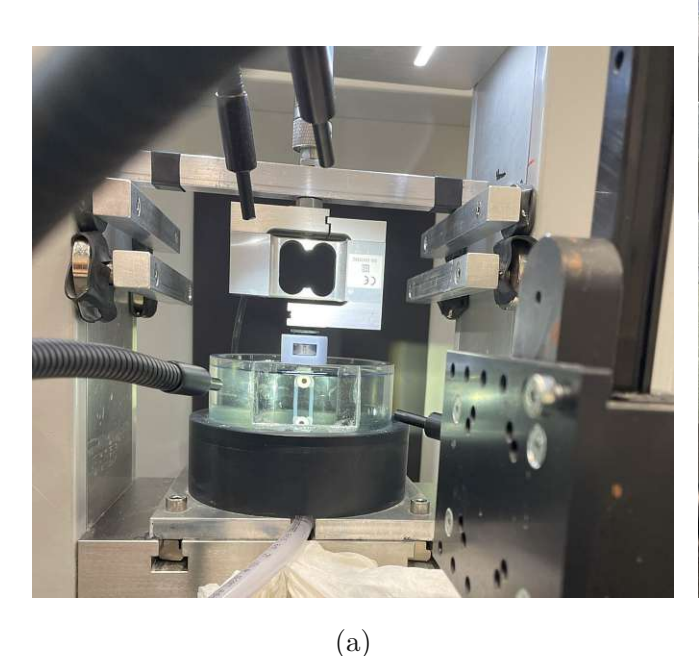


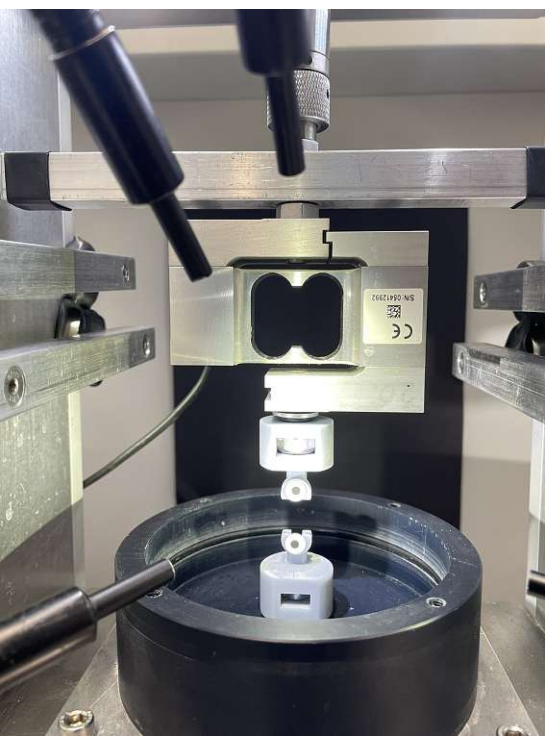
Figure 3.8.: Not to scale. CAD rendition of water bath, front, and front/side view shown

3.2.3. Testing Setup

Fig. 3.9a shows the complete testing setup with a fibrin ring mounted onto the adaptors. Fig. 3.9b is a closeup of the setup without the water bath. The black and white markers on the upper and lower adaptors allow for the position of the adaptors to be tracked using Tracker Video Analysis and Modeling Tool (Douglas Brown, Wolfgang Christian, Robert M Hanson, Davidson College, Davidson, NC, USA). The testing setup allowed for the fibrin rings to be tested in wet or dry conditions. The wet conditions used a water bath filled with PBS.







(b)

Figure 3.9.: (a) Water bath setup, (b) Closeup of the testing setup without the water bath.

3.2.4. Experimental Protocol

The following section overviews the general setup for running tests on the load frame, followed by instructions on how to run stress relaxation and cyclic loading experiments.

General Setup

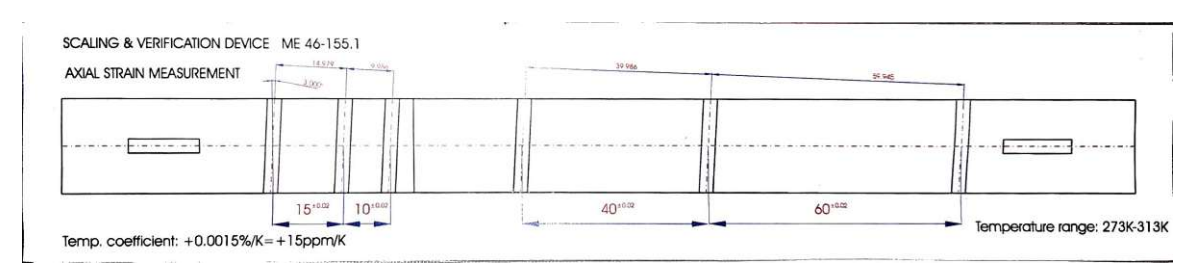
Before installing the load cell onto the load frame, the upper adaptor has to be installed on the load cell. The load cell used was very sensitive, so it was easier to install the adapter before it was placed on the load frame. Otherwise, the load cell is more likely to be damaged during adapter installation. The lower adaptor is installed directly onto the load frame. The load frame is turned on first, and then the load cell is installed on the upper piston. The user can log into the software and then manually align the upper and lower adaptors, ensuring that the user is careful not to pull on the load cell while adjusting the upper adapter. Using the alignment piece as seen in Fig. 3.10, the faces of the front of the adaptors become aligned to ensure that it is not twisted when the ring

is placed on the spools. The front face of the adaptor is parallel to the front face of the spool. Section 3.2.1 gives more details on the alignment process. Located on the upper and lower adapter half-spools are white sticker markers with a black dot in the center, provided by the laboratory. These are used to track the movement of the adapters.



Figure 3.10.: The upper and lower adaptor pieces are in the process of alignment.

After alignment, calibration photos are taken to be used as a reference. The process for taking the calibration photos is as follows: a calibration ruler is held in the same plane as the spools on the adaptors, and a snapshot is taken. The calibration ruler (Fig. 3.11a) is a scaling and verification device with set marked distances. This photo is the basis for calibration for that day's testing. Once the photo is taken, the camera system must not be moved or disturbed; otherwise, the process must be repeated. The black and white marker's diameter, acting as a known reference dimension, is measured using the video analysis software Tracker Video Analysis and Modeling Tool by measuring the scaling and verification device. There is a USB camera (MER2-630-60U3M, Daheng Imaging, Beijing, China) equipped with a 25 mm focal length lens with a tripod set up to capture video of every test, and this video data is used to measure the diameter of the markers and the diameter of the strands before the test begins. The diameter of the strands is used to calculate the CSA, which is later used to calculate stress.



(a) Schematic of calibration ruler with known set distances.



(b) Calibration ruler used in testing. The ruler was cut, and only one-half was used.

The tests are conducted in a water bath, and to minimize any error that may occur from refraction, the marker is measured again when under the solution, and that dimension is compared to the reference dimension. The strands are measured, and the value of one of the strands' diameter is calculated, which is the value used in Eqn. 3.1 to calculate the CSA.

Fig. 3.12a and 3.12b show an example of the reference dimension on the calibration, and Fig. 3.12c and 3.12d show an example of measuring one of the strands prior to mechanical testing.

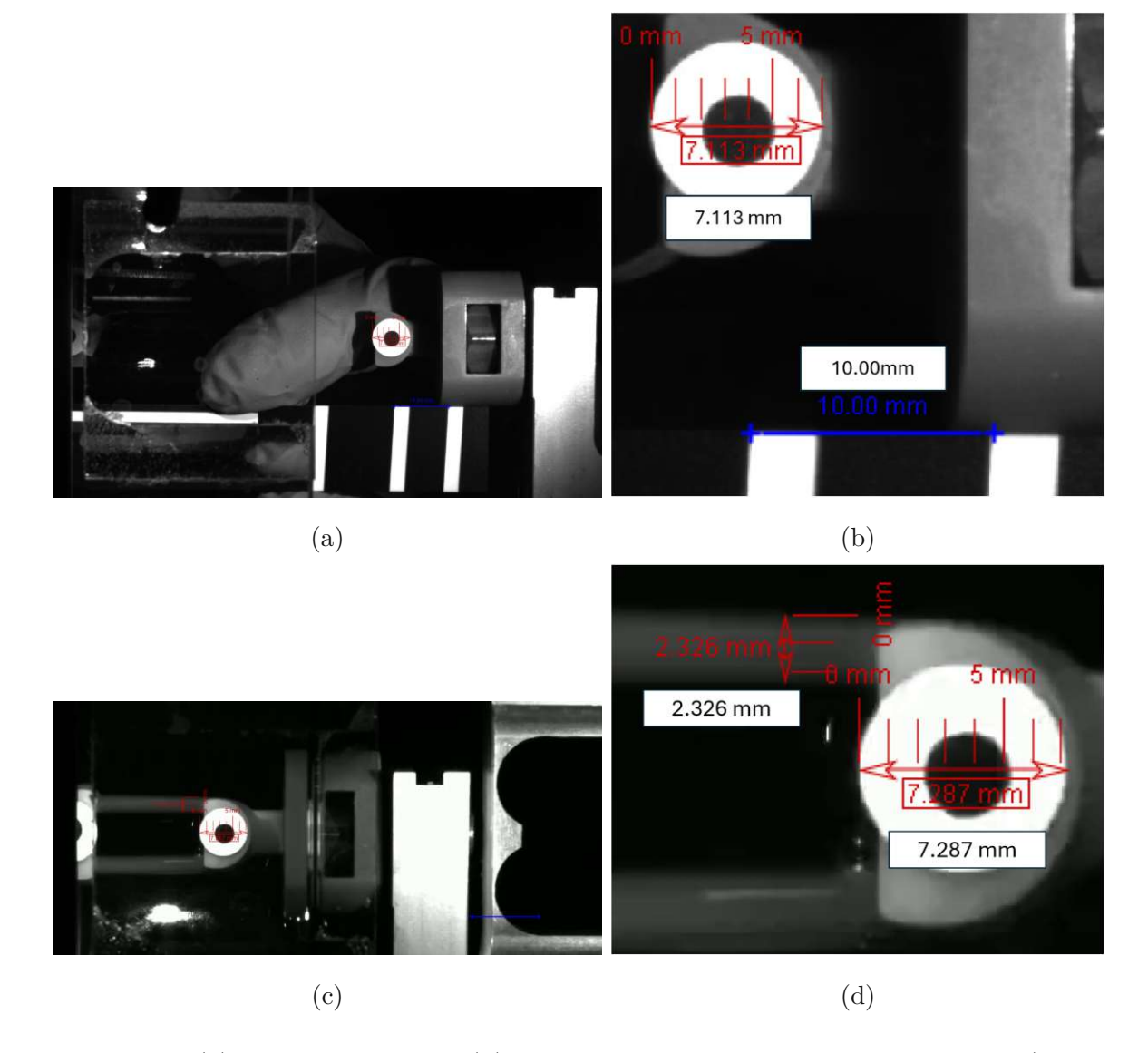


Figure 3.12.: (a) Initial calibration, (b) Zoomed-in photo of the initial calibration (in blue, 10.00mm reference dimension) to see the initial measurement of the marker (in red, 7.113mm), (c) Example of measuring a strand, (d) Zoomed-in photo of measuring the marker again (as it is under the PBS solution) and one of the strands to get the diameter of the strand)

In this example, a proportion (Eqn. 3.2) is set up to calculate the actual value of the diameter of the strand, as seen:

$$\frac{d}{ReferenceMarkerDim} = \frac{StrandDimUnderSolution}{MarkerDimUnderSolution}$$
 (3.2)

The reference marker dimension is 7.113 mm, which is the dimension from the calibration photo (Fig. 3.12b). The strand dimension under the solution is 2.326 mm, and the marker dimension under the solution is 7.287 mm (Fig. 3.12d). These values are plugged into the equation:

$$\frac{d}{7.113} = \frac{2.326}{7.287} \tag{3.3}$$

The actual value of the diameter based on the above is d = 2.27 mm. This value from Eqn. 3.3 is the input for Eqn. 3.1 and the corresponding CSA is used in calculating stress.

After calibration, the starting point for the tests needs to be set. The total length of the ring is 3 cm. Using a custom-made measurement block from heavy-weight cardstock, the block sits on the lower adaptor's top face (where the half-spool rises from); the upper adaptor is lowered until the bottom face of the upper adapter reaches the block. This sets the height between the upper adapter half-spool and the lower adapter half-spool to ensure that the length of the ring is 3 cm. This value can be saved in the load frame software as the zero position and used for all the tests that day. Fig. 3.13 illustrates this procedure.



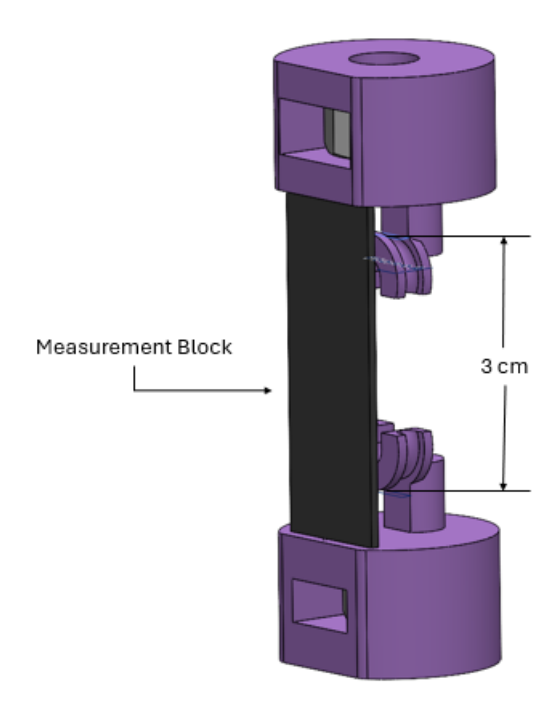


Figure 3.13.: The heavyweight cardstock piece is placed on the lower adapter. The upper adapter is lowered until the spool-side face contacts the measurement block (cardstock). This sets the starting distance and can be saved in the software as the zero position. This ensures that the length of the ring, when placed on the spools, is 3 cm.

38

Once the starting point is set, the water bath is installed. The water bath is installed after the calibration photos because there is limited space between the wall of the water bath and the adaptors. The water bath is filled with 400 mL of PBS and contains 100 μL of household dishwashing liquid concentrate. The dishwashing liquid concentrate is added to reduce surface tension effects between the adaptor and solution that may affect loading measurements.

The ring may be installed at this point, and testing can begin. To install the ring, the upper adaptor is raised until the upper spool is out of the solution. After hooking the ring over the spool, the piston is lowered until the bottom of the ring is below the lower adaptor spool. The lower portion of the ring is hooked below, hanging freely at this point, on the lower adaptor. The upper adaptor is raised to the starting point. Preloading the fibrin rings was impossible because the experiments operated at the lowest range of the load cell's capabilities. For example, the greatest load the rings experienced was 0.27 N; any attempt to preload the rings resulted in the rings relaxing and becoming slack.

Cyclic Loading

As mentioned in Chapter 1.2, this work seeks to identify the stresses occurring within the Magne Tissue bioreactor during mechanical stimulation of cell-seeded samples. One of the protocols used for tendon constructs within the bioreactor is cyclic loading, which is a way to stimulate the cells embedded in fibrin rings mechanically. The loading starts at 0%strain, then goes to 10% strain over one second, and then back to 0% strain over another second (10% strain applied at 0.5 Hz). With a period of two seconds, the MagneTissue bioreactor goes through this cyclic loading for six hours. After 18 hours of resting, in which only 3\% strain is applied at 0.5 Hz, the process repeats, but instead of going to 10% strain, the constructs are stretched to 12% strain. After six hours, there is another 18 hours of rest. Following the 18 hours of rest, the constructs are stretched to 14% strain. This process repeats every 2\% strain until the constructs are stretched to 20\% strain. Fig. 3.14 illustrates the protocol.

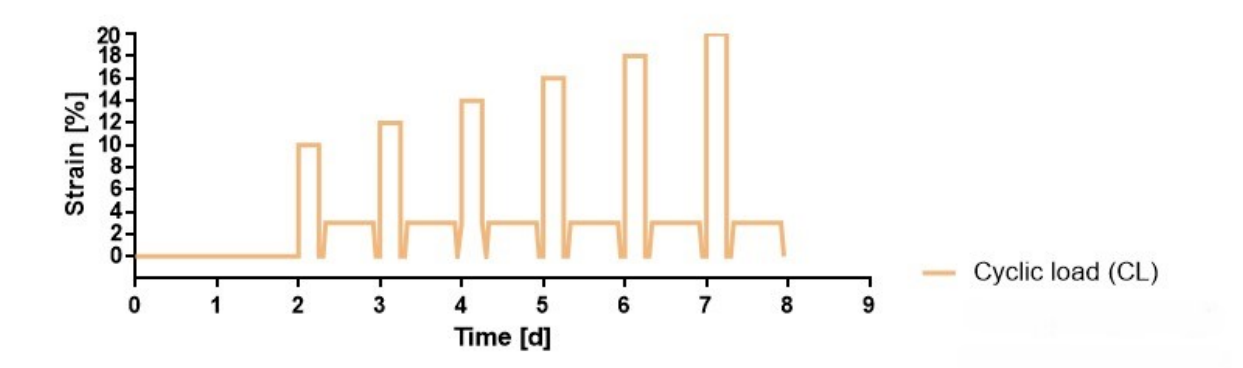


Figure 3.14.: Figure from Ekaterina Oleinik, M.Sc., a PhD student in the Institute of Lightweight Design and Structural Biomechanics. One of the protocols where initially 10% strain is applied for 6 hours per day at 0.5 Hz, then 3% strain at 0.5 Hz for 18 hours per day. After each resting phase, the cyclic load for the 6 hour phase increases by 2\%, up to 20\% by day 7.

Due to time limitations, running the load frame for six hours at a time was not feasible. Instead, a 30-minute cyclic loading test is conducted at 10% strain to identify the initial stresses the cells experience at the start of stimulation in the MagneTissue bioreactor. In addition, a separate group of fibrin rings is tested at 20% strain to understand the potential maximum stress the cells may experience.

Fig. 3.15 shows the 20% testing profile for the first 25 seconds of testing. There is a onesecond ramp-up to the set maximum strain, which is held for one second. This plateau hold was deliberately inserted due to a limitation of the load cell used. The forces that the load cell reads during these tests are at the lower end of the load cell's capabilities, so whenever the piston moves up or down, the load cell picks up the movement, resulting in magnitudes of noise that cannot be filtered out. The plateaus allow the forces to stabilize, providing a moment for the data to be analyzed. After the hold, there is a one-second ramp down, followed by another hold. This process repeats for 30 minutes. Data points were sampled at 10 Hz frequency.

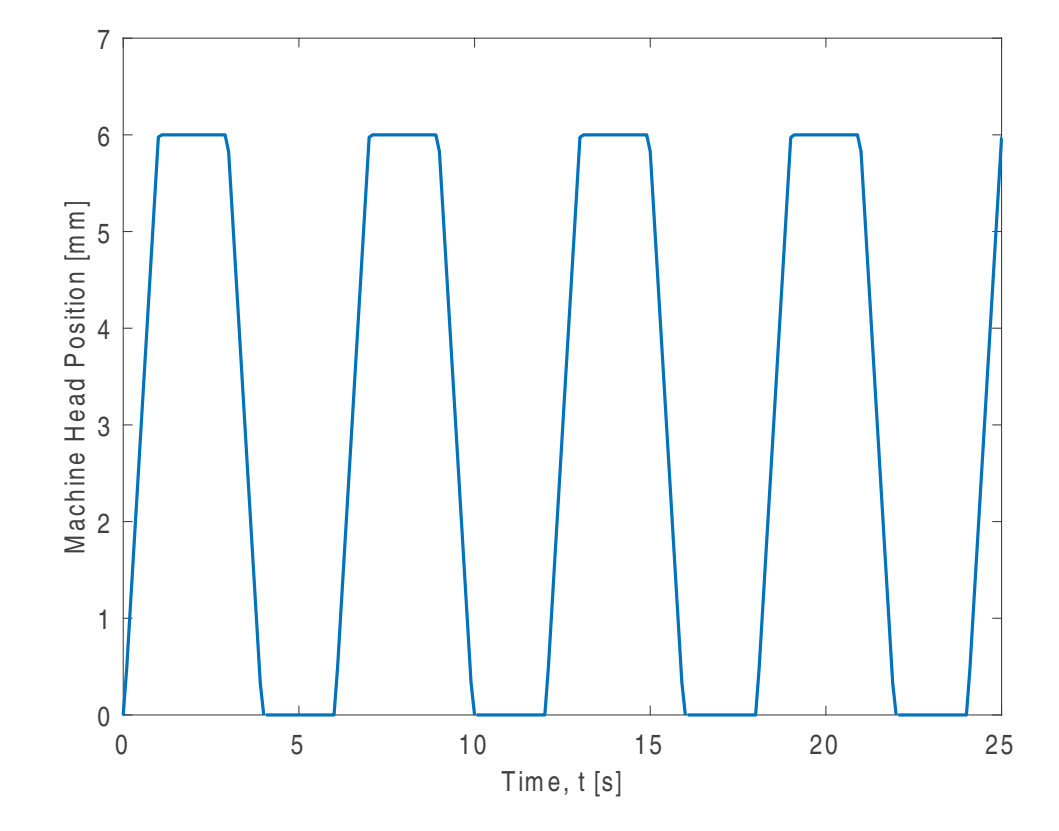


Figure 3.15.: Displacement profile for the 20% Strain, Cyclic Test. Over one second, the machine head displaces 6 mm, holds for two seconds, and then, over one second, goes to 0 mm displacement.

3. Methodology

Since the test starts with the rings at an initial length of 3 cm, to achieve 10% strain, the machine head moves up 3 mm. Similarly, to achieve 20% strain, the machine head moves up 6 mm, as seen in Fig. 3.15.

Stress Relaxation

The second test conducted is stress relaxation. During the 30-minute cyclic test, there is some expectation known from experiments in the bioreactor that as the fibrin ring is being loaded and unloaded repeatedly, there will be some relaxation or stretching. Stress relaxation is conducted to compare to the cyclic loading results. Fig. 3.16 shows the 10% testing profile. Like with the cyclic loading testing, there is a one-second ramp-up. However, the ramp-up is followed by a five-minute hold during which stress can relax.

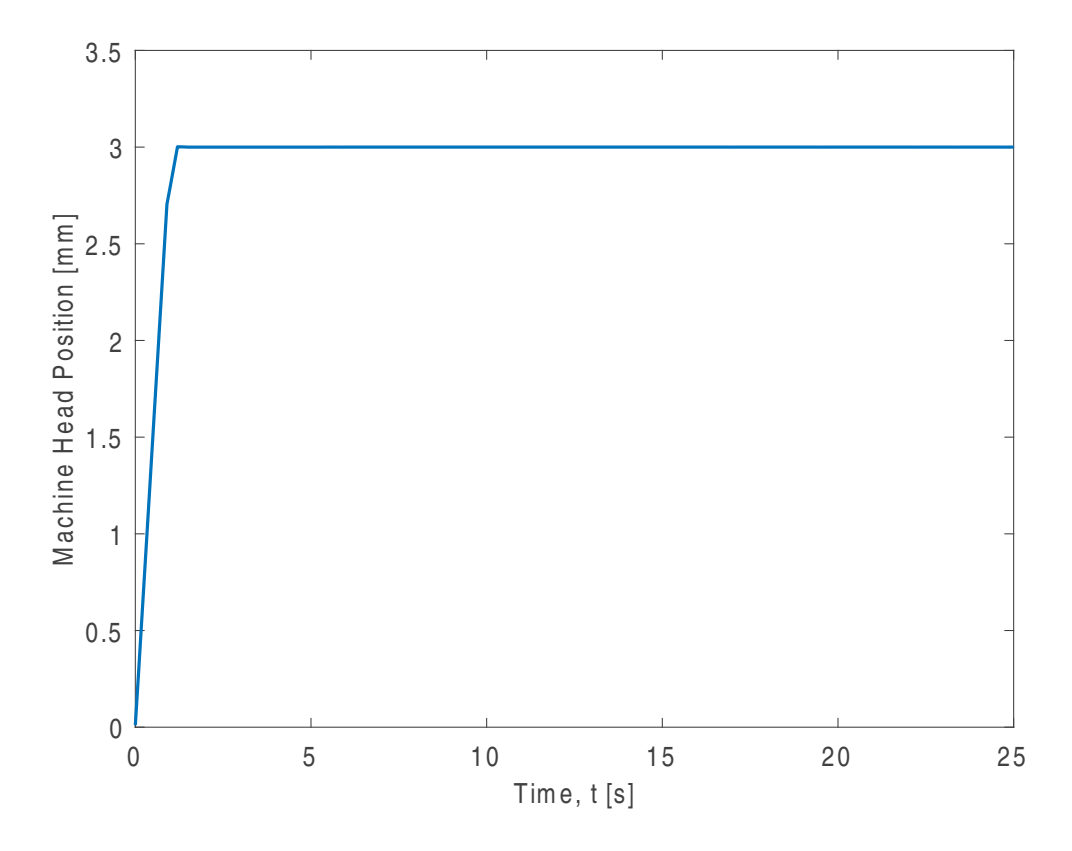


Figure 3.16.: Displacement profile for the 10% Strain, Stress Relaxation Test. Over one second, the machine head displaces to 3 mm, which stays there for the test duration.

Post-Test

Following the end of either cyclic loading or stress relaxation, the fibrin ring is removed and disposed of according to laboratory practices. Likewise, the PBS solution is emptied. The load cell is removed, the upper adaptor is removed from the load cell, and the lower adaptor is removed from the test stand. Both adaptors are cleaned following laboratory practices.

3.2.5. Data Processing

This section details how the results are processed from the mechanical cyclic loading and stress relaxation tests.

Both the cyclic loading and stress relaxation testing utilize two different strains: 10% and 20%. Two groups of rings are tested at 10% strain: rings (1) with cells that had a culture period of two days and (2) cell-free rings. Three different groups of rings have 20% strain applied: rings (1) with cells cultured for two days, (2) with cells cultured for nine days, and (3) cell-free rings.

In the figure legends, "2-cell" refers to groups of fibrin rings cultured for two days, while "9-cell" refers to fibrin rings cultured for nine days. Data was processed using Matlab (Matlab, 2024a, MathWorks, Inc., Natick, Massachusetts, USA).

3.2.6. Cyclic Loading Data Processing

The following example illustrates the data processing steps, consistently applied to all cyclic loading experiments. In the initial observation of Fig. 3.17, it is evident that the data exhibits oscillations and artifacts from testing. The sensitivity of the load cell causes noisy data because the load cell operates near its lower limit and thus causes oscillating waves around the stress value whenever the machine's head moves up or down due to friction within the actuator. Hence, plateaus are incorporated to assist in stabilizing the readings and act as noise reduction.

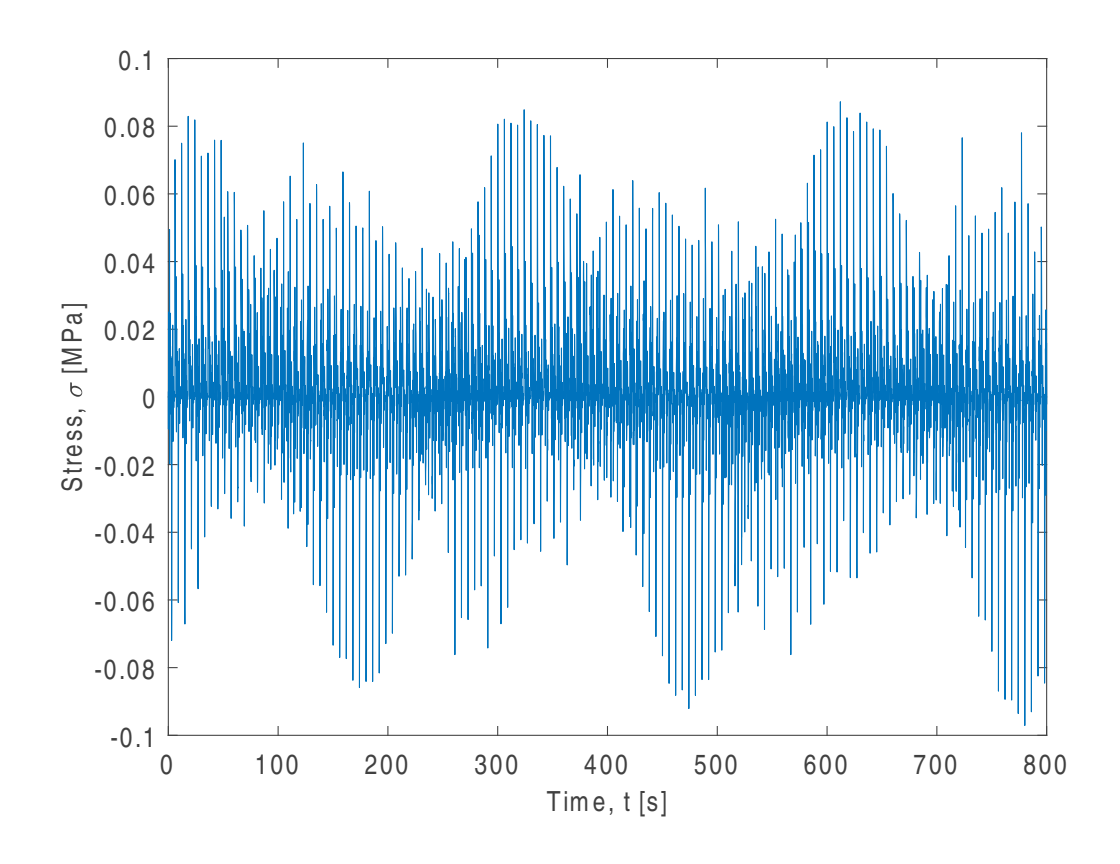


Figure 3.17.: Raw data from the first trial of the 2-cell group, 20% strain from the cyclic loading test. Due to the load cell operating near its lower limit and the soft, low-stiffness nature of the rings, force oscillations are generated whenever the machine head moves up or down, resembling the behavior of an underdamped system.

Fig. 3.18 shows a zoomed-in view of Fig. 3.17, with the positional data on top. This zoomed-in view shows the data oscillating around some upper value due to the 2-second upper plateau hold, then oscillating around zero due to the 2-second lower plateau hold. This figure also shows that the largest spikes occur when the head ramps up or down.

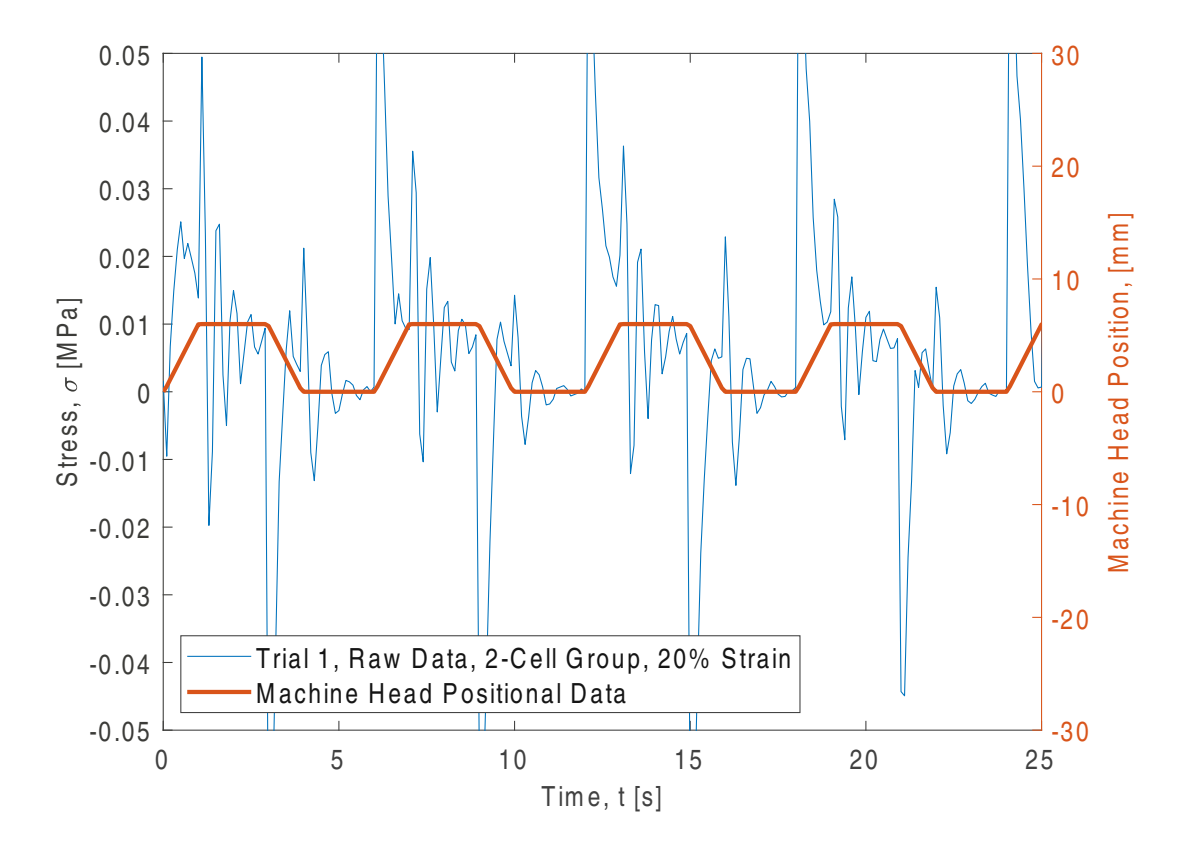


Figure 3.18.: Raw data from the first trial of the 2-cell group, 20% strain, from the cyclic loading test, and the positional data from the head of the loading frame. At any given plateau region, there is the characteristic behavior of an underdamped system, where the waveform oscillates around some value with decreasing amplitude over time. The largest spikes in the data occur whenever the machine head moves up or down.

The areas of interest are the plateau regions, especially the upper ones. The upper regions are of interest because they represent where the fibrin ring is held at the respective strain value. This upper region is the data that can be compared to the stress relaxation data. The plateau data can be cleaned up further by isolating those segments as seen in Fig. 3.19.

This data is still noisy, but it can be cleaned up further by:

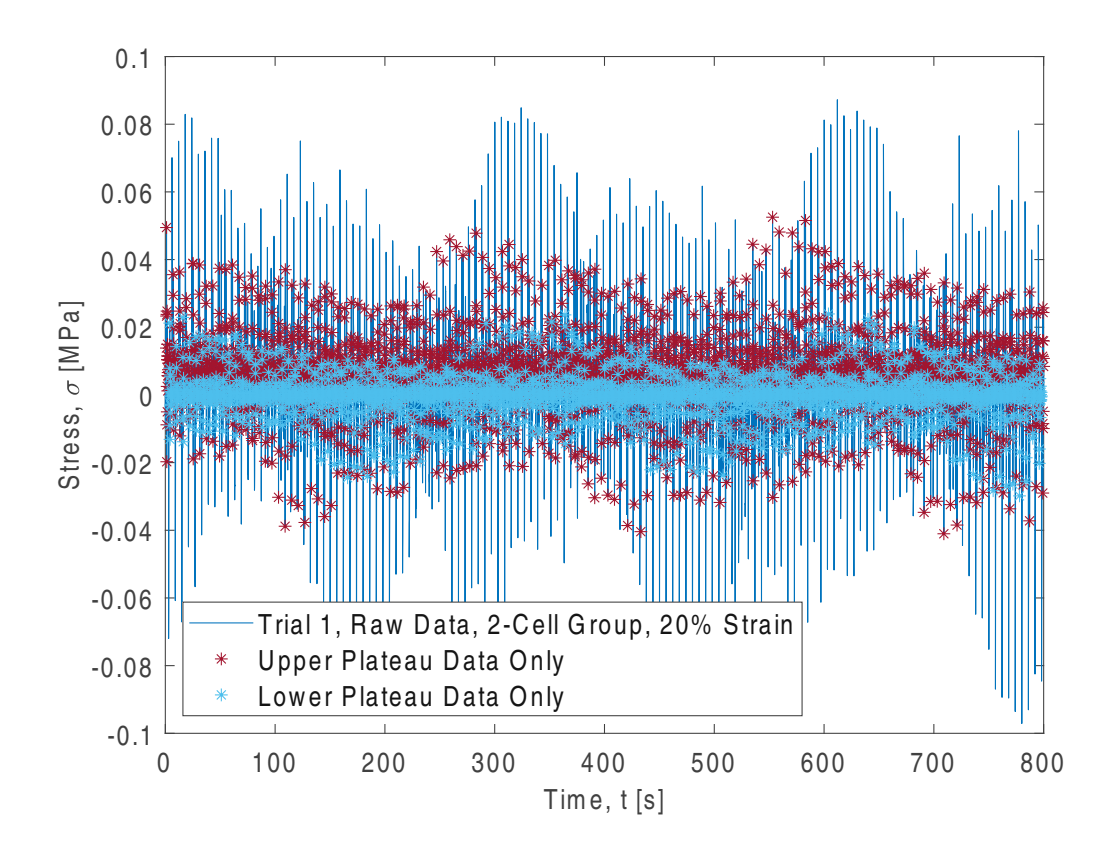


Figure 3.19.: Upper and lower plateau data, with maroon representing only the upper plateau data and light blue representing only the lower plateau segments. In this view, there is a band of data for the lower plateau and an upper band for the upper plateau. The next steps in data processing involve smoothing the noisy data to isolate the realistic values.

- 1. Running the upper plateau data through a moving median with a window size of 900 and then
- 2. Taking that smoothed data and rerunning it through a moving mean with a window size of 450

Fig. 3.20 shows the upper and lower plateau data results after smoothing individually. The upper plateau data represents the state when the machine head is holding the sample at 20% strain, while the lower plateau data corresponds to when the sample is held at 0%strain.

There should be no stress on the sample at 0% strain. However, even at 0% strain, the recorded force often oscillates around zero, resulting in a non-zero value during testing because the machine may not zero out perfectly at the start of the test. This is another limitation of the test setup. The force results recorded are on the lower end of the load cell's working range, and without the ability to preload the samples, the recorded force at 0\% strain oscillates around zero. A non-perfect zeroing of the test leads to recording a small non-zero force when the sample is at zero 0% strain during the test. The average value of the lower plateau data is calculated to address this issue. If this average is greater than zero, the entire data set (both upper and lower plateaus) is adjusted downward so that the lower plateau values average zero. Conversely, if the average value of the lower plateau data is below zero, the entire data set is adjusted upward by the corresponding offset. Fig. 3.20 considers the offset, and the data is adjusted accordingly. However, the data still contains segments due to the removed ramp sections.

The next step is to remove the segmentation and adjust the time scale, resulting in continuous data, as shown in Fig. 3.21.

The upper plateau data are now in a form that allows comparisons to the stress relaxation data found in Section 4.3. The next step is to normalize the smoothed data. This process is also done for stress relaxation and serves as another comparison; every stress value (σ_i) is divided by the maximum stress value (σ_{max}) as seen in Eqn. 3.4:

$$\sigma_i^* = \frac{\sigma_i}{\sigma_{max}} \tag{3.4}$$

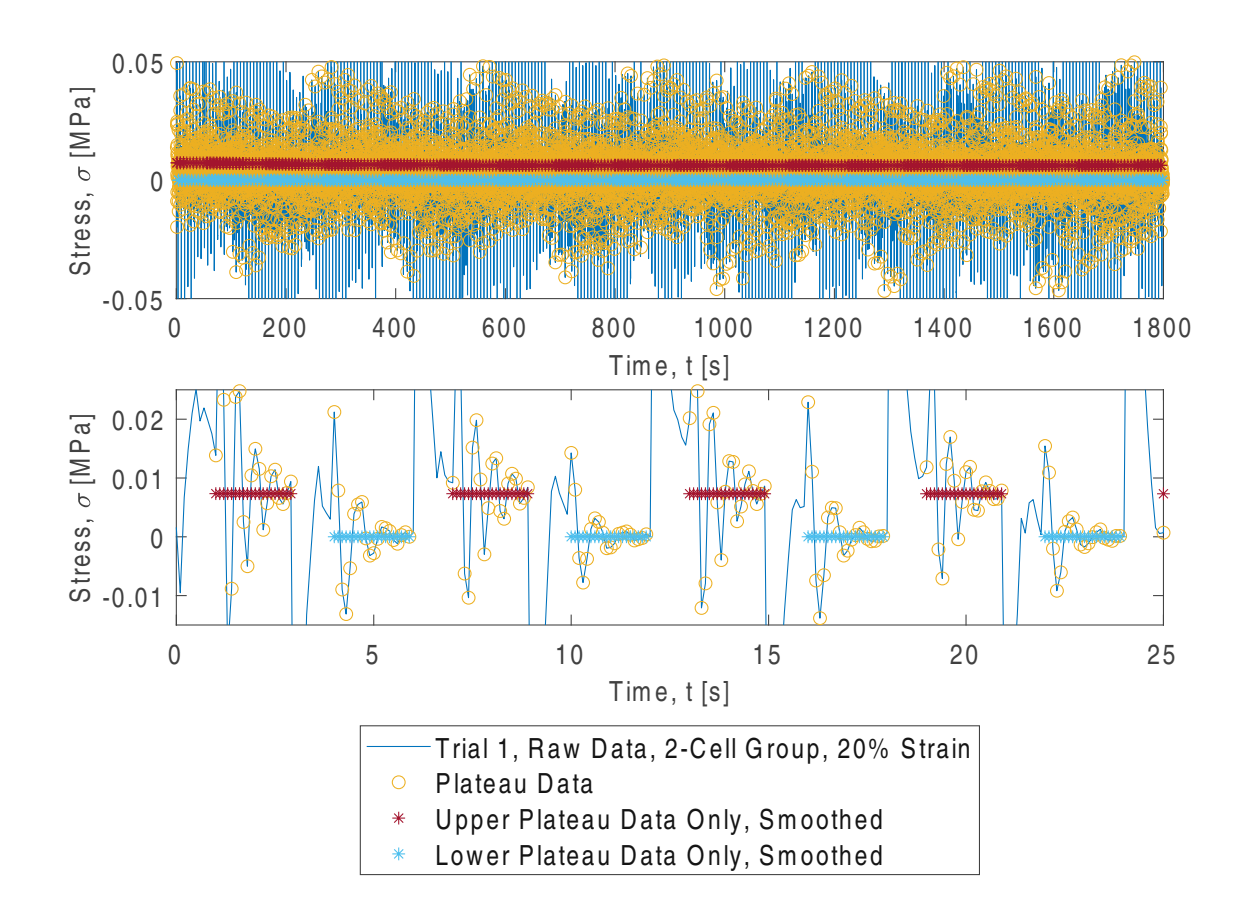


Figure 3.20.: The upper and lower graphs display the same data, with differences in time scale (x-axis) and magnitude of stress (y-axis). The solid blue line represents the raw data from the first trial of the 2-cell group at 20% strain from the cyclic loading test. The yellow scatter indicates the upper and lower plateau data segments before processing with the moving median and mean. The maroon scatter represents the smoothed upper plateau data, while the light blue scatter represents the smoothed lower plateau data. The lower graph shows the oscillation of the raw data around the smoothed upper and lower plateau segments, where average values of the lower plateau data have been adjusted to 0 N, and the upper and lower plateau data have been shifted accordingly.

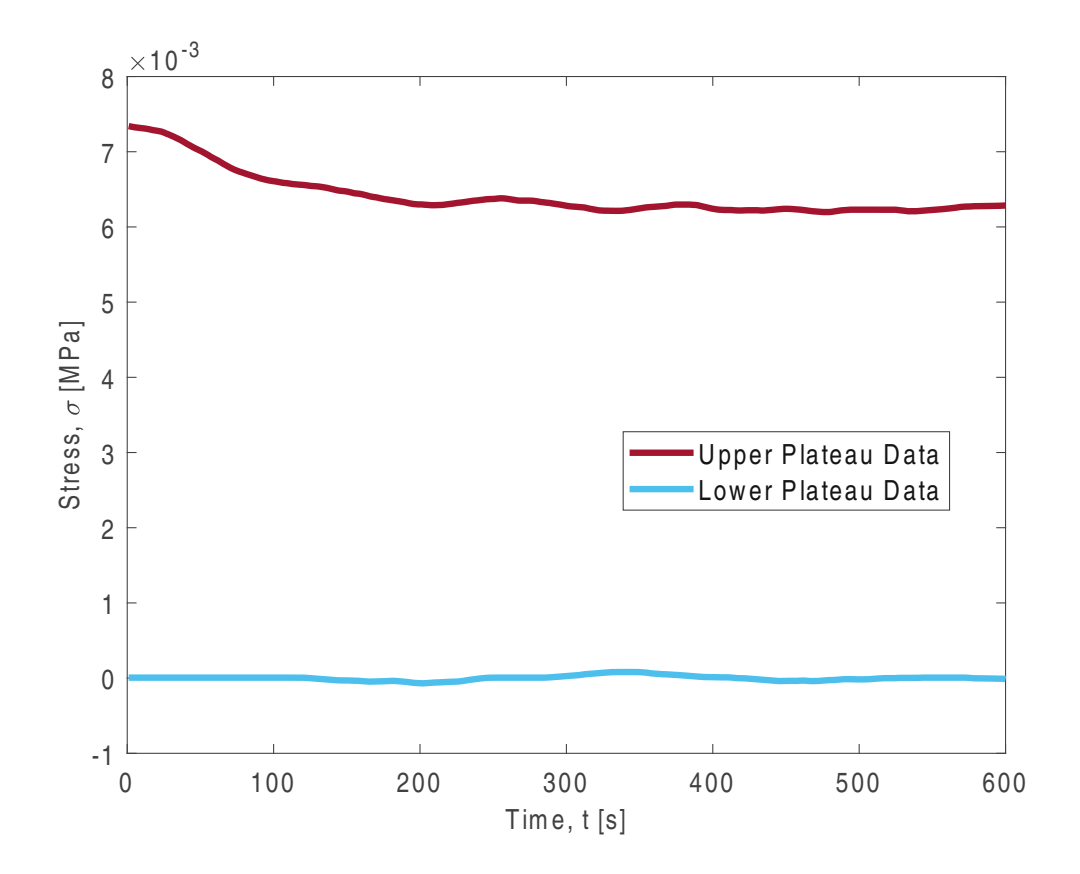


Figure 3.21.: Stitched upper and lower plateau data from the processed results of the first trial from the 2-cell group at 20% strain from the cyclic loading test. This figure eliminates any gaps between the plateaus in the upper and lower regions to present a continuous data line. All data have been adjusted such that the light blue lower plateau data line averages zero.

3. Methodology

Where the normalized stress, σ^* , is dimensionless. Normalizing the data allows for comparing different trials across different data groups and gives a sense of the shape of the curves and how they stack up to one another. It indicates whether the trials and groups are relaxing at similar rates. Normalizing the data also relates the final data point to the maximum data point. In the case of this data, the maximum data point should also correspond to the initial data point, as from that point onwards, the fibrin ring undergoes relaxation, and the corresponding stress decreases.

The last data processing step applies a three-term Prony series to the normalized data. Fig. 3.22 results from the normalization and fitting. The figure shows the Prony series curve fit overlaid the normalized data. The curve fit has an R^2 value of 0.9974.

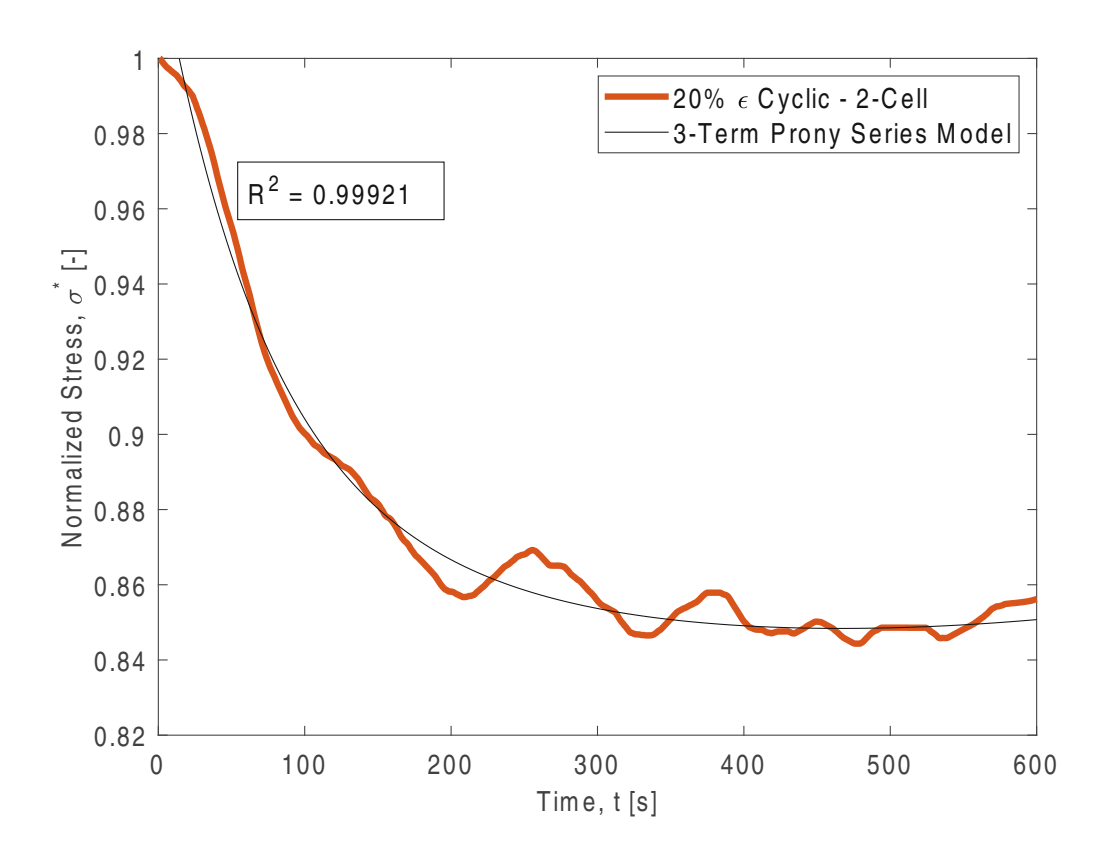


Figure 3.22.: Upper plateau data after normalization (orange line). The data comes from the first trial from the 2-cell group at 20% strain from the cyclic loading test. The black line is the 3-term Prony series model ($R^2=0.99921$). After 600 seconds, the final normalized stress value is 0.8563 [-]. This value can also be expressed as the final stress being 85.63% of the initial stress. The threetime constant (τ) values are: $\tau_1 = 72.7s$, $\tau_2 = 1000.0s$, and $\tau_3 = 5207.6s$.

Time constants, extracted from the Prony series model, allow comparisons between the different groups. While a three-term Prony series is fitted to the normalized data, the first two time constants are constrained to the order of 10 seconds and 100 seconds, respectively. These two-time constants are later used in the analysis. The third time constant, approximately 1000 seconds, is included solely for model convergence. It is excluded from the analysis because the data spans from 0 to 600 seconds, and extending the projection into the 1000-second range would be purely speculative. In addition, after finding the third time constant, the series can be refit with two parameters where the starting parameters are the parameters found from the three-term fit.

3.2.7. Stress Relaxation Data Processing

This section outlines the raw data processing from trial one of the no-cell group subjected to a 10% strain hold after the ramp-up period. Fig. 3.23 shows the raw data.

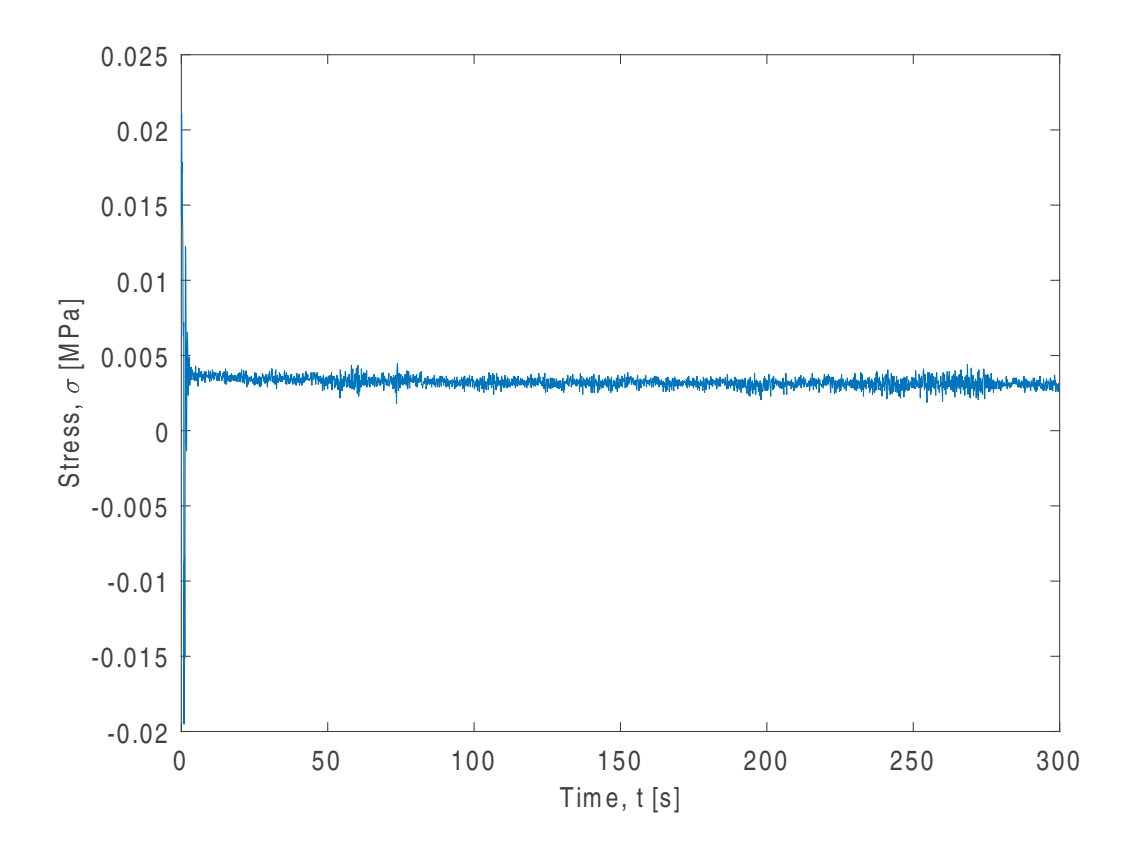


Figure 3.23.: Raw data from the first trial of the cell-free group, stress relaxation test at 10% strain. As with the cyclic loading, on the initial one-second ramp-up to the holding strain level, there are large oscillations in the data before the amplitude rapidly decreases. The stress relaxation test runs for 300 seconds.

As seen from Fig. 3.23, in the first few seconds of the test, there are large peaks followed by the data oscillating around a variable stress value.

Fig. 3.24 shows the same data but with y-axis limits from 0 MPa to 0.005 MPa (5 kPa). In this zoomed-in view, the raw data trends toward decreasing MPa while oscillating around variable stress values.

Denoising the data occurs in three steps:

1. Run the data through a lowpass filter with a cutoff frequency of 0.001 Hz



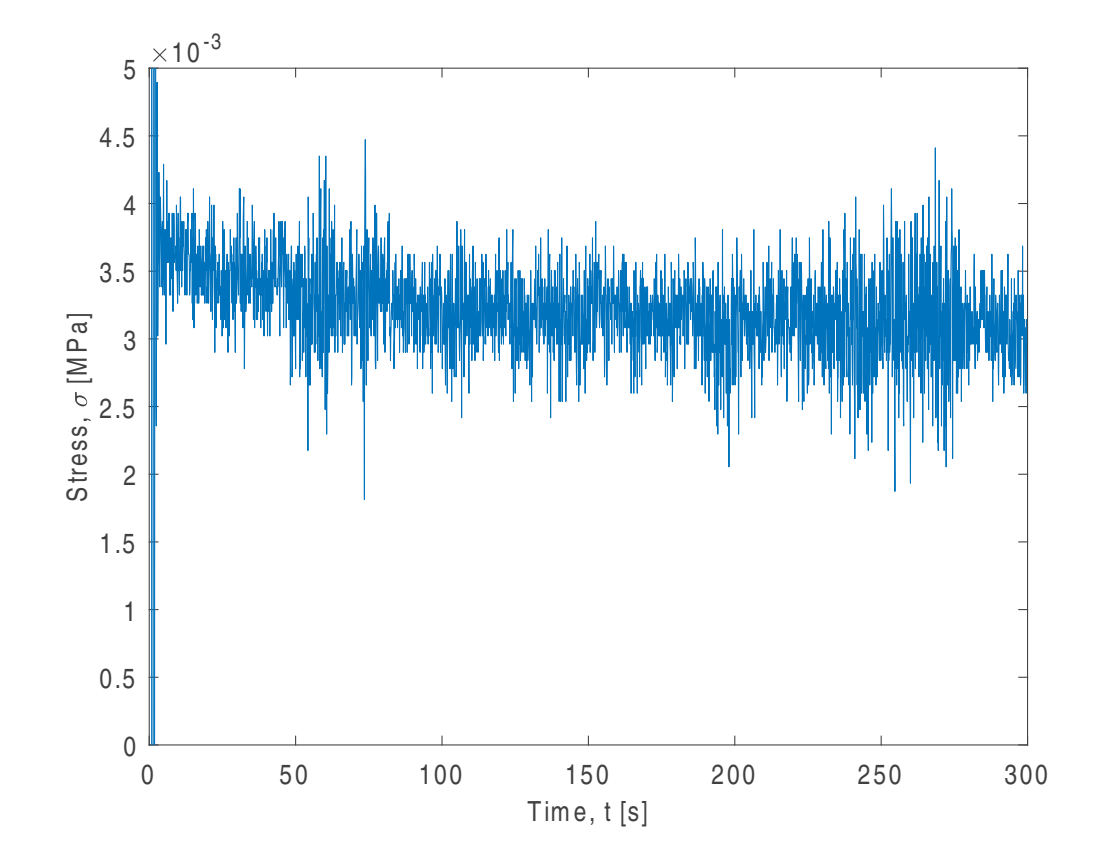


Figure 3.24.: Zoomed-in view of the raw data from the first trial of the cell-free group, 10% strain from the stress relaxation test. This figure shows the waveform oscillating around decreasing stress values.

3. Methodology

- 2. Smooth the data by running the filtered data through a moving median with a window size of 200
- 3. Take that smoothed data and further smooth it by running it through a moving mean with a window size of 200

Like processing the cyclic loading data, other methods and different moving window sizes were tried for processing these data sets. The abovementioned ones worked best for the stress relaxation data sets. Furthermore, the data starts not at 0 seconds but after 1 second to exclude any noise from the ramp-up over 1 second. As seen with cyclic loading testing, moving the head up or down generates noise. To reduce the influence of the noise on the data, the data begins after the machine head stops after reaching the test strain. Similar to the cyclic loading scenario, the force oscillates around zero before the test begins, and the ring is placed on the test stand. In cyclic loading data processing, this is addressed by averaging the lower plateau data and adjusting the plateaus accordingly. This way of offsetting is not an option for stress relaxation testing because, after the rampup, the machine head is held at the testing strain. The average stress relaxation curves are adjusted to address this issue so that the initial stress aligns with the corresponding cyclic loading test. The initial ramp-up time is one second, which is the same ramp-up time for the first cycle of the cyclic loading test.

Similarly to the cyclic test, the data was normalized and fit with a Prony series in the same manner.

Fig. 3.25 shows the filtering results and smoothing of the data on top of the raw data. Fig. 3.26 shows the Prony series curve fit overlaid the normalized, smoothed, and filtered data. The curve fit has an R^2 value of 0.98662.

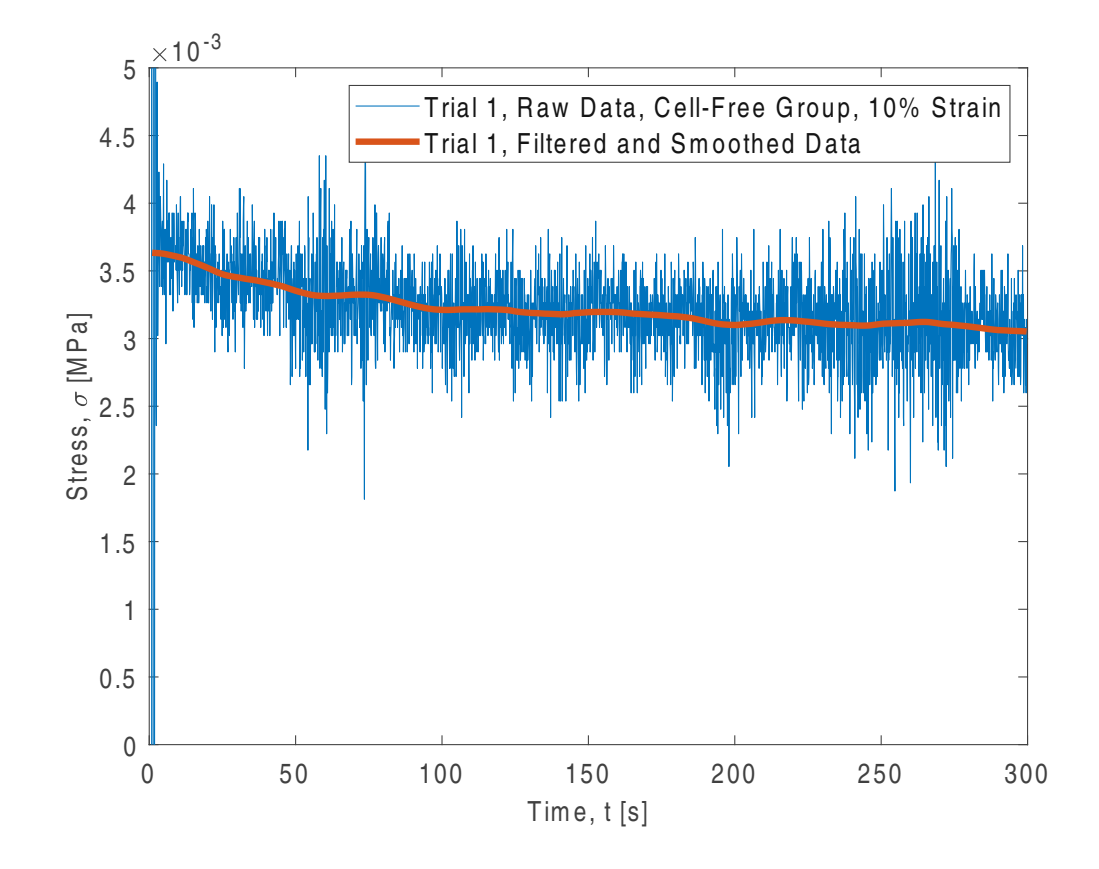


Figure 3.25.: The blue line represents the raw data from the first trial of the cell-free group at 10% strain from the stress relaxation test. The orange line represents the smoothed data after it passed through a lowpass filter with a cutoff of 0.001 Hz and subsequent smoothing through a moving median and average.

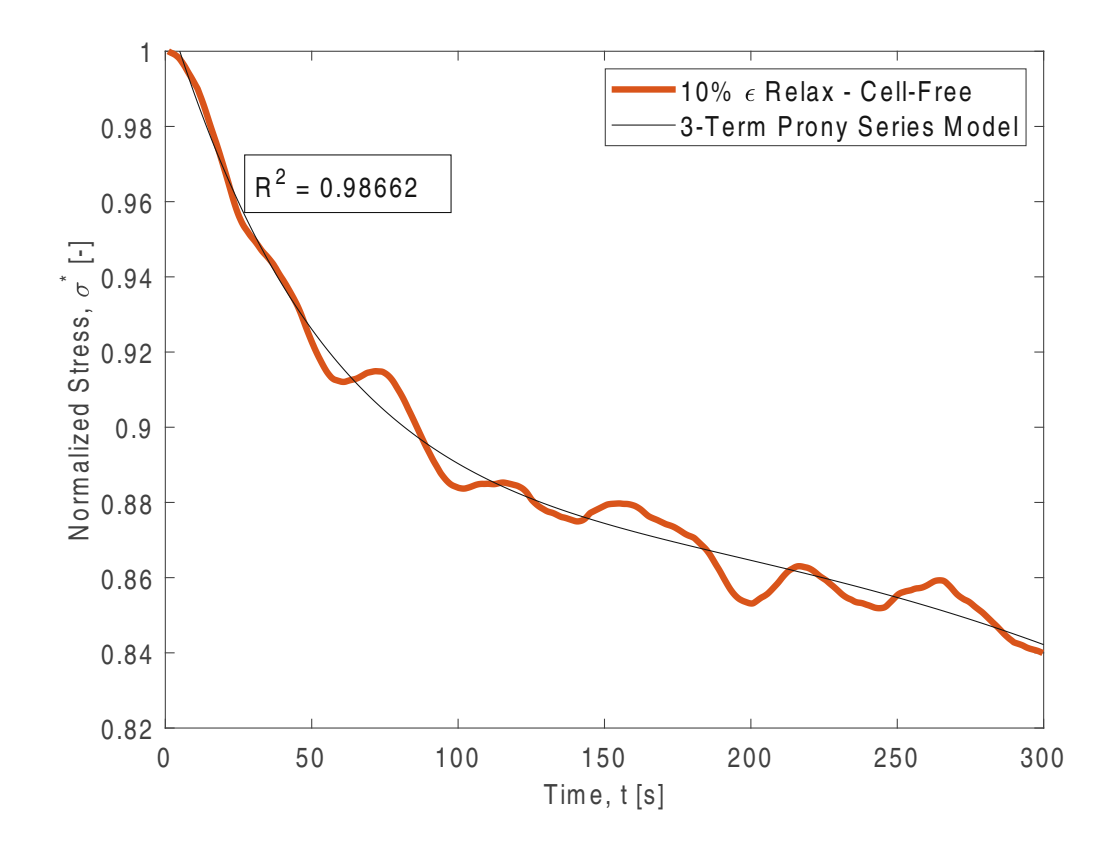


Figure 3.26.: The orange line is the normalization of the data from the first trial from the cell-free group at 10% from the stress relaxation test. The black line is the 3-term Prony series model that fits the normalized data with an \mathbb{R}^2 value of 0.98662. After 300 seconds, the final normalized stress value is 0.84 [-]. This value can be expressed as the final stress being 84.0% of the initial stress. The three-time constant (τ) values are: $\tau_1 = 64s$, $\tau_2 = 251s$ and $\tau_3 = 2050s$. Like with the cyclic loading testing, the τ_3 value is excluded from analysis because the data is only from 0 seconds to 300 seconds, but τ_3 is included for model convergence purposes.

3.2.8. Instantaneous and Equilibrium Moduli

The instantaneous moduli were calculated by taking the initial stress (σ_0) and dividing it by the strain (ϵ_0) . The equilibrium moduli were calculated by taking the last stress value (σ_{∞}) and dividing it by the strain (ϵ_0) .

3.2.9. Statistical Analysis

All groups had N=3 samples per group, except for the 10\% strain, cyclic, cell-free group and the 20% strain, cyclic, cell 9-day culture group, which had N=2 samples each. The groups with N=2 samples were excluded from direct comparisons to other groups due to sample size. All data was presented as mean + standard deviation (S.D.) for stress vs. time curves, except for the normalized data graphs. Both types of graphs were done in Matlab. The instantaneous and equilibrium moduli were plots as boxplots with the median and interquartile range. Fig. 4.17 and Fig. 4.19 were done in Matlab. Fig. 4.18 and Fig. 4.20 were done in GraphPad Prism Software (GraphPad Software Inc., San Diego, USA). The bar graphs for the pooled data comparisons were made in GraphPad Prism Software by Ekaterina Oleinik, M.Sc., a PhD student in the Institute of Lightweight Design and Structural Biomechanics, whose help is gratefully acknowledged. Normal distribution of data was tested with Shapiro-Wilk normality test. Comparison between groups was calculated using the Unpaired t-test with Welch's correction or Mann-Whitney Test, and P-values < 0.10 were considered statistically significant. All statistical calculations were performed using GraphPad Prism Software.



Results

4.1. 10% and 20% Cyclic Loading Results

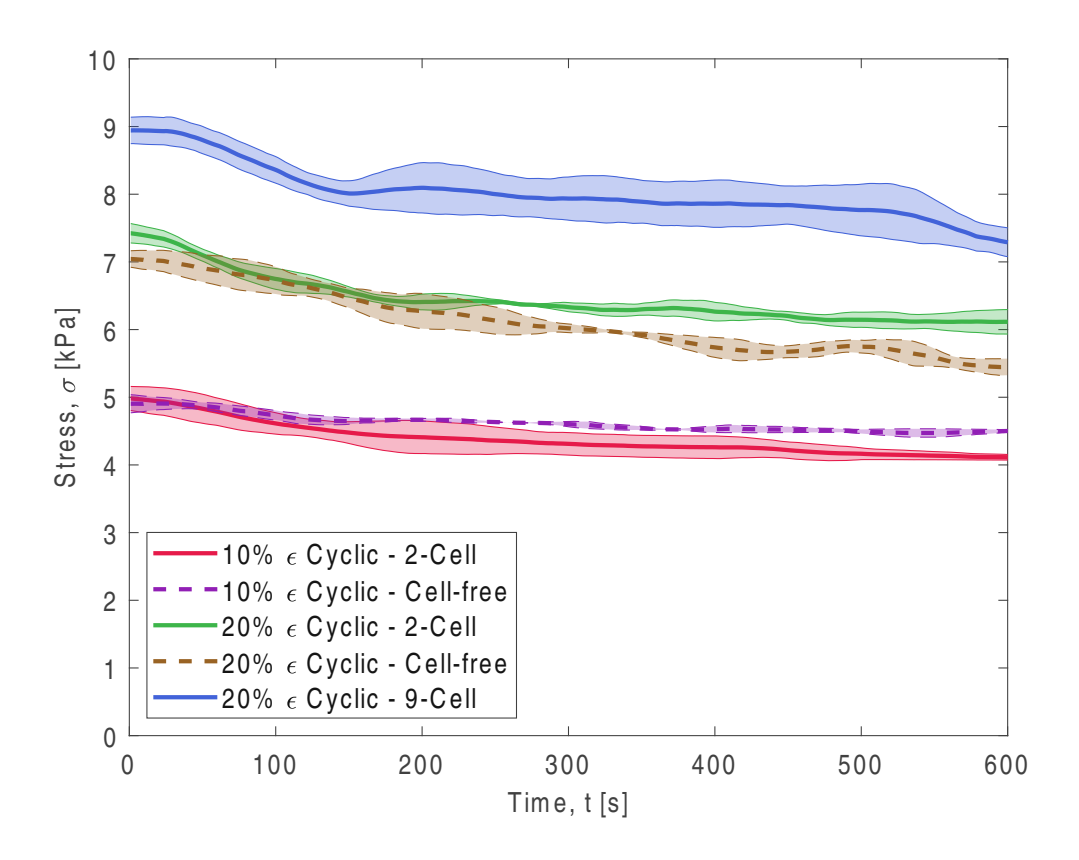


Figure 4.1.: Results of cyclic loading tests. Data is shown as the mean \pm SD. The 9-cell, 20% strain and cell-free, 10% strain groups have N=2 samples. The remaining groups have N=3 samples each. The 9-cell, 20% strain group experiences the greatest stress, followed by the 2-cell, 20% strain, and cell-free, 20% strain groups. Statistical analysis found that the maximum values for the 20% strain, 2-cell vs. the cell-free, are distinct (p-value ≤ 0.1).

Fig. 4.1 shows all the results from the cyclic loading experiments. Data is shown as the mean (solid line) \pm the standard deviation (shaded areas). The maximum and minimum stress values for each group are found in Table 4.1. Due to N=2 samples for the 9-cell, 20\% strain and the cell-free, 10% strain, these groups are excluded from statistical analysis where they are directly compared to other data sets. However, the 10% strain group is included when pooling together all of the 10% data for analysis.

Table 4.1.: Mean maximum and minimum stress values for each group from the cyclic loading testing. Statistical testing results are summarized in (Tables A.1 and A.2)

Group Name	Maximum Stress Value [kPa]	Minimum Stress Value [kPa]
10% ε Cell-free	4.91 ± 0.09	4.47 ± 0.06
10% ε 2-Cell	4.98 ± 0.17	4.11 ± 0.04
20% ε Cell-free	7.04 ± 0.12	5.45 ± 0.12
20% ε 2-Cell	7.42 ± 0.14	6.11 ± 0.18
20% $arepsilon$ 9-Cell	8.94 ± 0.20	7.29 ± 0.21

When testing the maximum data sets for normality, the 10% 2-cell and the 20% cell-free groups are normally distributed, with p-values of 0.5184 and 0.2885, respectively (Shapiro-Wilk). The 20% 2-cell group found a p-value of 0.0061 when testing for normality. When testing the minimum sets for normality, the 10% 2-cell, 20% 2-cell, and the 20% cellfree are all found to be normally distributed with p-values of 0.1012, 0.5536, and 0.7369, respectively.

Table A.1 and A.2 summarize the results of statistical testing performed between the groups for the maximum and minimum values, respectively. When looking at the maximum, significant differences are found between all groups, with p-values less than or equal to 0.10. This suggests that the maximum values for 10% 2-cell, 20% 2-cell, and the 20% cell-free groups are distinct, and in the case of the 20% 2-cell and the 20% cell-free, the presence of cells does have an impact on the maximum stress the constructs experience. Evidence also shows that the 10% 2-cell and the 20% 2-cell are significantly different. This is further tested by pooling the 10% 2-cell and cell-free data (N=5) and the 20% 2-cell and cell-free (N=6). When checking the maximum groups for normality, both groups are normally distributed, with the 10% strain group having a p-value of 0.3794 and the 20% strain group having a p-value of 0.6481. For the minimum groups, the 10% strain group has a p-value of 0.2164, and the 20% strain group has a p-value of 0.4000. The t-test results with Welch's correction find p-values less than 0.001 for both the maximum (Fig. 4.2a and minimum groups (Fig. 4.2b). Significant differences between 10% strain and 20% strain are found for both maximum and minimum values, indicating that the strain significantly affects the constructs' response at different strain levels.

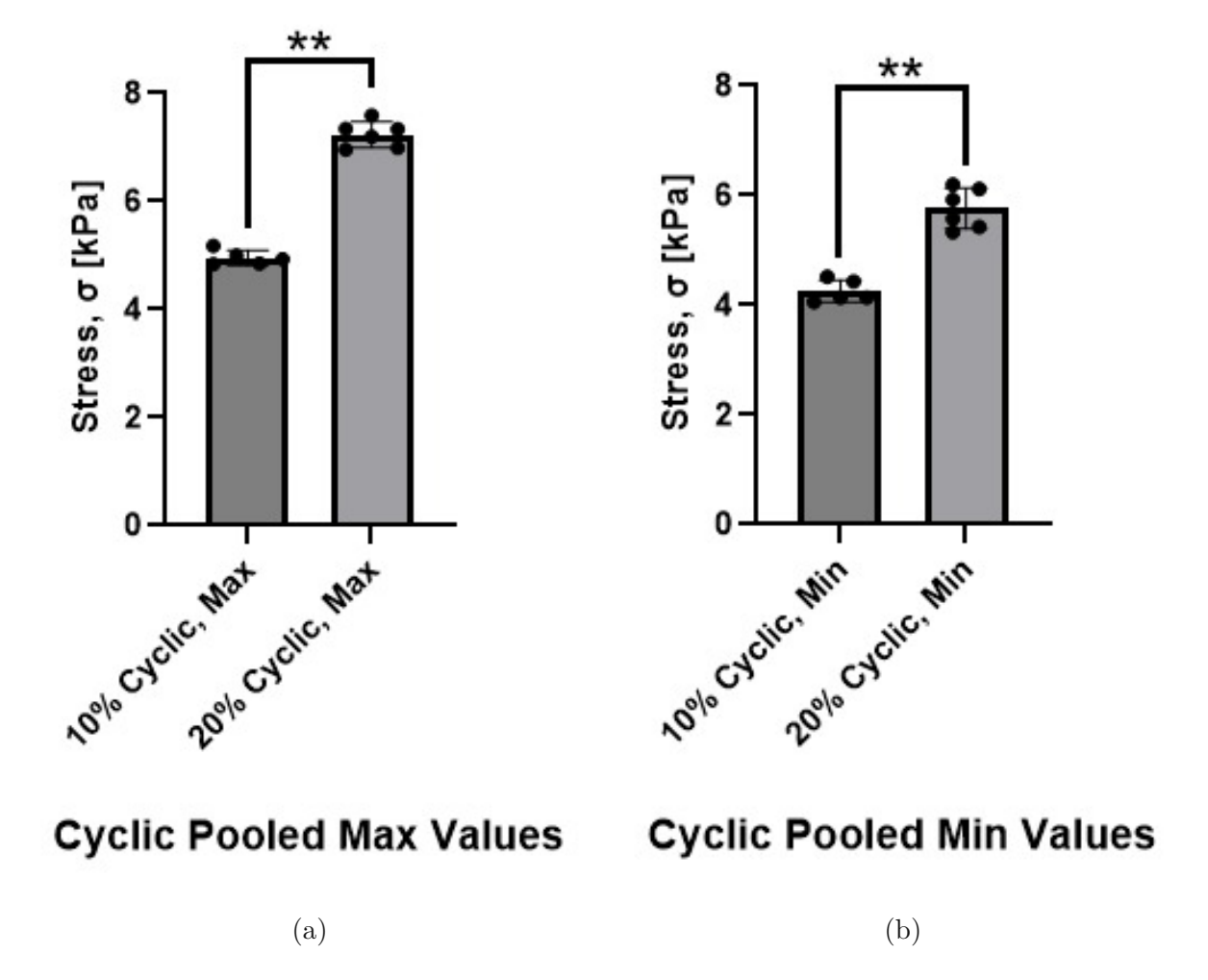


Figure 4.2.: Two asterisks (**) refer to a P-value between 0.01 and 0.001. 10% 2-cell and cell-free data (N=5) was pooled together. 20% 2-cell and cell-free data (N=6) was pooled together. The maximum and the minimum pooled comparisons had p-values less than 0.001.

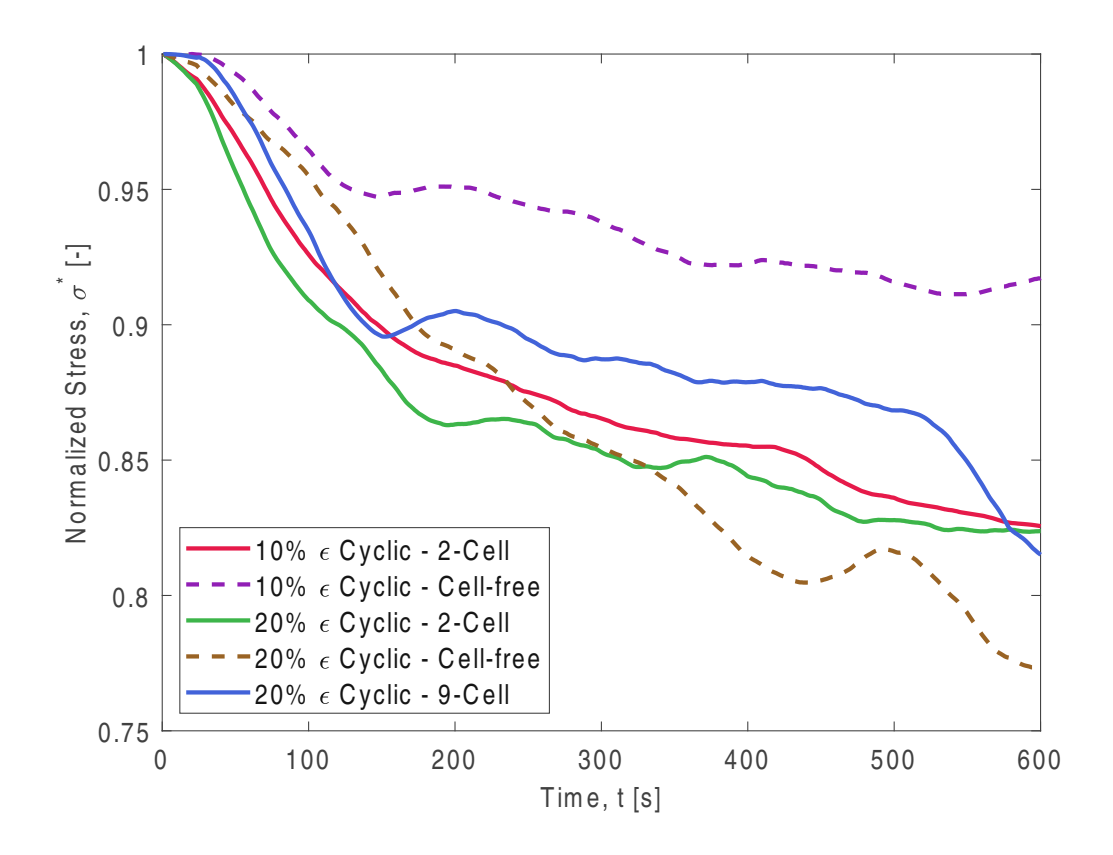


Figure 4.3.: Normalized cyclic loading test results, data shown as mean \pm SD. The 9cell, 20% strain and the cell-free, 10% strain groups have N=2 samples. The remaining groups have N=3 samples each. By the end of the test, the cell-free, 10% group retained the highest percentage of the initial stress, whereas the cell-free, 20% group had the lowest. When pooling together all the 10% strain data into one group and the 20% 2-cell and cell-free into a group (excluding the 9-cell), the 10% strain data retained a higher final percentage of the initial stress, compared to the 20% strain group (p-value=0.0644). The 2-cell group at 20% strain and the 2-cell group at 10% strain had similar final percentages of the initial stress (p-value > 0.9999).

Fig. 4.3 shows the normalized results, and Table 4.2 contains each group's final normalized stress values. Table A.3 summarizes the statistical test results for the final normalized stress values. When testing for normality, the 10% 2-cell and 20% cell-free groups are normally distributed, with p-values of 0.9046 and 0.5034, respectively. The 20\% 2-cell had a p-value of 0.0473 when testing for normality. After direct comparisons of the groups, all comparisons except the 10% 2-cell compared to the 20% 2-cell had p-values less than or equal to 0.10. The 10% cell-free group retained the highest percentage of

the initial stress, whereas the 20% cell-free retained the lowest. The 20% 2-cell group and the 10\% 2-cell group had similar final percentages of the initial stress (p-value > 0.9999). The 10% 2-cell and cell-free were pooled together (N=5), while the 20% 2-cell and cell-free (N=6) were pooled together. Running a normality test on the data sets found that both are normally distributed with p-values of 0.8841 (10% strain) and 0.8013 (20% strain). Comparing the two sets using a t-test with Welch's correction results in a p-value of 0.0644 (Fig. 4.4), suggesting a difference between the 10% strain and 20%strain groups when comparing the final normalized stress values. The 10% group has a mean of 0.8616 where, whereas the 20% group has a mean of 0.7989, suggesting that the 10% group has a higher final percentage of the initial stress after 600s.

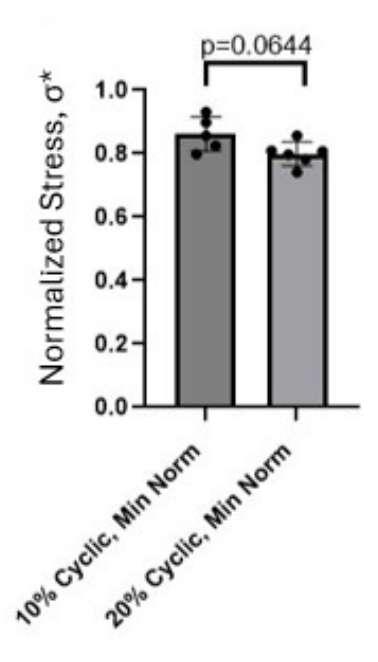


Figure 4.4.: Normalized cyclic pooled minimum value results. The 10% group had N=5 samples while the 20% group had N=6 samples.

Table 4.2.: Final normalized stress values for each group from the cyclic loading testing.

Group Name	Final σ^* Value [-]
20% $arepsilon$ 9-Cell	0.814 ± 0.006
20% $arepsilon$ 2-Cell	0.824 ± 0.028
20% ε Cell-free	0.774 ± 0.029
10% ε 2-Cell	0.826 ± 0.029
10% ε Cell-free	0.915 ± 0.024



4.2. 10% and 20% Stress Relaxation Results

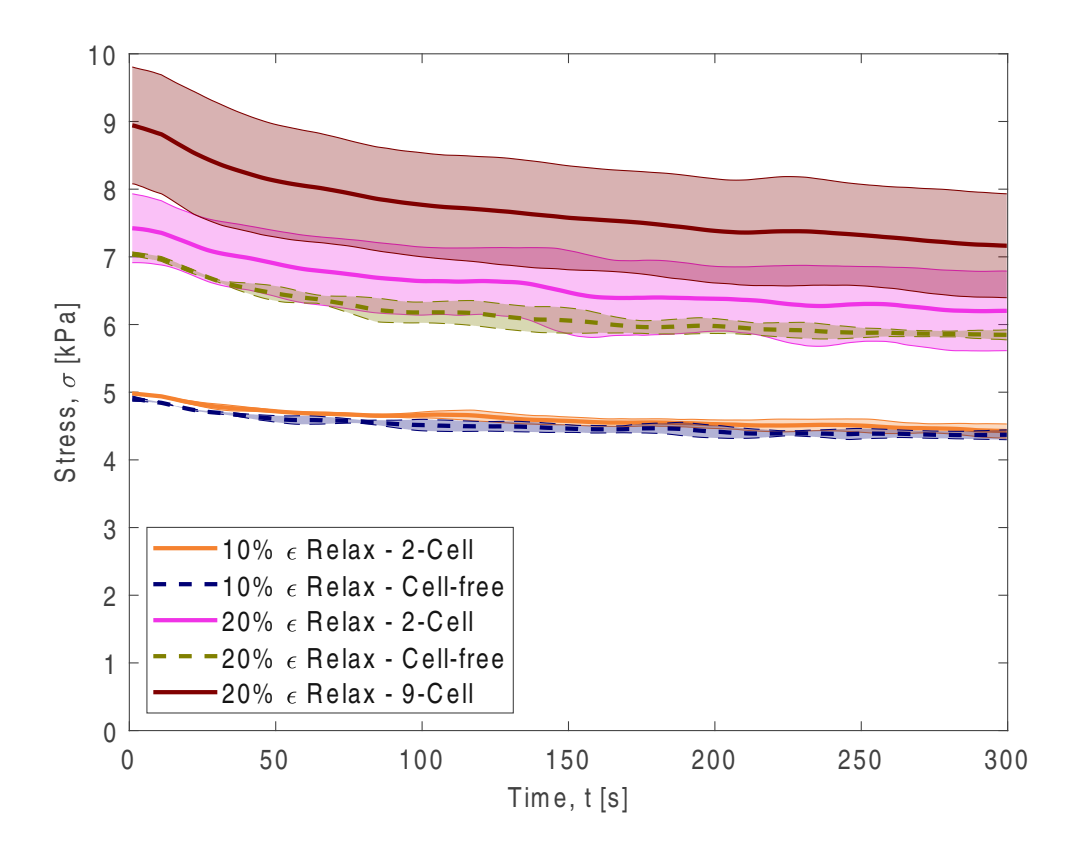


Figure 4.5.: Stress relaxation curves. Five groups are represented here. Data is shown as mean \pm SD, N=3 for each group. The 9-cell, 20% strain group experiences the greatest stress (p-value=0.10 when compared to the 20% strain 2-cell group), followed by the 20% 2-cell and cell-free groups (p-value=0.70, the 20% 2-cell and the 20% cell-free groups do not statistically differ). The 2-cell, 10% strain group had slightly higher initial stress than its counterpart, the cell-free, 10% strain group (p-value=0.0523).

Fig. 4.5 displays the stress relaxation results, and Table 4.3 displays the maximum and minimum stress values for each group. The shaded areas represent the standard deviation from the mean. All experiments had N=3 samples.

Table 4.3.: Mean maximum and minimum stress values from the relaxation loading testing. The stress relaxation mean curves have their initial stress aligned with the corresponding cyclic data to account for zeroing issues in the test setup, which is why the maximum values are the same as in Table 4.1.

Group Name	Maximum Stress Value [kPa]	Minimum Stress Value [kPa]
10% ε Cell-free	4.91 ± 0.04	4.37 ± 0.06
10% ε 2-Cell	4.98 ± 0.02	4.43 ± 0.10
20% ε Cell-free	7.04 ± 0.03	5.85 ± 0.06
20% ε 2-Cell	$\textbf{7.42} \pm \textbf{0.51}$	6.20 ± 0.59
20% ε 9-Cell	8.94 ± 0.86	7.16 ± 0.77

For the maximum data values, the 10% 2-cell, 10% cell-free, and the 20% cell-free are normally distributed with p-values of 0.5958, 0.8609, and 0.8907, respectively. The 10% cell-free and 20% 9-cell had p-values of 0.0312 and 0.0178, respectively. The minimum data values are all found to be normally distributed with p-values greater than 0.1.

Table A.4 and A.5 summarize the results of statistical testing performed between the groups for the maximum and minimum values, respectively. For the maximum values, all groups have p-values less than or equal to 0.10 except for the 20% cell-free compared to the 20% 2-cell (0.7000). Furthermore, when pooling the maximum values of the 10% 2-cell and cell-free together (N=6) and the 20% 2-cell and cell-free together (N=6), a p-value of 0.0022 is obtained. This shows significant differences between the 10% strain and 20% strain groups when the constructs undergo stress relaxation loading (Fig. 4.6a). Comparing within the 10% strain group, cell-free vs. 2-cell, a p-value of 0.0523 is obtained, denoting significant differences in the maximum stress (at 10% strain) the constructs experience when there is the presence of cells. While the 20% counterparts (2-cell vs. cell-free) do not show significant differences, comparing the 20% 2-cell to the 20% 9-cell and comparing the 20% cell-free to the 20% 9-cell results in p-values of 0.1000, suggesting that there are differences when cells have been cultured for 9 days. The standard deviation for the 20% 2-cell is large compared to the standard deviation of the 20% cell-free. The average maximum stress for the 20% strain cell-free is within one standard deviation of the 20% strain 2-cell.

For the minimum values, comparing the 10% 2-cell and 10% cell-free results in a p-value

of 0.3262, the 20% 2-cell vs. 20% cell-free results in a p-value of 0.3910, and the 20%2-cell vs. the 20% 9-cell results in a p-value of 0.1593. All other groups have p-values less than or equal to 0.10. For the minimum values, the distinction between 2-cell and cell-free is not as clear for stress relaxation loading, except for 20% cell-free vs. 20% 9-cell (p-value=0.0931). Like the maximum values, the 10% 2-cell and cell-free values (N=6) and the 20% 2-cell and cell-free (N=6) minimum values are pooled. With a p-value of less than 0.001, there are significant differences between how the constructs experience 10%strain and 20% strain after testing for 300s (Fig.4.6b).

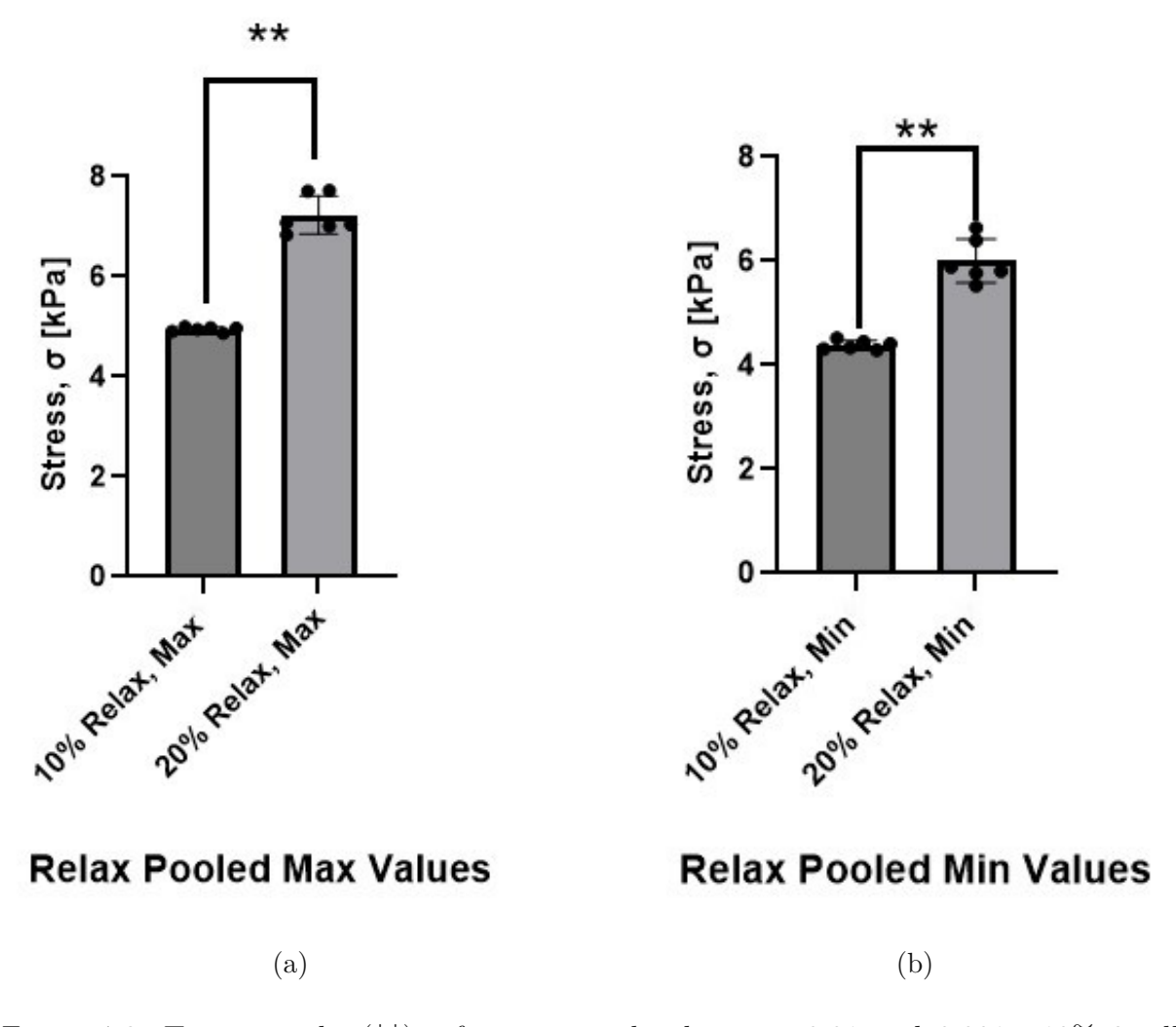


Figure 4.6.: Two asterisks (**) refer to a p-value between 0.01 and 0.001. 10% 2-cell and cell-free data (N=6) was pooled together. 20\% 2-cell and cell-free data (N=6) was pooled together. The maximum pooled comparison had a p-value of 0.0022, and the minimum pooled comparisons had a p-value less than 0.001.

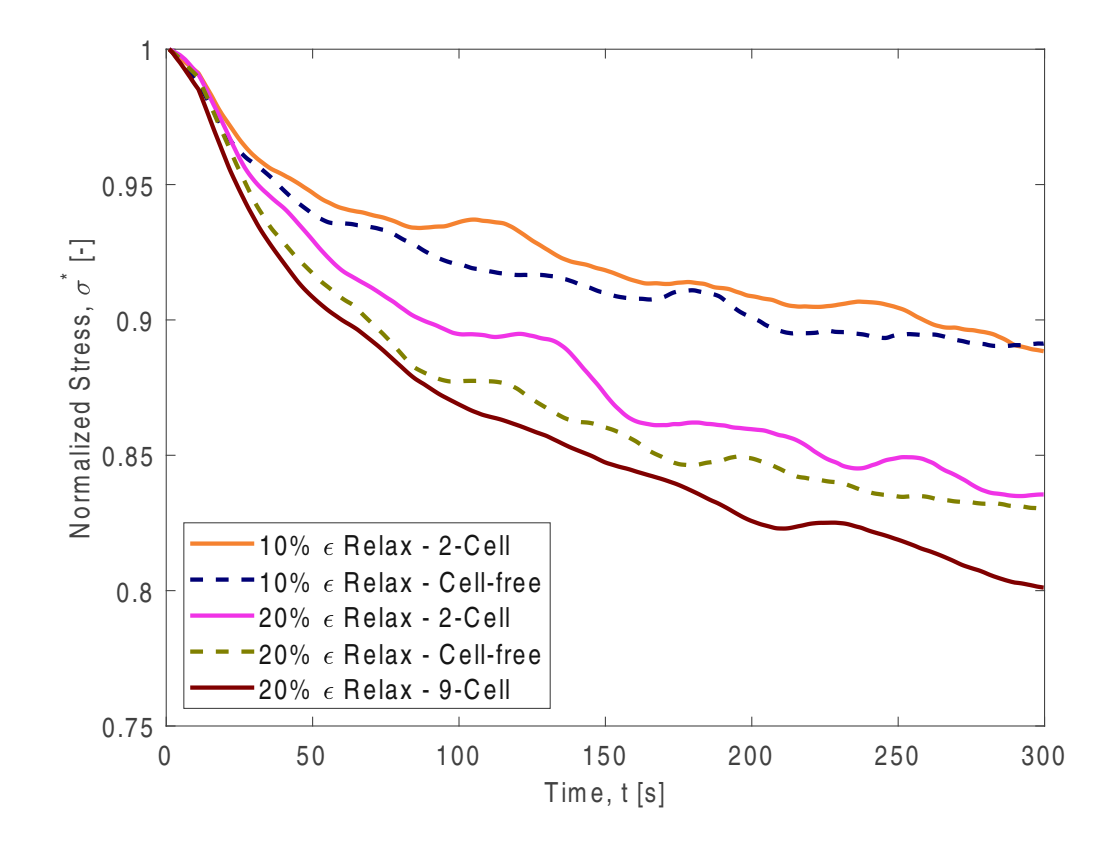


Figure 4.7.: Normalized stress relaxation test results. There are five groups of data, with each group showing the normalized mean of the individual samples that comprise it. All groups have N=3 samples each. By the end of the test, 10% strain groups (2-cell and cell-free) retained the highest percentage of the initial stress, compared to the 20% strain groups (2-cell and cell-free) (pvalue = 0.0391

4. Results

The normalized results are shown in Fig. 4.7, and Table 4.4 contains each group's final normalized stress values. Table A.6 summarizes the statistical testing results for the final normalized stress values. Testing for normality finds only the 10% 2-cell (0.6500), 20% 2cell (0.4349), and 20% 9-cell (0.2768) groups are normally distributed. Directly comparing all groups finds all p-values except for the 10% 2-cell compared to the 20% cell-free (0.10), 10% cell-free compared to the 20% cell-free (0.10), and the 10% cell-free compared to the 20% 9-cell (0.10) less than or equal to 0.10. The 10% 2-cell and cell-free values (N=6) and the 20% 2-cell and cell-free (N=6) final normalized values are pooled together. With a p-value of 0.0391, there are differences between the 10% strain and 20% strain groups (Fig. 4.8. The 10% group has a mean of 0.889 compared to the 20% group's mean of 0.8329; like with the cyclic loading case, the 10% group has a higher final percentage of the initial stress after 300s.

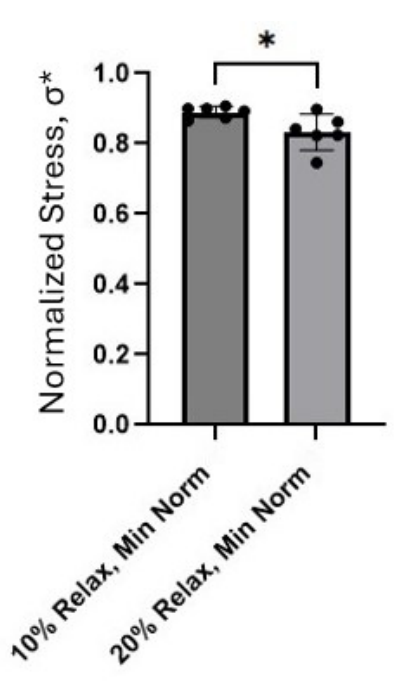


Figure 4.8.: Normalized relaxation pooled minimum value results. Both groups had N=6 samples, and the results of a Welch's t-test found a p-value of 0.0391. One asterisk (*) refers to a p-value between 0.1 and 0.01.



Table 4.4.: Final normalized stress values for each group from the relaxation loading testing.

Group Name	Final σ^* Value [-]
20% $arepsilon$ 9-Cell	0.8011 ± 0.09
20% ε 2-Cell	0.8355 ± 0.08
20% ε Cell-free	0.8303 ± 0.01
10% ε 2-Cell	0.8884 ± 0.02
10% ε Cell-free	0.8913 ± 0.01

4.3. Cyclic and Stress Relaxation Comparison

4.3.1. 10% Strain

This section compares the cyclic and stress relaxation data at 10% strain and 20% strain. The figures illustrate the comparison of each condition's initial and final stresses.

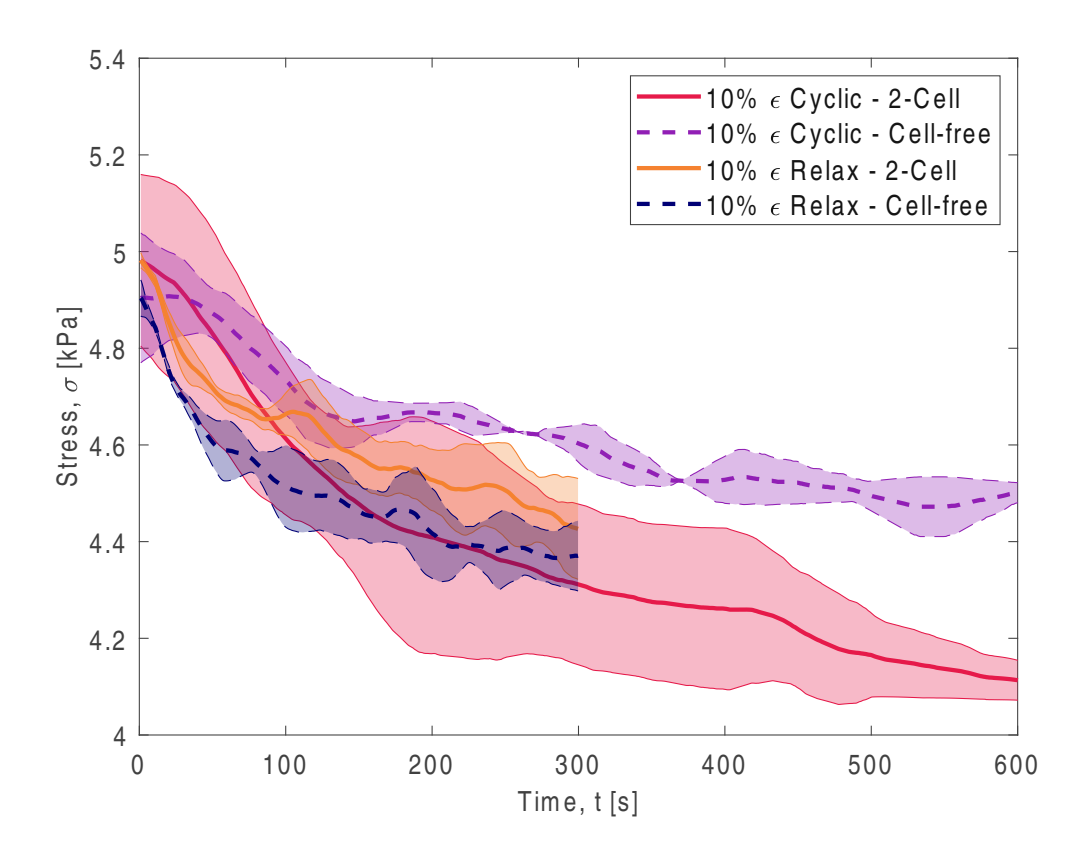


Figure 4.9.: Stress data from the cyclic loading and stress relaxation tests conducted at 10% strain. The stress relaxation mean curves have their initial stress aligned with the corresponding cyclic data to account for zeroing issues in the test setup. Data is shown as the mean with \pm SD. Each group consists of N=3 samples, except for the 10% strain cell-free group from the cyclic loading test, which has N=2 samples.

4.9 plots the 2-cell and cell-free groups from the 10% strain, cyclic, and stress relaxation testing, and Table 4.5 displays the maximum and the stress values at 300s for each group. The relaxation testing is 300s long; the corresponding time point for the cyclic loading testing is pulled so a comparison can be made. Data is shown as mean (solid line) \pm SD (shaded area). All groups have N=3 samples except for the 10% strain, cell-free cyclic loading (N=2).

Table 4.5.: Mean maximum and stress values at t=300s from the cyclic and relaxation loading testing at 10% strain. The stress relaxation mean curves have their initial stress aligned with the corresponding cyclic data to account for zeroing issues in the test setup, which is why the maximum values are the same for corresponding groups.

Group Name	Maximum Stress Value [kPa]	Stress Value at 300s [kPa]
Cyclic Cell-free	4.91 ± 0.09	4.60 ± 0.04
Cyclic 2-Cell	$\textbf{4.98} \pm \textbf{0.17}$	4.31 ± 0.17
Relax Cell-free	4.91 ± 0.04	4.37 ± 0.06
Relax 2-Cell	$\textbf{4.98} \pm \textbf{0.02}$	4.43 ± 0.10

The 10% cyclic cell-free group is excluded from direct comparison to the other groups due to the N=2 sample size. For the stress values at 300s, all groups are found to be normally distributed with p-values greater than 0.1. The 10% cyclic groups (N=5) are pooled together, while the 10% relaxation groups (N=6) are pooled together. Both groups for the pooled maximum values and the values at 300s are normally distributed with p-values greater than 0.1.

Table A.7 and A.8 summarize the results of the p-values from statistical testing performed between the groups for the maximum values and values at 300s, respectively. For the maximum values, all groups have p-values greater than 0.10 except for the 10% relax 2cell compared to the 10% relax cell-free (p-value=0.0523). A t-test with Welch's correction on the pooled maximum values (10% cyclic vs. 10% relaxation) results in a p-value of 0.8202 (Fig. 4.10a). The initial stress at the start (also the maximum stress) that the constructs experience is the same regardless of loading type at 10% strain.

For the minimum values, all p-values are greater than 0.10; after 300s of testing, the constructs have similar levels of stress when directly comparing 10% strain, cyclic 2-cell

4. Results

to relax 2-cell (0.3790) or cyclic 2-cell compared to relax cell-free (p-value=0.7686). When pooling together all of the 10% cyclic data (N=5), including the two samples from the 10% cyclic cell-free group, the results of the t-test with Welch's correction find there are no differences after 300s (p-value=0.6751) (Fig. 4.10b). After 300s, regardless of the loading type at 10% strain, the constructs experience similar stress levels.

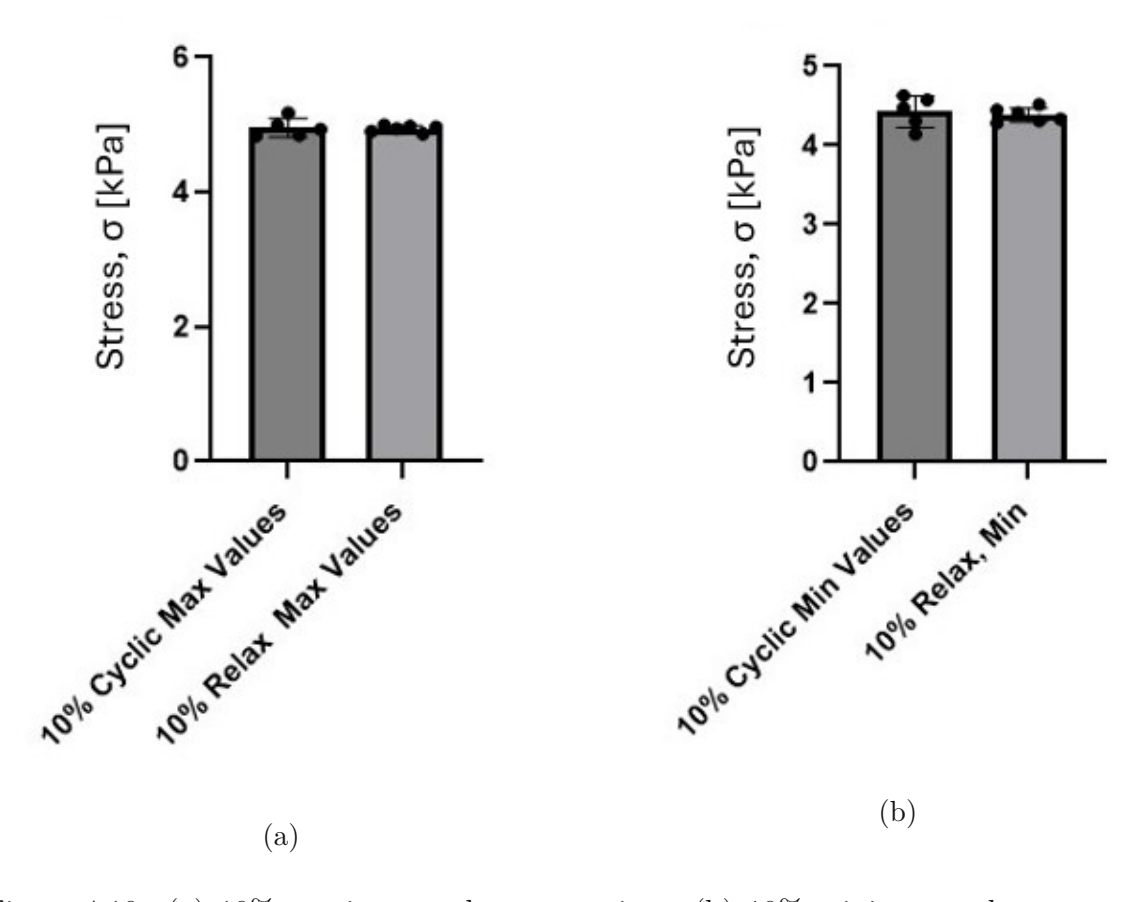


Figure 4.10.: (a) 10% maximum value comparison, (b) 10% minimum value comparison (time after t=300s). No significant differences were found for either comparison. Cyclic data had N=5 samples, and relaxation data had N=6 samples.

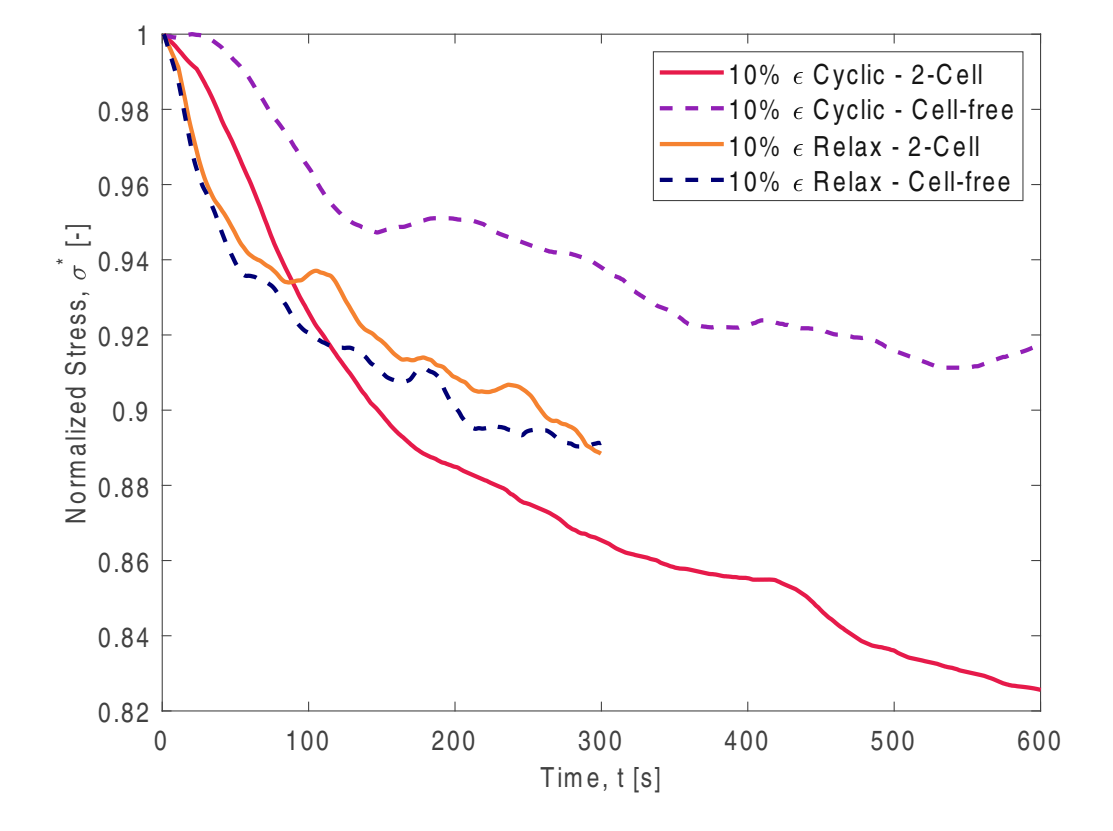


Figure 4.11.: Normalized stress data from the cyclic loading and stress relaxation test conducted at 10% strain. Regardless of the loading type, the constructs at 10% strain have similar normalized stresses at 300s (p-value=0.8410).

Fig. 4.11 contains all the 10% normalization, and Table 4.6 contains each group's final normalized stress values after 300s. Table A.9 summarizes the p-values by comparing all of the 10% final normalized stress values. Testing for normality finds all groups except the 10% strain relax cell-free group normally distributed (p-value=0.0122). The 10% cyclic data pooled together and the 10% relaxation data pooled together also follow a normal distribution. All p-values are greater than 0.10 when directly comparing groups and when the cyclic data (N=5) and relaxation data (N=6) are pooled and compared (p-value=0.8410) (Fig. 4.12). Regardless of the loading mechanism, constructs at 10% strain have similar normalized stress at 300s.

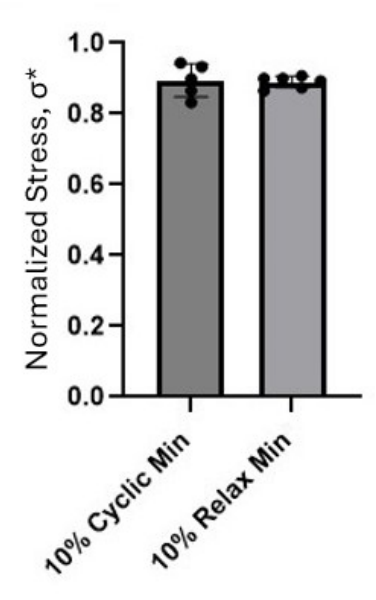


Figure 4.12.: Normalized pooled 10% cyclic and relaxation comparison. Cyclic data had N=5 samples, and relaxation data had N=6 samples. Min refers to the time after t=300s.

Table 4.6.: Normalized stress values at t=300s for each group from the cyclic and relaxation loading testing at 10% strain.

Group Name	Final σ^* Value at 300s[-]
Cyclic Cell-free	0.8011 ± 0.09
Cyclic 2-Cell	0.8355 ± 0.08
Relax Cell-free	0.8303 ± 0.01
Relax 2-Cell	0.8884 ± 0.02

4.3.2. 20% Strain

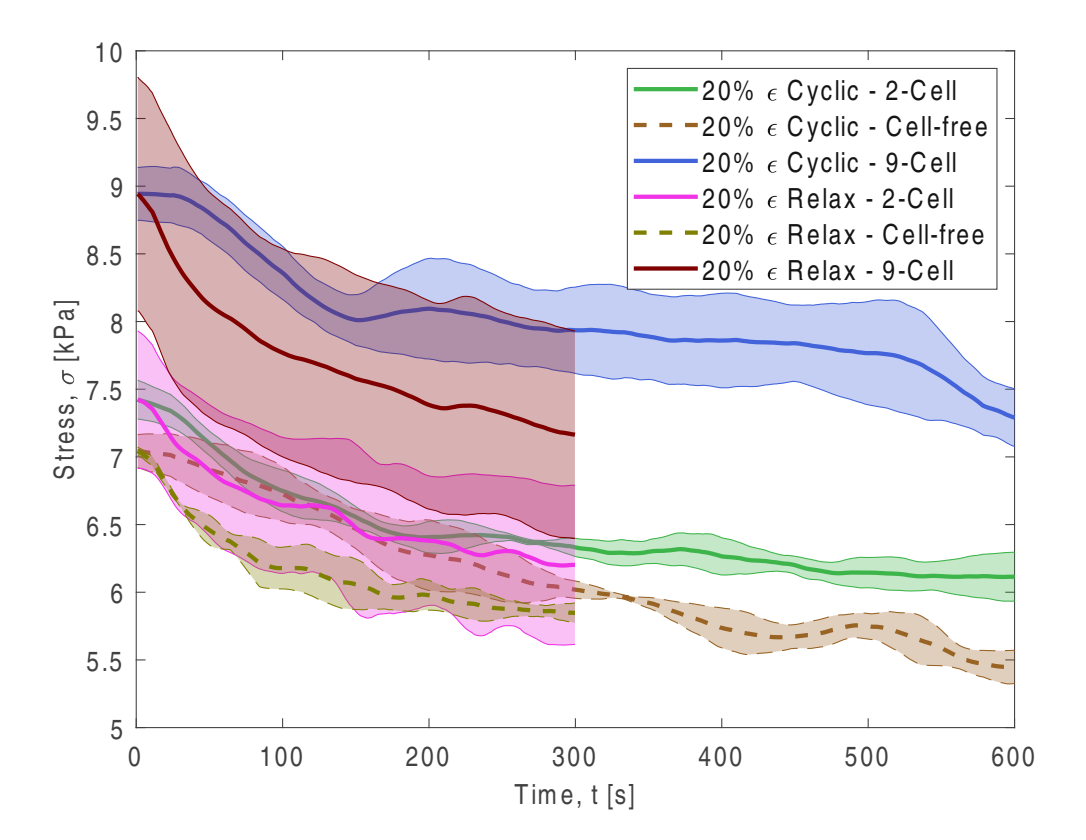


Figure 4.13.: This figure displays the stress data from the cyclic loading and stress relaxation testing conducted at 20% strain. The stress relaxation mean curves have their initial stress aligned with the corresponding cyclic curves to account for zeroing issues in the test setup. Data is shown as mean (solid line) ± SD (shaded areas). Each group consists of N=3 samples, except for the 20% strain 9-cell group from the cyclic loading test, which has N=2 samples.

Fig. 4.13 plots the 20% strain results for the 9-cell, 2-cell, and cell-free groups, and Table 4.7 displays the maximum and the stress values at 300s for each group. All groups have N=3 samples except for the 20% strain, 9-cell cyclic loading (N=2).

Table 4.7.: Mean maximum and stress values at t=300s from the cyclic and relaxation loading testing at 20% strain. The stress relaxation mean curves have their initial stress aligned with the corresponding cyclic data to account for zeroing issues in the test setup, which is why the maximum values are the same for corresponding groups.

Group Name	Maximum Stress Value [kPa]	Stress Value at 300s [kPa]
Cyclic Cell-free	$\textbf{7.04} \pm \textbf{0.12}$	6.02 ± 0.06
Cyclic 2-Cell	$\textbf{7.42} \pm \textbf{0.14}$	6.33 ± 0.07
Cyclic 9-Cell	8.94 ± 0.20	$\textbf{7.94} \pm \textbf{0.3}$
Relax Cell-free	$\textbf{7.04} \pm \textbf{0.03}$	5.85 ± 0.06
Relax 2-Cell	$\textbf{7.42} \pm \textbf{0.51}$	6.20 ± 0.59
Relax 9-Cell	8.94 ± 0.86	7.16 ± 0.77

The 20% cyclic 9-cell group is excluded from direct comparison to the other groups due to the N=2 sample size. At 300s, the data groups are all found to follow a normal distribution with p-values greater than 0.1. The 20% cyclic groups (N=8) are pooled together and are not normally distributed at the maximum values (p-value=0.0234) and 300s (p-value <0.0001). The 20% relaxation groups (N=9) pooled together are not normally distributed at the maximum values (p-value=0.0297) but are normally distributed at 300s (0.2010).

Table A.10 and A.11 summarizes the p-values from the statistical testing performed between maximum stress levels and values at 300s of the 20% cyclic and relaxation groups. Comparing 20% strain cyclic 2-cell to 20% strain relax 2-cell results in a p-value of 0.7000; in other words, the stress the constructs experience at the start of the test is similar in both loading cases. However, comparing cyclic 2-cell to relaxation cell-free results in a p-value of 0.1000, less than or equal to the 0.10 significance level. This suggests that either the presence of cells or the loading type affects the maximum stress at the start of the test. Cyclic cell-free, compared to relaxation cell-free, finds a p-value of 0.9574, and cyclic cell-free, compared to relaxation 2-cell, results in a p-value of 0.7000, finding no difference in the maximum stress the constructs experience at the start of the test. All groups had their maximum values (excluding the cyclic 9-cell) compared to the relaxation 9-cell; this resulted in p-values of 0.1000. In addition, comparing the 20% cyclic pooled (N=8) to the 20% relax pooled (N=9), a p-value of 0.7430 is obtained, suggesting that

there is no difference between the loading type on the stress the constructs experience at the start of the test (Fig. 4.14a).

For the minimum values, only comparing cyclic to relaxation, the 20% strain cyclic 2-cell vs. the relax cell-free and the cyclic cell-free vs. relax cell-free are significant with p-values of 0.0007 and 0.0193, respectively. After the 300s, these groups did not significantly differ in the stress the constructs experienced. When looking at the pooled data, cyclic (N=8) vs. relaxation (N=9), a p-value of 0.5769 indicates no significant difference between the loading type after 300s (Fig. 4.14b).

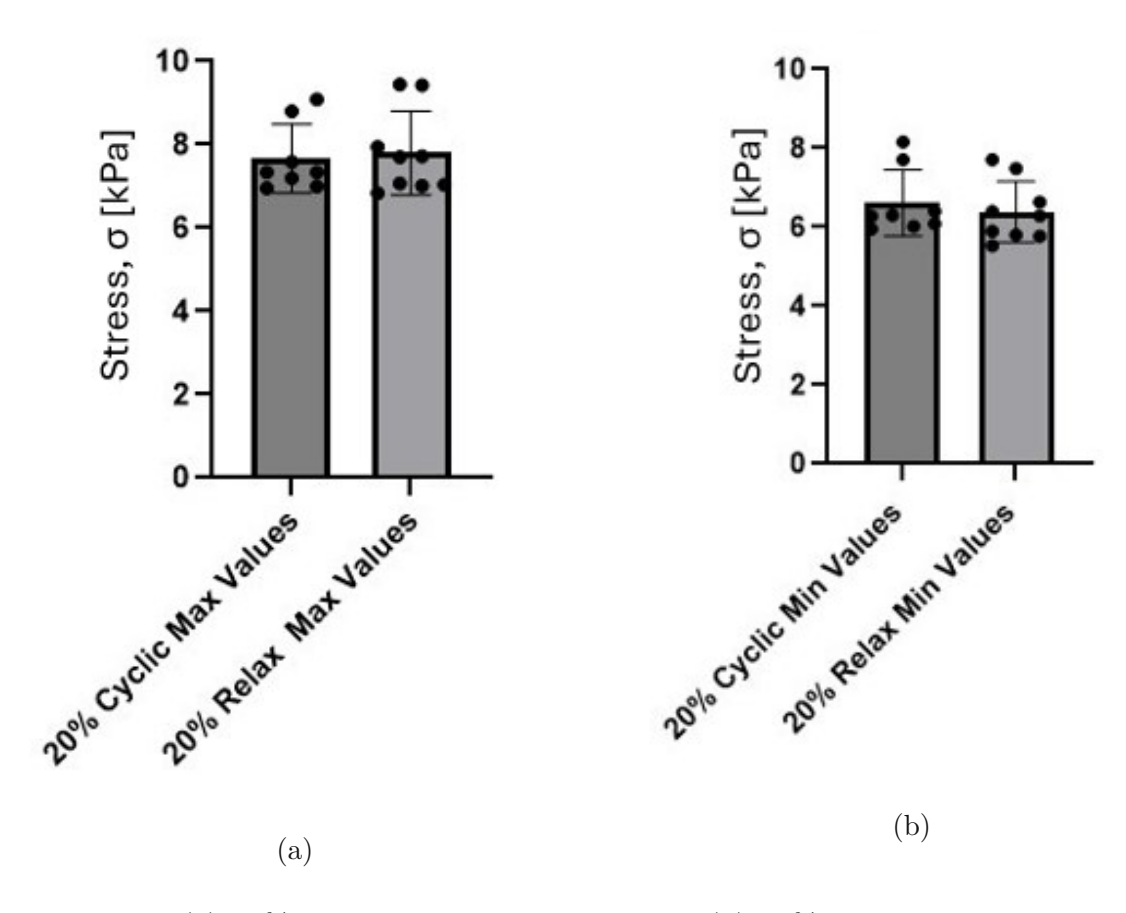


Figure 4.14.: (a) 20% maximum value comparison, (b) 20% minimum value comparison (time after t=300s). Cyclic data had N=8 samples, and relaxation data had N=9 samples.



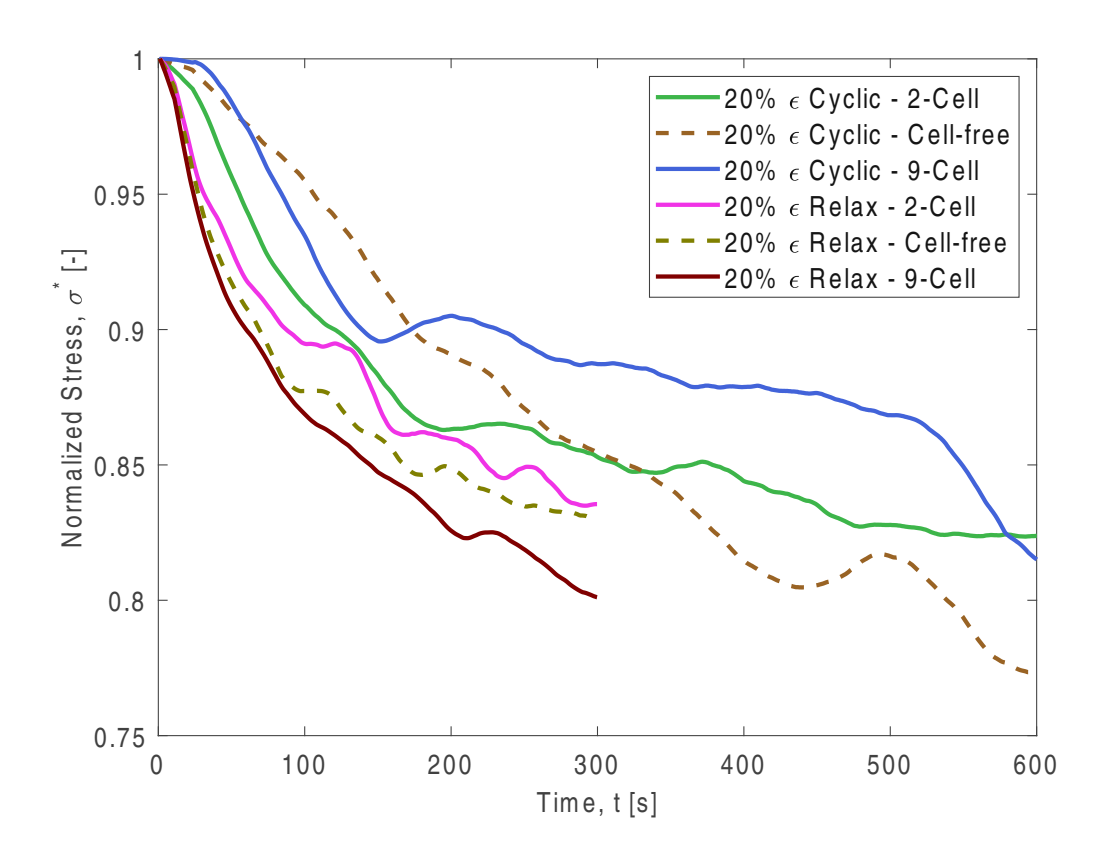


Figure 4.15.: Normalized stress results from the cyclic loading and stress relaxation testing conducted at 20% strain. After 300s, the loading type (cyclic pooled vs. stress relaxation pooled) does have a significant impact on the normalized stress at 300s (p-value=0.0745).

Fig. 4.15 displays the 20% strain normalization, and Table 4.8 contains each group's normalized stress values after 300s. Table A.12 looks at the p-values from statistical testing performed between the final normalized stress values of all the 20% strain groups. All groups follow a normal distribution except for the 20% cell-free relaxation group (pvalue=0.0793). The relaxation group pooled together also follows a normal distribution, while the pooled cyclic loading does not. Significant differences exist between the relaxation cell-free group and the cyclic cell-free group, as well as between the relaxation cell-free group and the cyclic 2-cell group. Furthermore, there are significant differences when comparing the pooled cyclic data (N=8) and the pooled relaxation data (N=9) (p-value=0.0745), suggesting that at 20% strain, there are differences in the normalized stress value at 300s (Fig. 4.16).

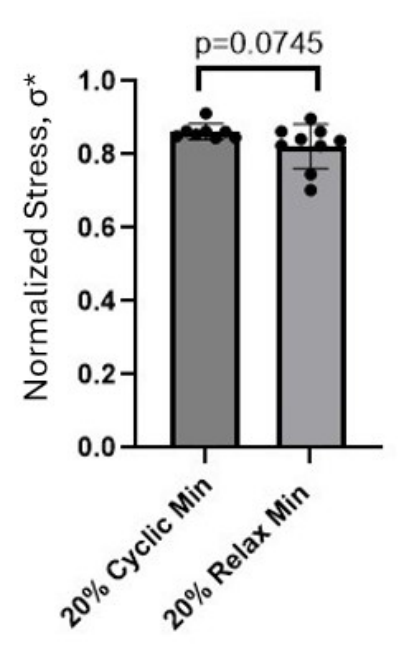


Figure 4.16.: Normalized pooled 20% cyclic and relaxation comparison. Cyclic data had N=8 samples, and relaxation data had N=9 samples. Min refers to the time after t=300s.

Table 4.8.: Normalized stress values at t=300s for each group from the cyclic and relaxation loading testing at 20% strain.

Group Name	Final σ^* Value at 300s[-]
Cyclic Cell-free	0.8547 ± 0.01
Cyclic 2-Cell	0.8530 ± 0.01
Cyclic 9-Cell	0.8873 ± 0.04
Relax Cell-free	0.8303 ± 0.01
Relax 2-Cell	0.8355 ± 0.08
Relax 9-Cell	0.8011 ± 0.09

4.3.3. Instantaneous and Equilibrium Moduli

The values for the instantaneous modulus and the equilibrium modulus are shown in Table 4.9. Table A.13 and A.14 summarize the p-values from statistical testing performed between groups for the instantaneous moduli and the equilibrium moduli, respectively. The instantaneous modulus for the 10% strain cyclic 2-cell and 10% strain relaxation 2-cell are the same value due to offsetting the initial relaxation stress value to the initial cyclic stress value to account for zeroing issues. This pattern is the same for each corresponding group (10% cell-free, 20% 2-cell, cell-free, 9-cell).

A visual representation of the 10% and 20% strain instantaneous boxplots is shown in Fig. 4.17. The equilibrium boxplots for 10% strain and 20% strain are shown in Fig. 4.19.

Table 4.9.: This table depicts each group's mean instantaneous (σ_0/ε_0) and equilibrium modulus $(\sigma_{\infty}/\varepsilon_0)$.

Group Name	$\sigma_0/arepsilon_0$ [kPa]	$\sigma_{\infty}/arepsilon_0$ [kPa]
10% Cyclic 2-Cell	49.8 ± 1.77	41.1 ± 0.41
10% Cyclic Cell-free	49.0 ± 1.34	45.0 ± 0.19
10% Relax 2-Cell	49.8 ± 0.16	47.5 ± 1.04
10% Relax Cell-free	49.0 ± 0.37	43.7 ± 0.73
20% Cyclic 2-Cell	37.1 ± 0.72	30.6 ± 0.91
20% Cyclic Cell-free	35.2 ± 0.61	27.2 ± 0.61
20% Cyclic 9-cell	44.7 ± 0.98	36.4 ± 1.06
20% Relax 2-Cell	37.1 ± 2.54	31.0 ± 2.94
20% Relax Cell-free	35.2 ± 0.15	29.2 ± 0.37
20% Relax 9-Cell	44.7 ± 4.32	35.8 ± 3.84

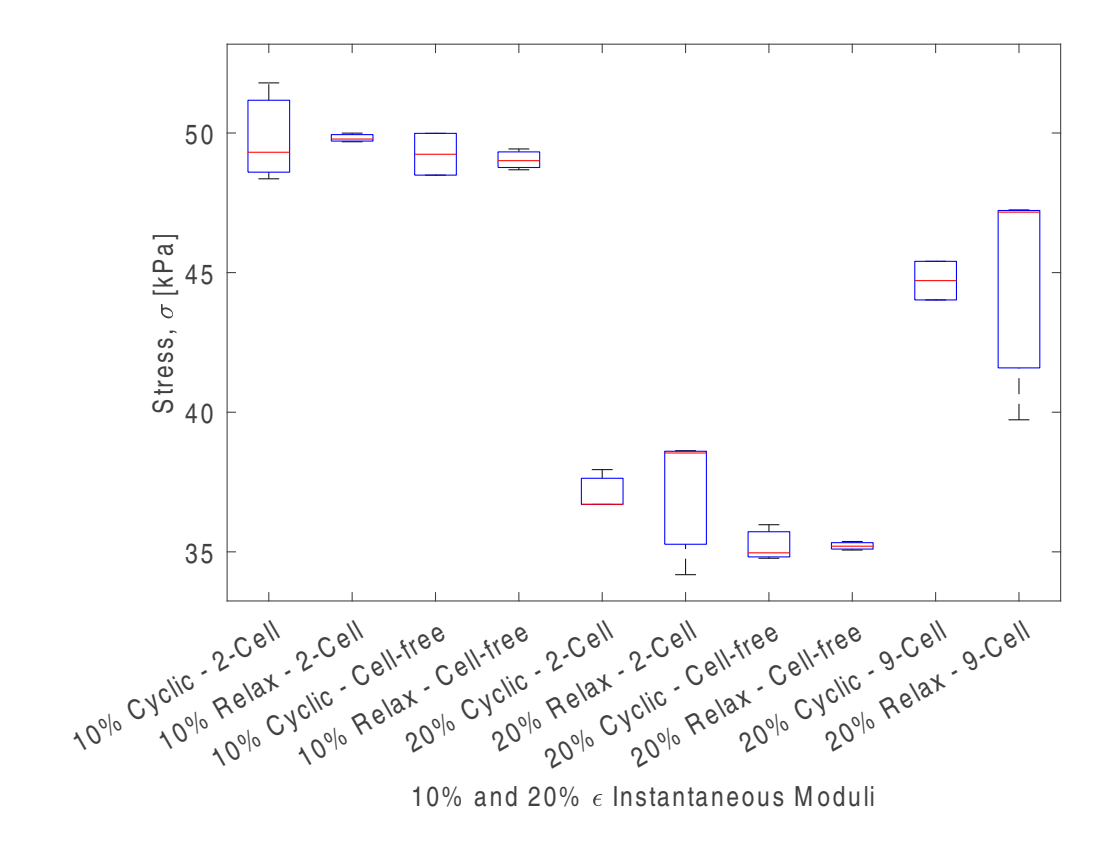


Figure 4.17.: Boxplots of the instantaneous moduli (σ_0/ε_0) for the 10% and 20% strain groups. Data is shown as median (red line) with minimum (lower whisker) to maximum (upper whisker) values.

TU **Sibliothek**, Die approbierte gedruckte Originalversion dieser Diplomarbeit ist an der TU Wien Bibliothek verfügbar wien vour knowledge hub

Doing group comparisons of the instantaneous moduli found six comparisons that are not significant:

- 10% cyclic 2-cell vs. 10% relax 2-cell (>0.9999)
- 10% cyclic 2-cell vs. 10% relax cell-free (0.5275)
- 20% cyclic 2-cell vs. 20% relax 2-cell (0.7000)
- 20% cyclic cell-free vs. 20% relax 2-cell (0.7000)
- 20% cyclic cell-free vs. 20% relax cell-free (0.9574)
- 20% relax 2-cell vs. 20% relax cell-free (0.7000)

Because the 10% cyclic cell-free and the 20% cyclic 9-cell groups had N=2 samples, they were excluded from direct comparisons. The 10% strain cyclic 2-cell and the 10% strain relax 2-cell groups had the greatest instantaneous moduli, suggesting that these two groups had the greatest initial elastic response of the groups. The 10% groups were of similar instantaneous moduli, with only the 10% relax 2-cell vs. the 10% relax cellfree being significantly different (0.0523). The 20\% relax 9-cell had the second highest modulus after the 10% groups. The 20% groups (consisting of the 2-cell and cell-free groups) had the lowest instantaneous moduli and were not significantly different from each other. Fig. 4.18 visually compares the 10% strain, cyclic and relaxation, 2-cell and cell-free groups, the 20% strain, cyclic and relaxation, 2-cell and cell-free groups, and the 20% strain, cyclic and relaxation 9-cell groups for the instantaneous moduli.

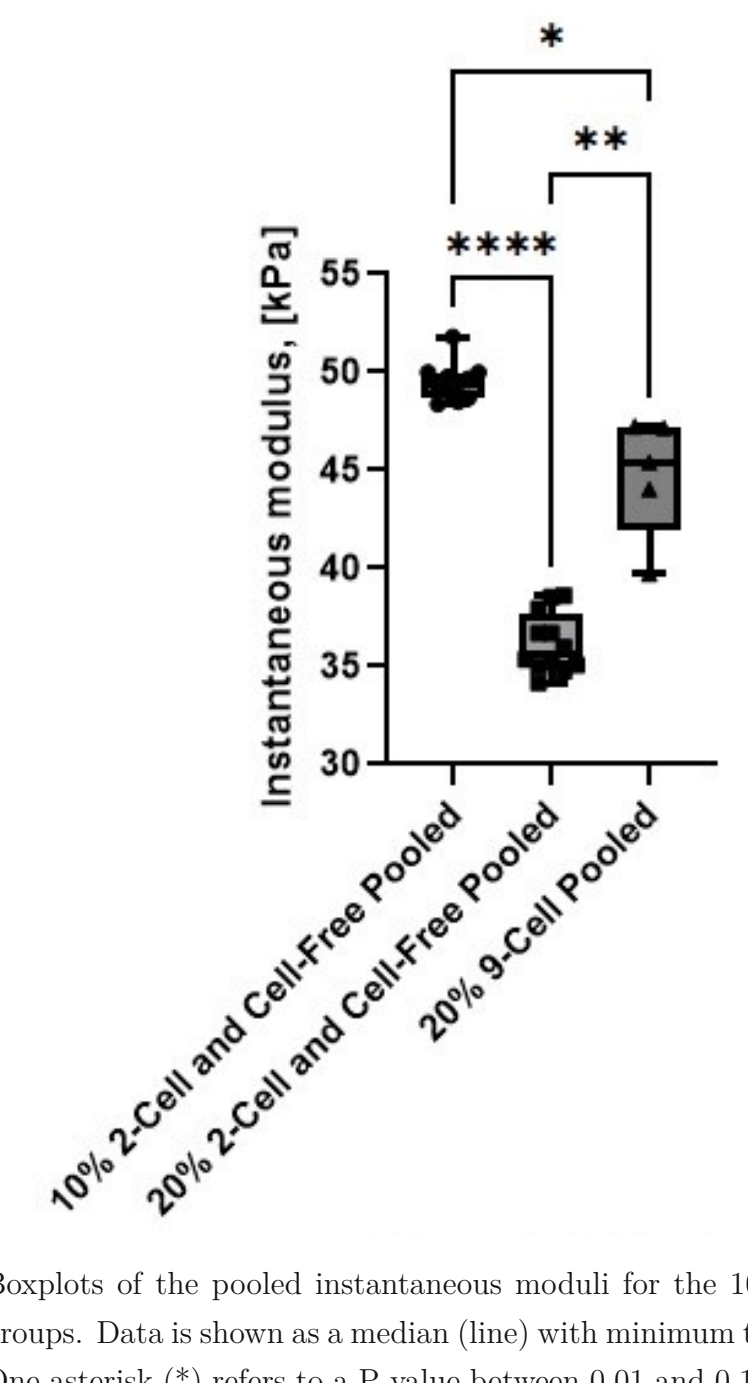


Figure 4.18.: Boxplots of the pooled instantaneous moduli for the 10% and 20% strain groups. Data is shown as a median (line) with minimum to maximum values. One asterisk (*) refers to a P-value between 0.01 and 0.1, two asterisks (**) refer to a P-value between 0.01 and 0.001, and four asterisks (****) refer to a p-value less than 0.0001.

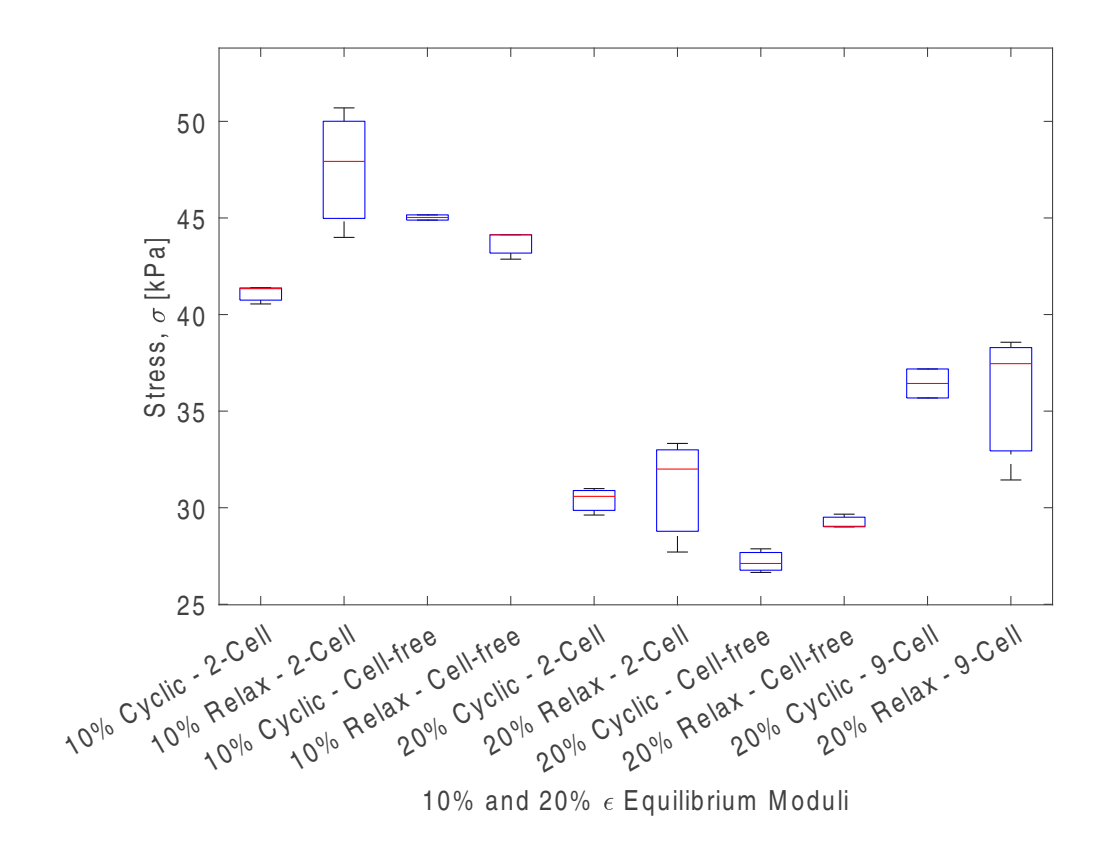


Figure 4.19.: This figure illustrates the equilibrium moduli for the 10% and 20% strain groups. Data is shown as median (red line) with minimum (lower whisker) to maximum (upper whisker) values. For some plots, the whiskers are missing or only single-sided.

The equilibrium moduli found eight comparisons that are not significant:

- 10% cyclic 2-cell vs. 20% relax 9-cell (0.1383)
- 10% relax 2-cell vs. 10% relax cell-free (0.4000)
- 20% cyclic 2-cell vs. 20% relax 2-cell (0.7562)
- 20% cyclic 2-cell vs. 20% relax cell-free (0.2000)
- 20% cyclic 2-cell vs. 20% relax 9-cell (0.1299)
- 20% cyclic cell-free vs. 20% relax 2-cell (0.1493)
- 20% relax 2-cell vs. 20% relax cell-free (0.7000)
- 20% relax 2-cell vs. 20% relax 9-cell (0.1647)

4. Results

Similar to the instantaneous moduli, the 10% strain groups had the greatest equilibrium moduli, followed by the 20% strain 9-cell groups and the 20% strain 2-cell and cell-free groups. Fig. 4.20 visually compares the 10% strain, cyclic and relaxation, 2-cell and cell-free groups, the 20% strain, cyclic and relaxation, 2-cell and cell-free groups, and the 20% strain, cyclic and relaxation 9-cell groups for the equilibrium moduli.

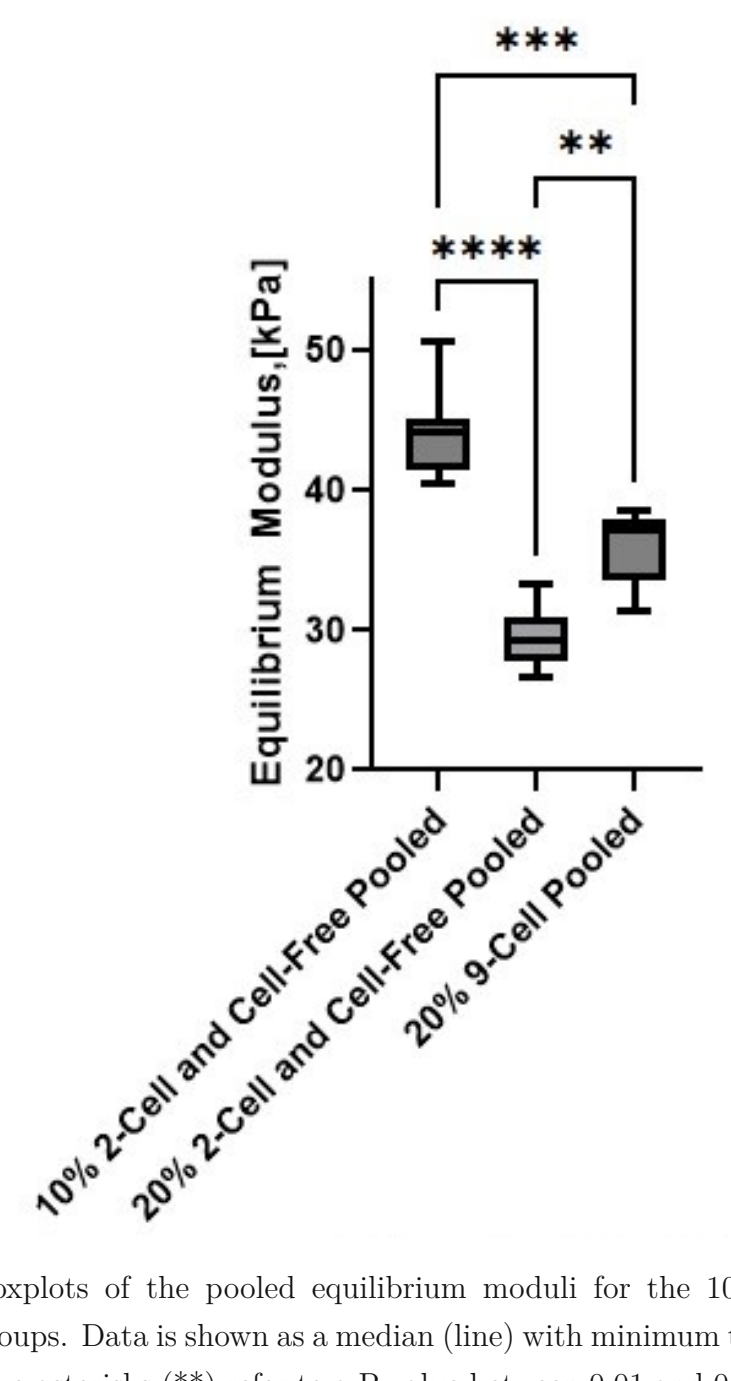


Figure 4.20.: Boxplots of the pooled equilibrium moduli for the 10% and 20% strain groups. Data is shown as a median (line) with minimum to maximum values. Two asterisks (**) refer to a P-value between 0.01 and 0.001, three asterisks (***) refer to a p-value between 0.0001 and 0.001, and four asterisks (****) refer to a p-value less than 0.0001.

4.3.4. Prony Series Modelling

Fig. 4.21 displays the 10% strain Prony series curve fit approximations, and Fig. 4.22 plots the 20% strain Prony series fit approximations. Prony series models are fitted for all the curves. Table 4.10 shows the mean values of the time constants and R^2 values for the 10% strain cyclic and relaxation groups. Table 4.11 shows the mean values of the time constants and R^2 values for the 20% strain cyclic and relaxation groups. Table A.15 and A.16 summarize the p-values from statistical testing performed between groups for τ_1 and τ_2 , respectively. Due to N=2 samples for the 10% cyclic cell-free and the 20% cyclic 9-cell groups, they were excluded from direct comparisons.

Table 4.10.: This Table depicts the mean Prony series time constants τ_1 and τ_2 and R^2 value for the 10% strain, cyclic and relaxation groups, 2-cell and cell-free.

Group Name	$ au_1$ [s]	$ au_2$ [s]	\mathbb{R}^2 Value
10% Cyclic 2-Cell	96 ± 3.66	$\textbf{343} \pm \textbf{420.92}$	0.99
10% Cyclic Cell-free	79 ± 17.96	634 ± 448.08	0.96
10% Relax 2-Cell	36 ± 35.33	802 ± 295.20	0.99
10% Relax Cell-free	37 ± 23.88	451 ± 481.79	0.98

For the τ_1 values, there were only four significant comparisons:

- 10% cyclic 2-cell vs. 10% relax 2-cell (0.0949)
- 10% cyclic 2-cell vs. 10% relax cell-free (0.0459)
- 10% cyclic 2-cell vs. 20% relax cell-free (0.0240)
- 10% cyclic 2-cell vs. 20% relax 9-cell (0.0068)

Excluding the 10% strain, cyclic 2-cell group, none of the other comparisons were significant, indicating that all constructs have similar τ_1 relaxation times (except for the 10% strain, cyclic 2-cell group).

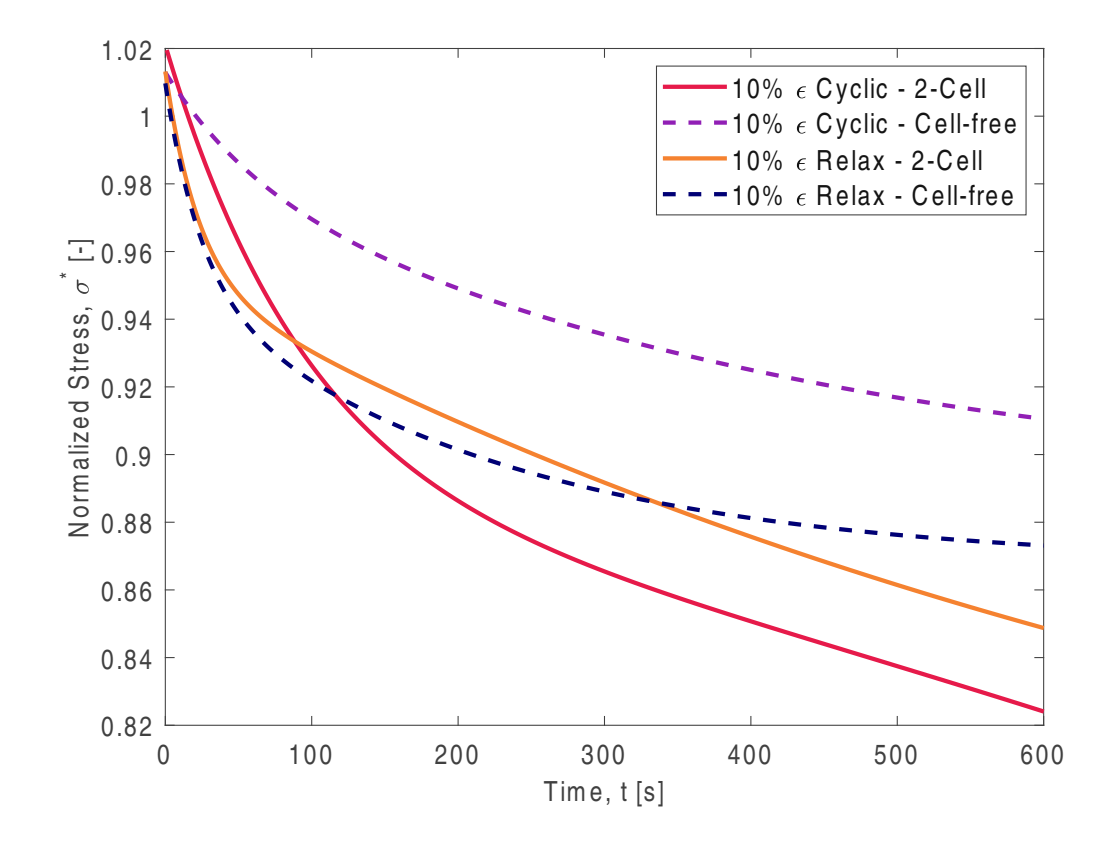


Figure 4.21.: Depicted here are the Prony series models for cyclic loading and relaxation testing conducted at 10% strain.

Table 4.11.: This Table depicts the mean Prony series time constants τ_1 and τ_2 and R^2 value for the 20% strain, cyclic and relaxation groups, 2-cell and cell-free.

Group Name	$ au_1$ [s]	$ au_2$ [S]	\mathbb{R}^2 Value
20% Cyclic 2-Cell	64 ± 40.89	491 ± 461.44	1.00
20% Cyclic Cell-free	68 ± 34.33	955 ± 39.15	0.98
20% Cyclic 9-cell	$100 \pm 3.53 \text{e-}04$	$1000 \pm 7.07 ext{e-}05$	0.99
20% Relax 2-Cell	50 ± 30.67	1000 ± 0	0.98
20% Relax Cell-free	35 ± 18.14	115 ± 21.71	0.99
20% Relax 9-Cell	31 ± 11.97	528 ± 408.91	1.00

For the τ_2 values, there were only eight significant comparisons:

- 10% cyclic 2-cell vs. 20% cyclic cell-free (0.1000)
- 10% cyclic 2-cell vs. 20% relax 2-cell (0.1000)
- 10% relax 2-cell vs. 20% relax cell-free (0.0561)
- 20% cyclic 2-cell vs. 20% relax 2-cell (0.1000)
- 20% cyclic cell-free vs. 20% relax cell-free (0.0002)
- 20% relax 2-cell vs. 20% relax cell-free (0.1000)
- 20% relax 2-cell vs. 20% relax 9-cell (0.1000)
- 20% relax cell-free vs. 20% relax 9-cell (0.1000)

There are more significant differences for the τ_2 values. However, there is no discernible pattern for this set of groups.

4.4. Post Testing Qualitative View of Constructs

Lastly, following testing, the rings have a characteristic bowing shape to the strands, as seen in Fig. 4.23. When removed from the loading frame, the fibrin rings do not immediately return to their original shape. The rings displayed some residual strain when removed from the load frame. This phenomenon affects both rings with cells and cell-free rings. However, after some time, the rings with cells will eventually contract.

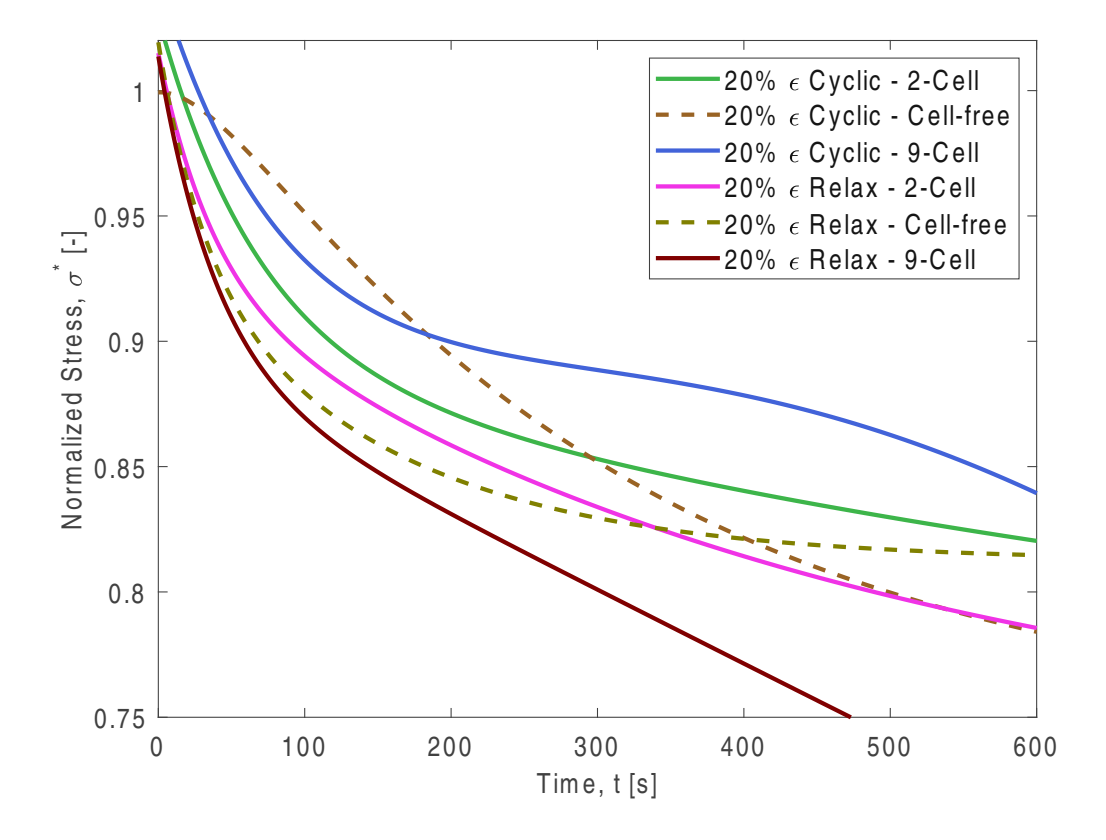


Figure 4.22.: Illustrated here are the Prony series models for the cyclic and loading relaxation testing conducted at 20% strain.

Although quantifying the extent of plastic strain for the cell-free rings is beyond the scope of this thesis, it is essential to note this behavior. It indicates potential limitations in the material's ability to recover after deformation, which could have significant implications for its use as a scaffold in tissue engineering.

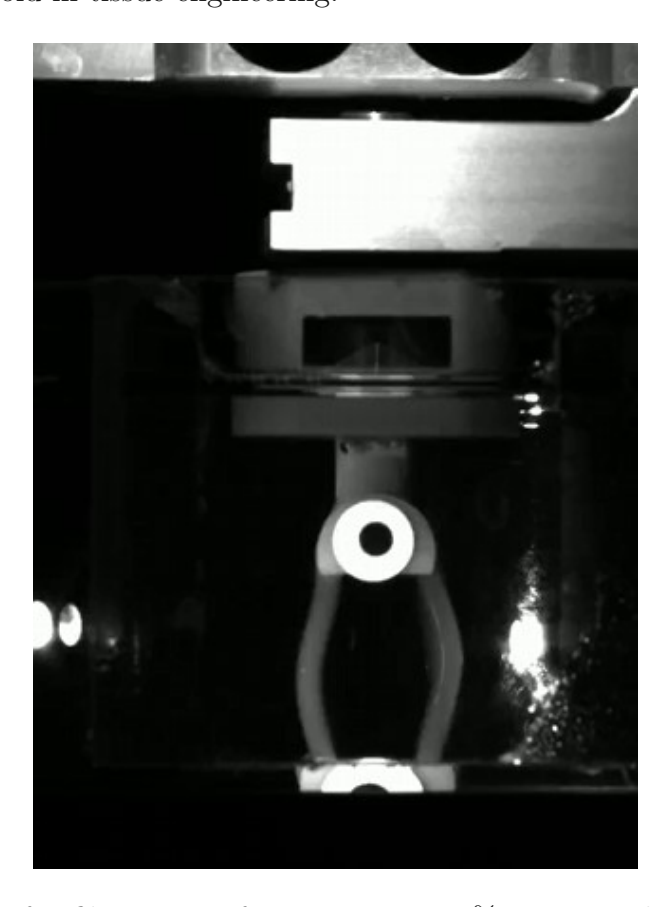


Figure 4.23.: Photo of a fibrin ring after testing at 20% strain with cyclic loading. The ring contains cells cultured for two days.

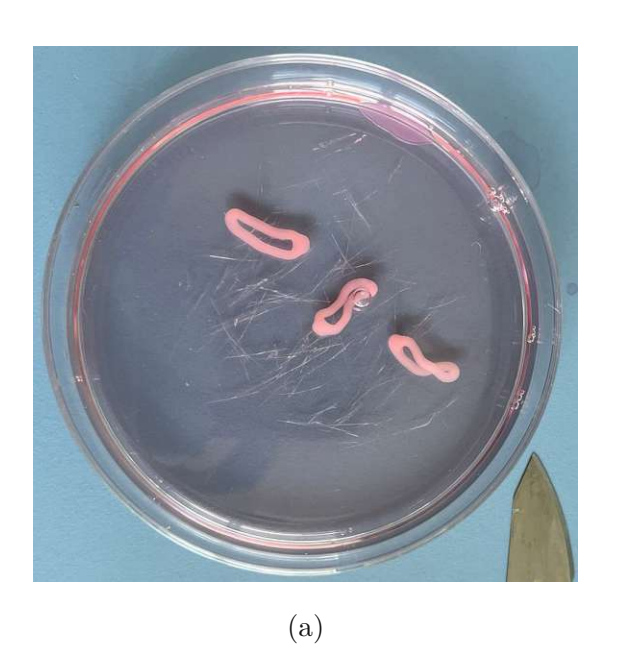
5. Discussion

This thesis aimed to develop a setup for mechanical testing of ring-shaped fibrin hydrogels and validate the setup with cell-free constructs and constructs with cells. Similar reasoning to Heher et al., in our experimental setup, the final concentration of 20 mg/mL for fibrinogen and 0.625 KIU/mL of thrombin were chosen because the casting process was more reliable and the scaffolds were more stable than using 10 mg/mL concentration of fibrinogen [11], but also because the homogeneity of the fibrin meshwork increases with lower thrombin concentrations [39].

There were no significant differences between the maximum stresses experienced between the 20% pooled cyclic groups (N=8) compared to the 20% pooled relaxation groups (N=9) (p-value=0.7430) (Fig. 4.14a) or after 300 s (p-value=0.5769) (Fig. 4.14b). For 10% strain, no significant differences were found neither for the maximum stresses (pvalue=0.8202) nor the stresses after 300s (p-value=0.6751). When considering the strain only for the constructs within the MagneTissue bioreactor (10%) [11], the loading type does not appear to matter up to 300 s. However, in previous works, the MagneTissue protocol applied static strain at 10% for 6 h followed by 18 h at strain 3% and found that this protocol gave optimal results. Heher et al. found that 10% strain (for 6 h) was optimal in "terms of cell alignment, myoblast fusion, myogenic differentiation, and myotube maturity" [11]. In addition, their preliminary studies found that 1 h of cyclic stimulation led to differences in myogenic differentiation compared to 1 h of static stimulation [11]. However, this contrasts with the results found in this thesis; no significant differences were found between the maximum stresses nor the minimum stresses when comparing cyclic strain and relaxation loading at 10% or 20% strain levels. If 10% cyclic stimulation vs. static (relaxation) stimulation led to differences in terms of myogenic differentiation, etc., then it would reason there would be differences found in stress levels experienced. These differences in results reported here vs. Heher et al. were likely due to the 5 min testing time compared to 60 min, and the conditions under which they tested were different; they tested under dry conditions. However, a follow-up test of 1h stimulation for both cyclic and relaxation loading would provide further insight. It is possible that the 5 min testing time here was too short of a time scale to compare the cyclic and relaxation loading schemes.

92

Within the relaxation group, we found significant differences in maximum stresses between cell-free, 2-cell groups (10% and 20% strain) and 9-cell groups (20% strain). The lowest stress value found was the 10% strain cell-free group, which had a value of 4.91 ± 0.04 kPa. The largest stress value found was the 20% strain 9-cell group with a value of 8.94 \pm 0.86 kPa. The full breakdown can be found in Table 4.3. Differences within the loading group are due to the presence of cells and the duration of the cell culture, where the 9-cell group had the longest culture time of 9 days (2-cell had a culture time of 2 days). Likewise, for the cyclic stimulation groups, there were significant differences between the 20% strain 2-cell and the 20% cell-free groups (p-value=0.1000) for the maximum stress value. For minimum stress, there was a significant difference between the 20% 2-cell and 20% cell-free groups (p-value=0.0044). In each of these cases for maximum stress, the constructs with cells experienced higher stress levels than their cell-free counterpart. The 9-cell cases experienced the greatest levels; as previously mentioned, the presence of cells and the duration of culturing for the constructs directly affected the stiffness of the rings. Cells were attaching to the matrix and contracting it, which qualitatively can be seen; 2 days after casting, if left floating in a petri dish, the cells contract, as seen in Fig. 5.1.



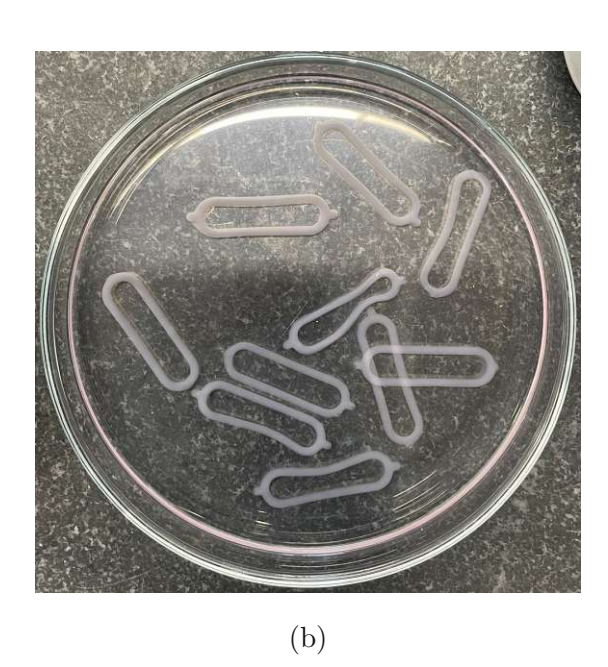


Figure 5.1.: (a) Rings containing cells (b) Cell-free rings

The groups with cells experienced higher stress levels, with the 9-cell group experiencing the greatest stress levels. There are some possible reasons for this phenomenon. In an unpublished study on the same type of fibrin rings, conducted by Ekaterina Oleinik,

using the same cell type, cell density, and fibrin concentration as this thesis, it was found that there was a significant upregulation of collagen I (col1a) and collagen III (col3) expression in a floating group (which has the same conditions as the 9-cell group in this thesis), suggesting that the cells remodeled the fibrin ring.

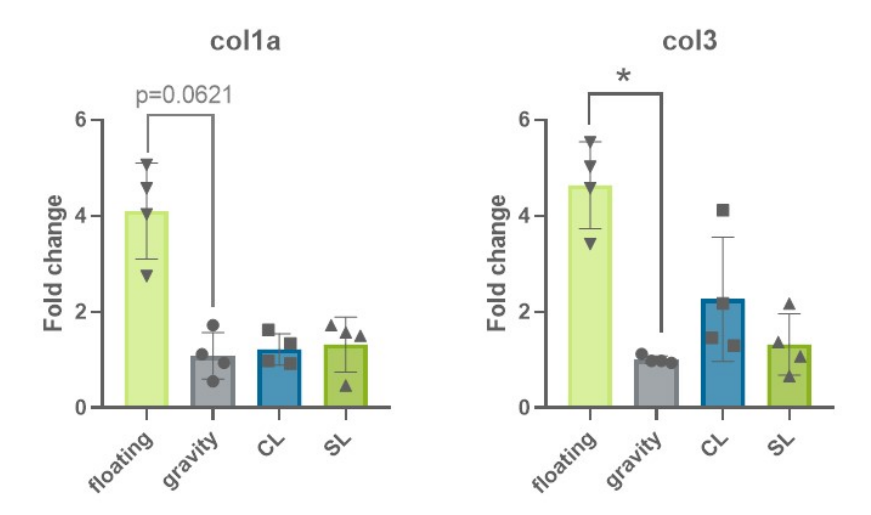


Figure 5.2.: qPCR analysis of collagen I (col1a) and collagen III (col3) expression by calculation of the ratio of these genes to GAPDH: floating - floating control, gravity – gravity control, CL – cyclic loading, SL – static loading. Data are shown as median with standard deviation (SD), n=4. Statistical analysis was done with a nonparametric Kruskal - Wallis test followed by Dunn's posthoc test using GraphPad Prism 8.2.1. Values were considered statistically significant for p<0.05. Figure from Ekaterina Oleinik, M.Sc., a PhD student in the Institute of Lightweight Design and Structural Biomechanics.

The remodeling of the ECM from fibrin to a mixture of colla and coll would explain the higher stresses that the 9-cell group experienced compared to the 2-cell and cell-free groups, which eventually means that the 9-cell group rings have higher stiffness. These findings are consistent with other published studies conducted with collagen and fibrinbased hydrogels, where it was shown that hydrogel stiffness increases as the collagen/fibrin content increases [40] [41], but at the expense of extensibility [42].

Additionally, comparisons can be made regarding the instantaneous and the equilibrium moduli for 10% and 20% strain cyclic and relaxation groups (Table A.14). For both the instantaneous and equilibrium moduli, the 10% data was pooled and compared to the 20% cell-free and 2-cell pooled groups and the 20% 9-cell groups. Significant differences were found between the groups when pooled. The average instantaneous modulus for the

20% cell-free and 2-cell pooled group (and the lowest) was 36.2 ± 1.5 kPa (Fig. 4.18), which is on the same order of magnitude as other stress relaxation experiments on fibrin in published studies; an article by Jimenez et al. found the instantaneous modulus was 31.8 ± 3.5 kPa and 23.1 ± 2.9 kPa for the equilibrium modulus for 4 mg/mL of fibringen and 0.5 U of thrombin [43]. The mean equilibrium modulus for the 20% pooled groups found in this study is 29.5 ± 2.0 kPa. For the 20% 9-cell groups, it was found to be 44.7 \pm 3.1 kPa (instantaneous modulus) and 36.0 ± 2.3 kPa (equilibrium modulus). The mean instantaneous and equilibrium moduli for the 10% pooled group were 49.5 ± 1.0 kPa and 44.3 ± 3.0 kPa, respectively. In a different study, Tomasch et al. used the same type of hydrogel, with the same concentration of fibringen and thrombin [38]. Although they tested their rings in dry conditions and performed a tensile test by pulling to failure, they calculated an apparent tensile modulus of about 22 kPa, which was in ranges similar to our instantaneous modulus [38]. Again, while their value was lower, there were differences in our test setup vs. theirs, which would account for differences (wet vs. dry conditions, lower strain levels vs. pulling to failure, etc.).

The stress relaxation response was captured by fitting a Prony series to the normalized curves. The cyclic loading curves were normalized similarly and fitted with a Prony series. The constructs showed two independent time scales. For the short-term relaxation time, τ_1 , excluding the 10% strain, cyclic 2-cell group, there were no significant differences between the groups, suggesting that all groups (excluding 10% strain, cyclic 2-cell) relax similarly. The τ_1 values ranged from 31 s to 100 s, which is of the same order (47.8 s - 73.5 s) from a study by Jimenez et al. on fibrin gels undergoing stress relaxation [43]. However, the long-term relaxation time ranged from 115 s to 1000 s, whereas in the Jimenez et al. study, their values ranged from 1590 s to 1700s [43]. For their study, they had lower fibringen concentrations (2 mg/mL and 4 mg/mL compared to our 20 mg/mL) [43], which attributed to the discrepancy.

While the plastic deformation of the rings was not quantitatively measured here, it was noted. Previous studies found that fibrin uncrosslinked fibers can be stretched 2.2 times their length, and partially cross-linked fibers could be pulled over 2.8 times and recover without permanent damage [44]. However, another more recent study found that the elastic limit of fully cross-linked fibrin fibers to be less than or equal to 50%, and in some cases, many fibers showed permanent deformation at strains as low as 10% [45], which

5. Discussion

aligned with what we had seen in our experiments. It was likely that the fibrin constructs created for this work were highly cross-linked, which would explain the plastic deformation at a lower strain, as cross-linking makes fibers stiffer, less extensible, and thus more susceptible to plastic deformation [45]. Notably, however, the rings with cells would contract after some time, but the cell-free constructs would not; it appeared that the presence of cells and the remodeling of the ECM affected the extensibility and irreversibility.

To summarize, the key findings were:

- 1. At the maximum stress values (the initial stress) and after 300s, there were no significant differences between cyclic groups and relaxation groups for both 10% strain and 20% strain
- 2. The presence of cells affected the stiffness of the rings due to their ability to contract and remodel the ECM from fibrin to a mixture of colla and col3
- 3. The 9-cell groups experienced higher levels of stress than all other groups due to the composite nature of the material
- 4. Post-test, the cell-free rings experienced irreversible plastic deformation

5.1. Advancements and Prospective Developments

A greater number of samples would be the best improvement for this thesis in terms of definitively capturing the trends seen. Enhancing the stability of the load frame by lowering the friction during head movement and replacing the 10 N load cell with a 1 N load cell would reduce the need for extensive data processing. Additionally, future experiments could focus on quantifying the amount of plastic strain experienced by the fibrin rings or conducting a follow-up study, where 1 h of cyclic loading is compared to 1 h of static loading, which could better serve as a comparison to the 1 h cyclic loading and 1 h static loading that was conducted by Heher et al.

5.2. Limitations

It was essential to highlight limitations encountered during this thesis, as they had some bearing on the discussion. First, the dynamic load frame and load cell setup were not ideal, as the recorded loads were near the lower limit of the load cell's capacity. Additionally, force oscillations were observed whenever the head moved despite efforts to stabilize the piston with lubrication. However, one of the most significant limitations recognized was the sample size. At most, there were biological triplicates (N=3) for each group, but in some cases, groups only had two samples.

6. Conclusion

Given their incidence rates, common in athletic and aging populations, tendons' inability to self-heal makes their injury particularly problematic and limits treatment options. Fibrin hydrogels are very popular for tissue engineering applications and serve as a scaffolding base. This work aims to provide a protocol for studying the mechanical properties of the fibrin rings, especially regarding determining the stresses the fibrin rings experience within the bioreactor.

The main aspects of this work include:

- designing an experimental setup for mechanical testing
- developing a test protocol
- testing the mechanical properties of fibrin rings without and with cells

The constructs with cells experience higher stress levels and are stiffer than cell-free rings. It can be elaborated further that the 9-cell groups exhibit the highest stress levels due to cell-mediated remodeling and heightened collagen production. For the initial stresses experienced, there is no significant difference due to the loading type for either 10% or 20% strain levels. Additionally, there was no significant difference between cyclic loading and stress relaxation loading after 300 s. The cell-free constructs show irreversible plastic deformation after testing.

This thesis has limitations. In the best case, the sample size is biological triplicates, while in the worst case, there are only two samples. Some experimental limitations include instability in the load frame when the load cell moves despite efforts to stabilize the piston with lubrication and a 10 N load cell near its sensitivity limits for the applied loads. These factors require extensive data post-processing to produce usable data.

These preliminary results have important implications for tissue engineering in the case of tendon repair. The cell-mediated enhancement of the fibrin rings and their stiffness can render such constructs relevant for tendon scaffolding. Plastic deformation, as obtained during experimentation, constitutes a complication in this respect, hinting at possible permanent changes in the scaffold structure that may lead to a loss of functionality in clinical applications if these tendons are stretched into their plastic deformation region. During

culturing, maintaining constant stress levels is ideal. Plastic deformation affects stress levels; therefore, understanding the forces involved and the accumulation of permanent strain would allow for better control and tunability of the fibrin rings.

Therefore, this thesis constitutes the basis for understanding the mechanical properties of fibrin-based scaffolds for tendon tissue engineering applications and allows for several follow-up studies that will further stimulate the pursuit of strategies for improving tissue engineering approaches for tendons. While challenges still exist, mainly with plastic deformation, refinement of mechanical testing methodologies, and limited sample size, this study contributes to the literature on tissue engineering.

TU Sibliothek, Die approbierte gedruckte Originalversion dieser Diplomarbeit ist an der TU Wien Bibliothek verfügbar wien knowledge hub. The approved original version of this thesis is available in print at TU Wien Bibliothek.

A. P-Values from Statistical Testing

A.1. Cyclic Testing P-Values

Table A.1.: Table of p-values from statistical testing performed between the maximum values of the respective groups. With the significance level set to 0.10, all pvalues are less than or equal to 0.10, indicating significant differences between the groups. 20% strain 9-cell and 10% strain cell-free are excluded due to N=2 sample size. A * denotes the data set is normally distributed. When two normally distributed data sets are compared, a t-test with Welch's correction is used; otherwise, the statistical method is a Mann-Whitney U test.

Group Name	10% 2-Cell*	20% 2-Cell	20% Cell-free*
10% 2-Cell*	1	0.1000	0.0002
20% 2-Cell	0.1000	1	0.1000
20% Cell-free*	0.0002	0.1000	1

Table A.2.: Table of p-values from statistical testing performed between the **minimum** values of the respective groups. With the significance level set to 0.10, all pvalues are less than or equal to 0.10, indicating significant differences between the groups. 20% strain 9-cell and 10% strain cell-free are excluded due to N=2 sample size. A * denotes the data set is normally distributed. When two normally distributed data sets are compared, a t-test with Welch's correction is used; otherwise, the statistical method is a Mann-Whitney U test.

Group Name	10% 2-Cell*	20% 2-Cell*	20% Cell-free*
10% 2-Cell*	1	0.0006	0.0010
20% 2-Cell*	0.0006	1	0.0044
20% Cell-free*	0.0006	0.0044	1

Table A.3.: Table of p-values from statistical testing performed between the final normalized values of the respective groups. With the significance level set to 0.10, all groups except the 20% 2-cell compared to the 10% 2-cell have pvalues less than or equal to 0.10. 20% strain 9-cell and 10% strain cell-free are excluded due to N=2 sample size. A * denotes the data set is normally distributed. When two normally distributed data sets are compared, a t-test with Welch's correction is used; otherwise, the statistical method is a Mann-Whitney U test.

Group Name	10% 2-Cell*	20% 2-Cell	20% Cell-free*
10% 2-Cell*	1	>0.9999	0.0910
20% 2-Cell	>0.9999	1	0.1000
20% Cell-free*	0.0910	0.1000	1

A.2. Relaxation Testing P-Values

Table A.4.: Table of p-values from statistical testing performed between the **maximum** stress values of the groups. With the significance level set to 0.10, all groups except the 20% 2-cell compared to the 20% cell-free have p-values less than or equal to 0.10. A * denotes the data set is normally distributed. When two normally distributed data sets are compared, a t-test with Welch's correction is used; otherwise, the statistical method is a Mann-Whitney U test.

Group Name	10% 2-Cell*	10% Cell-free*	20% 2-Cell	20% Cell-free*	20% 9-Cell
10% 2-Cell*	1	0.0523	0.1000	< 0.0001	0.1000
10% Cell-free*	0.0523	1	0.1000	< 0.0001	0.1000
20% 2-Cell	0.1000	0.1000	1	0.7000	0.1000
20% Cell-free*	<0.0001	< 0.0001	0.7000	1	0.1000
20% 9-Cell	0.1000	0.1000	0.1000	0.1000	1

Table A.5.: Table of p-values from statistical testing performed between the **minimum** stress values of the groups. With the significance level set to 0.10, all groups except the 10% cell-free compared to the 10% 2-cell, the 20% cell-free compared to the 20% 2-cell, and the 20% 9-cell compared to the 20% 2-cell have p-values less than or equal to 0.10. A * denotes the data set is normally distributed. A t-test with Welch's correction is used when comparing two normally distributed data sets.

Group Name	10% 2-Cell*	10% Cell-free*	20% 2-Cell*	20% Cell-free*	20% 9-Cell*
10% 2-Cell*	1	0.3262	0.0311	0.0002	0.0235
10% Cell-free*	0.3262	1	0.0304	< 0.0001	0.0232
20% 2-Cell*	0.0311	0.0304	1	0.3910	0.1593
20% Cell-free*	0.0022	< 0.0001	0.3910	1	0.0931
20% 9-Cell*	0.0235	0.0232	0.1593	0.0931	1

Table A.6.: Table of p-values from statistical testing performed between the **final nor**malized stress values of the groups. With the significance level set to 0.10, all p-values except are greater than 0.10 except for 10% 2-cell compared to 20% cell-free, 10% cell-free compared to 20% cell-free, and 10% cell-free compared to 20% 9-cell. A * denotes the data set is normally distributed. When two normally distributed data sets are compared, a t-test with Welch's correction is used; otherwise, the statistical method is a Mann-Whitney U test.

Group Name	10% 2-Cell*	10% Cell-free	20% 2-Cell*	20% Cell-free	20% 9-Cell*
10% 2-Cell*	1	>0.9999	0.3668	0.1000	0.2156
10% Cell-free	>0.9999	1	0.2000	0.1000	0.1000
20% 2-Cell*	0.3668	0.2000	1	0.7000	0.6372
20% Cell-free	0.1000	0.1000	0.7000	1	>0.9999
20% 9-Cell*	0.2156	0.1000	0.6372	>0.9999	1

A.3. Cyclic and Stress Relaxation Comparison

A.3.1. 10% Strain

Table A.7.: Table of p-values from statistical testing performed between the maximum stress values of the 10% cyclic and relaxation groups. All groups had N=3 samples except for the 10% cyclic cell-free (and therefore excluded from direct comparison). With the significance level set to 0.10, all p-values are greater than 0.10 except for the 10% relax 2-cell compared to the 10% relax cell-free group. A * denotes the data set is normally distributed. A t-test with Welch's correction is used when comparing two normally distributed data sets.

Croup Nama	10% Cyclic 10% Rela		10% Relax	
Group Name	2-Cell* 2-Cell*		Cell-free*	
10% Cyclic	1	> 0 0000	0.5275	
2-Cell*		>0.9999	0.5275	
10% Relax	>0.9999	1	0.0523	
2-Cell*	>0.9999	I	0.0023	
10% Relax	0.5275	0.0523	1	
Cell-free*	0.5275	0.0023	1	

A.3.2. 20% Strain

Table A.8.: Table of p-values from statistical testing performed between the stress values at 300s of the 10% cyclic and relaxation groups. All groups had N=3 samples except for the 10% cyclic cell-free (and therefore excluded from direct comparison). With the significance level set to 0.10, all p-values are greater than 0.10. A * denotes the data set is normally distributed. A t-test with Welch's correction is used when comparing two normally distributed data sets.

Croup Nama	10% Cyclic	10% Relax	10% Relax	
Group Name	2-Cell* 2-Cell*		Cell-free*	
10% Cyclic	1	0.2700	0.7696	
2-Cell*	I	0.3790	0.7686	
10% Relax	0.3790	1	0.3262	
2-Cell*	0.3790	ı	0.3202	
10% Relax	0.7686	0.3262	1	
Cell-free*	0.7000	0.3202	 	

Table A.9.: Table of p-values from statistical testing performed between the **normalized** stress values at 300s of the 10% cyclic and relaxation groups. All groups had N=3 samples except for the 10% cyclic cell-free (and therefore excluded from direct comparison). With the significance level set to 0.10, all p-values are greater than 0.10. A * denotes the data set is normally distributed. When two normally distributed data sets are compared, a t-test with Welch's correction is used; otherwise, the statistical method is a Mann-Whitney U test.

	1		I	
Group Name	10% Cyclic	10% Relax	10% Relax	
Group Name	2-Cell* 2-Cell*		Cell-free	
10% Cyclic	4	0.0700	0.0000	
2-Cell*	l	0.3790	0.2000	
10% Relax	0.2700	1	> 0.0000	
2-Cell*	0.3790	I	>0.9999	
10% Relax	0.2000	>0.9999	1	
Cell-free	0.2000	<i>></i> ∪.ฮฮฮฮ	 	

Table A.10.: Table of p-values from statistical testing performed between the **maximum** stress values of the 20% cyclic and relaxation groups. All groups had N=3 samples except for the 20% cyclic 9-cell (and therefore excluded from direct comparison). The significance level is set to 0.10. A * denotes the data set is normally distributed. When two normally distributed data sets are compared, a t-test with Welch's correction is used; otherwise, the statistical method is a Mann-Whitney U test.

Croup Nama	20% Cyclic	20% Cyclic	20% Relax	20% Relax	20% Relax
Group Name	2-Cell Cell-free* 2-Cell		Cell-free*	9-Cell	
20% Cyclic	1	0.1000	0.7000	0.1000	0.1000
2-Cell	l	0.1000	0.7000	0.1000	0.1000
20% Cyclic	0.1000	1	0.7000	0.9574	0.1000
Cell-free*	0.1000	l	0.7000	0.9374	0.1000
20% Relax	0.7000	0.7000	1	0.7000	0.1000
2-Cell	0.7000	0.7000	I	0.7000	0.1000
20% Relax	0.1000	0.9574	0.7000	1	0.1000
Cell-free*	0.1000	0.557 +	0.7000	'	0.1000
20% Relax	0.1000	0.1000	0.1000	0.1000	1
9-Cell	0.1000	0.1000	0.1000	0.1000	1

Table A.11.: Table of p-values from statistical testing performed between the stress values at 300s of the 20% cyclic and relaxation groups. The significance level is set to 0.10. A * denotes the data set is normally distributed. A t-test with Welch's correction is used when comparing two normally distributed data sets.

Group Name	20% Cyclic	20% Cyclic	20% Relax	20% Relax	20% Relax	
	2-Cell*	Cell-free*	2-Cell*	Cell-free*	9-Cell*	
20% Cyclic	1	0.0043	0.7111	0.0007	0.2004	
2-Cell*	I	0.0043	0.7111	0.0007	0.2004	
20% Cyclic	0.0043	1 0.6656		0.0193	0.1218	
Cell-free*	0.0043	ı	0.0000		0.1210	
20% Relax	0.7111	0.6656	1	0.3910	0.1593	
2-Cell*	0.7111	0.0000	1	0.0010	0.1000	
20% Relax	0.0007	0.0193	0.3910	1	0.0931	
Cell-free*	0.0001	0.0190 0.3910		ı	0.0001	
20% Relax	0.2004	0.1218	0.1593	0.0931	1	
9-Cell*	0.2004	0.1210	0.1000	0.0001	'	

Table A.12.: Table of p-values from statistical testing performed between the **normalized** stress values at 300s of the 20% cyclic and relaxation groups. The significance level is set to 0.10. A * denotes the data set is normally distributed. When two normally distributed data sets are compared, a t-test with Welch's correction is used; otherwise, the statistical method is a Mann-Whitney U test.

Group Name	20% Cyclic	20% Cyclic	20% Relax	20% Relax	20% Relax	
	2-Cell*	Cell-free*	2-Cell*	Cell-free	9-Cell*	
20% Cyclic	1	0.8297	0.7387	0.1000	0.4047	
2-Cell*	I	0.0297	0.7367	0.1000	0.4047	
20% Cyclic	0.8297	1	0.7154	0.1000	0.3923	
Cell-free*	0.0297	0.7134		0.1000	0.0020	
20% Relax	0.7387	0.7154	1	0.7000	0.6372	
2-Cell*	0.7307	0.7104	1	0.7000	0.0072	
20% Relax	0.1000	0.1000	0.7000	1	>0.9999	
Cell-free	0.1000	0.1000	0.7000		Z0.0999	
20% Relax	0.4047	0.3923	0.6372	>0.9999	1	
9-Cell*	0.1017	0.0020	0.0072	<i>></i> 0.0000		

Table A.13.: Table of p-values from statistical testing performed between the instantaneous moduli values of the 10% and 20% cyclic and relaxation groups. The significance level is set to 0.10. A * denotes the data set is normally distributed. When two normally distributed data sets are compared, a t-test with Welch's correction is used; otherwise, the statistical method is a Mann-Whitney U test.

P-Values from Statistical Testing

Group Name	10% Cyclic	10% Relax	10% Relax	20% Cyclic	20% Cyclic	20% Relax	20% Relax	20% Relax
Group Name	2-Cell*	2-Cell*	Cell-free*	2-Cell	Cell-free*	2-Cell	Cell-free*	9-Cell
10% Cyclic	4	> 0.0000	0.5075	0.4000	0.0004	0.4000	0.0046	0.1000
2-Cell*	I	>0.9999	0.5275	0.1000	0.0021	0.1000		
10% Relax	>0.9999	1	0.0523	0.1000	0.0003	0.1000	< 0.0001	0.1000
2-Cell*	<i>></i> 0.9999	l	0.0323	0.1000	0.0003	0.1000	<0.0001	0.1000
10% Relax	0.5275	0.0523	1	0.1000	< 0.0001	0.1000	< 0.0001	0.1000
Cell-free*	0.5275	0.0320	l	0.1000	<0.0001	0.1000	<0.0001	0.1000
20% Cyclic	0.1000	0.1000	0.1000	1	0.1000 0.70	0.7000	0.1000	0.1000
2-Cell	0.1000	0.1000	0.1000	'		0.7000	0.1000	
20% Cyclic	0.0021	0.0003	<0.0001	0.1000	1	0.7000	0.9574	0.1000
Cell-free*	0.0021	0.0000	<0.0001	0.1000	l	0.7000	0.557 4	0.1000
20% Relax	0.1000	0.1000	0.1000	0.7000	0.7000	1	0.7000	0.1000
2-Cell	0.1000	0.1000	0.1000	0.7000	0.7000	l	0.7000	0.1000
20% Relax	0.0046	< 0.0001	<0.0001	0.1000	0.9574	0.7000	1	0.1000
Cell-free*	0.0040	<0.0001	<0.0001	0.1000	0.007 +	0.7000	1	0.1000
20% Relax	0.1000	0.1000	0.1000 0.1000	0.1000	0.1000	0.1000	0.1000	1
9-Cell	0.1000	0.1000	0.1000	0.1000	0.1000	0.1000	0.1000	1



Table A.14.: Table of p-values from statistical testing performed between the equilibrium moduli values of the 10% and 20% cyclic and relaxation groups. The significance level is set to 0.10. A * denotes the data set is normally distributed. When two normally distributed data sets are compared, a t-test with Welch's correction is used; otherwise, the statistical method is a Mann-Whitney U test.

Group Namo	10% Cyclic	10% Relax	10% Relax	20% Cyclic	20% Cyclic	20% Relax	20% Relax	20% Relax
Group Name	2-Cell	2-Cell	Cell-free	2-Cell	Cell-free	2-Cell	Cell-free	9-Cell
10% Cyclic	1	0.0775	0.1000	0.0004	0.0001	0.0247	0.1000	0.1383
2-Cell	l l	0.0775	0.1000	<0.0001	<0.0001			
10% Relax	0.0775	1	0.4000	0.0102	0.0075	0.0033	0.1000	0.0170
2-Cell	0.0773	I	0.4000	0.0102	0.0075	0.0055	0.1000	0.0170
10% Relax	0.1000	0.4000	1	0.1000	0.1000	0.1000	0.1000	0.1000
Cell-free	0.1000	0.4000	1	0.1000	0.1000	0.1000	0.1000	0.1000
20% Cyclic	< 0.0001	0.0001 0.0102	0.1000	1	0.0044	0.7562	0.2000	0.1299
2-Cell	⟨0.0001	0.0102	0.1000	1	0.0044	0.7502	0.2000	0.1233
20% Cyclic	<0.0001	0.0075	0.1000	0.0044	1	0.1493	0.1000	0.0569
Cell-free	<0.0001	0.0070	0.1000	0.0044	'	0.1400	0.1000	0.0000
20% Relax	0.0247	0.0033	0.1000	0.7562	0.1493	1	0.7000	0.1647
2-Cell	0.0217	0.0000	0.1000	0.7002	0.1100	'	0.7 000	0.1017
20% Relax	0.1000	0.1000 0.1000 0.1000	0.1000	0.2000	0.1000	0.7000	1	0.1000
Cell-free	0.1000	0.1000	0.1000	0.2000	0.1000	0.7000	1	0.1000
20% Relax	0.1383	0.0170	0.1000	0.1299	0.0569	0.1647	0.1000	1
9-Cell	0.1000	0.0170	0.1000	0.1200	0.0000	0.1047	0.1000	1

Table A.15.: Table of p-values from statistical testing performed between the τ_1 values of the 10% and 20% cyclic and relaxation groups. The significance level is set to 0.10. A * denotes the data set is normally distributed. A t-test with Welch's correction is used when comparing two normally distributed data sets.

P-Values from Statistical Testing

Group Name	10% Cyclic	10% Relax	10% Relax	20% Cyclic	20% Cyclic	20% Relax	20% Relax	20% Relax
Group Name	2-Cell*	2-Cell*	Cell-free*	2-Cell*	Cell-free*	2-Cell*	Cell-free*	9-Cell*
10% Cyclic	4	0.0040	0.0450		0.0705	0.4470	0.0040	0.0000
2-Cell*	I	0.0949	0.0459	0.2991	0.2785	0.1176	0.0240	0.0068
10% Relax	0.0949	1	0.9783	0.4207	0.3281	0.6249	0.9761	0.8431
2-Cell*	0.0949	l	0.9765	0.4207	0.3201	0.0249	0.9701	0.0451
10% Relax	0.0459	0.9783	1	0.3867	0.2770	0.5794	0.9370	0.7476
Cell-free*	0.0433	0.9700	I	0.3007	0.2770	0.5754	0.9370	0.7470
20% Cyclic	0.2991	0.4207	0.3867	1	0.9123	0.6678	0.3528	0.2977
2-Cell*	0.2991	0.4207	0.3007	ı				
20% Cyclic	0.2785	0.3281	0.2770	0.9123	1	0.5500	0.2431	0.2003
Cell-free*	0.2703	0.0201	0.2770	0.5125	I	0.5500	0.2401	0.2000
20% Relax	0.1176	0.6249	0.5794	0.6678	0.5500	1	0.5137	0.4006
2-Cell*	0.1170	0.0240	0.07.04	0.0070	0.5500	1	0.0107	0.4000
20% Relax	0.0240	0.9761	0.9370	0.3528	0.2431	0.5137	1	0.7689
Cell-free*	0.0240	0.0701	0.0070	0.0020	0.2701	0.0101	l	0.7000
20% Relax	0.0068	0.0068 0.8431	0.7476	0.2977	0.2003	0.4006	0.7689	1
9-Cell*	0.0000	0.0401	0.7470					



Table A.16.: Table of p-values from statistical testing performed between the τ_2 values of the 10% and 20% cyclic and relaxation groups. The significance level is set to 0.10. A * denotes the data set is normally distributed. When two normally distributed data sets are compared, a t-test with Welch's correction is used; otherwise, the statistical method is a Mann-Whitney U test.

Group Name	10% Cyclic	10% Relax	10% Relax	20% Cyclic	20% Cyclic	20% Relax	20% Relax	20% Relax
	2-Cell	2-Cell*	Cell-free*	2-Cell*	Cell-free*	2-Cell	Cell-free*	9-Cell
10% Cyclic	1	0.2000	0.7000	0.7000	0.1000	0.1000	>0.9999	0.3000
2-Cell	'	0.2000	0.7000	0.7000	0.1000	0.1000	>0.9999	0.3000
10% Relax	0.2000	1	0.3534	0.3900	0.4651	0.4000	0.0561	0.4000
2-Cell*	0.2000	l	0.3334	0.3900	0.4031	0.4000	0.0301	0.4000
10% Relax	0.7000	0.3534	1	0.9215	0.2100	0.4000	0.3513	0.7000
Cell-free*	0.7000	0.3334	I	0.9213	0.2109 0.4000	0.4000	0.3313	0.7000
20% Cyclic	0.7000	0.3900	0.9215	1 0.2231 0	0.2221	0.1000	0.2939	>0.9999
2-Cell*	0.7000	0.3900	0.9213		0.1000	0.2939	<i>></i> 0.9999	
20% Cyclic	0.1000	0.4651	0.2109	0.2231	1	0.4000	0.0002	0.4000
Cell-free*	0.1000	0.4031	0.2109	0.2231	l	0.4000	0.0002	0.4000
20% Relax	0.1000	0.4000	0.4000	0.1000	0.4000	1	0.1000	0.1000
2-Cell	0.1000	0.4000	0.4000	0.1000	0.4000	l	0.1000	0.1000
20% Relax	> 0.0000	>0.9999 0.0561 0.3513 0.2939	0.2939	0.0002	0.1000	1	0.1000	
Cell-free*	<i>></i> 0.3333	0.0301	0.5515	0.2303	0.0002 0.1000	0.1000	I	0.1000
20% Relax	0.3000	0.4000	0.7000	>0.9999	0.4000	0.1000	0.4000	1
9-Cell	0.3000	0.4000	0.7000	>0.3333	0.4000	0.1000	0.1000	

References

- F. Wu, M. Nerlich, and D. Docheva, "Tendon injuries: Basic science and new repair proposals," General orthopaedics, vol. 2, pp. 891–921, 2017. DOI: 10.1302/2058-5241.2.160075.
- J. P. deJong, J. T. Nguyen, A. J. M. Sonnema, E. C. Nguyen, P. C. Amadio, and [2]S. L. Moran, "The incidence of acute traumatic tendon injuries in the hand and wrist: A 10-year population-based study," Clinics in Orthopedic Surgery, vol. 6, pp. 196-202, 2014. DOI: http://dx.doi.org/10.4055/cios.2014.6.2.196.
- T. A. H. Järvinen, P. Kannus, N. Maffulli, and K. M. Khan, "Achilles tendon disorders: Etiology and epidemiology," Foot and Ankle Clinics, vol. 10, pp. 255–266, 2005. DOI: 10.1016/j.fcl.2005.01.013.
- [4]S. Thomopoulos, W. C. Parks, D. B. Rifkin, and K. A. Derwin, "Mechanisms of tendon injury and repair," Journal of Orthopaedic Research, vol. 33, pp. 832–839, 2015. DOI: 10.1002/jor.22806...
- [5]M. Kvist, "Achilles tendon injuries in athletes," Sports Med, vol. 18, pp. 173–201, 1994. DOI: 10.2165/00007256-199418030-00004.
- [6] X. Zhang, D. Bogdanowicz, C. Erisken, N. M. Lee, and H. H. Lu, "Biomimetic scaffold design for functional and integrative tendon repair," Journal of Shoulder and Elbow Surgery, vol. 21, no. 2, pp. 266–277, 2012. DOI: 10.1016/j.jse.2011.11.016.
- T. Zhao, Q. Qi, S. Xiao, et al., "Integration of mesenchymal stem cell sheet and bgfg-loaded fibrin gel in knitted plga scaffolds favorable for tendon repair," Journal Materials Chemistry B, vol. 13, pp. 2201–2211, 2019. DOI: https://doi.org/10. 1039/C8TB02759E.
- [8] B. Hashemibeni, M. Mardani, M. Bahrami, A. Valiani, M. S. Mehr, and M. Pourentezari, "Comparison of fibrin and plga/fibrin scaffolds for chondrogenesis of human adipose derived stem cells by icariin," Journal of Kerman University of Medical Sciences, vol. 27, no. 1, pp. 14-23, 2020. DOI: https://doi.org/10.22062/jkmu.2020. 89592.

- H. K. Makadia and S. J. Siegel, "Poly lactic-co-glycolic acid (plga) as biodegradable controlled drug delivery carrier," *Polymers*, vol. 3, no. 3, pp. 1377–1397, 2011. DOI: https://doi.org/10.3390/polym3031377.
- [10] T. A. Ahmed, E. V. Dare, and M. Hincke, "Fibrin: A versatile scaffold for tissue engineering applications," Tissue Engineering: Part B, vol. 14, no. 2, pp. 199–215, 2008. DOI: https://doi.org/10.1089/ten.teb.2007.0435.
- P. Heher, B. Maleiner, J. Prüller, et al., "A novel bioreactor for the generation of [11]highly aligned 3d skeletal muscle-like constructs through orientation of fibrin via application of static strain," Acta Biomaterialia, vol. 24, pp. 251–265, 2015. DOI: https://doi.org/10.1016/j.actbio.2015.06.033.
- B. P. Chan and K. W. Leong, "Scaffolding in tissue engineering: General approaches [12]and tissue-specific considerations," European Spine Journal, vol. 17, pp. 467–479, 2008. DOI: 10.1007/s00586-008-0745-3.
- M. Brovold, J. Almeida, I. Pla-Palacin, et al., "Naturally-derived biomaterials for [13]tissue engineering applications," Advances in Experimental Medicine and Biology, 2018. DOI: https://doi.org/10.1007/978-981-13-0947-2 23.
- M. W. Mosesson, "Fibringen and fibrin structure and functions," Journal of Throm-[14]bosis and Haemostasis, vol. 3, pp. 1894–1904, 2005. DOI: 10.1111/j.1538-7836. 2005.01365.x.
- J. W. Weisel and C.-E. H. Dempfle. "Fibringen structure and function." (), [On-[15]line]. Available: https://oncohemakey.com/fibrinogen-structure-and-function/. (accessed: 12.15.2024).
- E. Sproul, S. Nandi, and A. Brown, "Fibrin biomaterials for tissue regeneration [16]and repair," in Peptides and Proteins as Biomaterials for Tissue Regeneration and Repair, M. A. Barbosa and M. C. L. Martins, Eds. Woodhead Publishing, 2019, pp. 151–173, ISBN: 9780081008034.
- M. Pieters and A. S. Wolberg, "Fibringen and fibrin: An illustrated review," Research and Practice in Thrombosis and Haemostasis, vol. 3, pp. 191–172, 2019. DOI: 10.1002/rth2.12191.

- E. Ranjit, S. Hamlet, R. George, A. Sharma, and R. M. Love, "Biofunctional approaches of wool-based keratin for tissue engineering," Journal of Science: Advanced Materials and Devices, 2022. DOI: https://doi.org/10.1016/j.jsamd.2021.10. 001.
- [19] M. R. Islam and M. L. Oyen, "Mechanical characterization of hydrogels," The Mechanics of Hydrogels, 2022. DOI: https://doi.org/10.1016/B978-0-08-102862-9.00014-2.
- W. Bian and N. Bursac, "Engineered skeletal muscle tissue networks with con-[20]trollable architecture," Biomaterials, 2009. DOI: https://doi.org/10.1016/j. biomaterials.2008.11.015.
- J. Rosser and D. Thomas, "10 bioreactor processes for maturation of 3d bioprinted [21]tissue," 3D Bioprinting for Reconstructive Surgery, 2018. DOI: https://doi.org/ 10.1016/B978-0-08-101103-4.00010-7.
- M. Larsen, R. Mishra, M. Miller, and D. Dean, "Chapter 17 bioprinting of bone," [22]in Essentials of 3D Biofabrication and Translation, A. Atala and J. J. Yoo, Eds. Elsevier, 2015, pp. 293-308, ISBN: 978-0-12-800972-7.
- E. Gdoutos and M. Konsta-Gdoutos, "Tensile testing," in Mechanical Testing of [23]Materials, E. Gdoutos and M. Konsta-Gdoutos, Eds. Springer, Cham, 2024, pp. 1– 34, ISBN: 9783031459900.
- C. Cai and K. Zhou, "Chapter 7 metal additive manufacturing," in Digital Manufacturing, C. D. Patel and C.-H. Chen, Eds. Elsevier, 2022, pp. 247–298, ISBN: 9780323950626.
- [25]T. E. Engineer. "Understanding material strength, ductility and toughness." (), [Online]. Available: https://efficientengineer.com/material-strengthductility-toughness/. (accessed: 12.15.2024).
- A. Oza, R. Vanderby, and R. Lakes, "Creep and relaxation in ligament: The-[26]ory, methods and experiment," in Mechanics of Biological Tissue, G. A. Holzapfel and R. W. Ogden, Eds. Springer, Berlin, Heidelberg, 2006, pp. 379–397, ISBN: 9783540311843.
- [27]J. Bergström, "6 - linear viscoelasticity," in Mechanics of Solid Polymers, J. Bergström, Ed. William Andrew, 2015, pp. 309–351, ISBN: 9780323311502.

- [28]A. Schiavi and A. Prato, "Evidences of non-linear short-term stress relaxation in polymers," Polymer Testing, vol. 59, 2017. DOI: https://doi.org/10.1016/j. polymertesting.2017.01.030.
- K. S. Fancey, "A mechanical model for creep, recovery and stress relaxation in polymeric materials." Journal of Materials Science, vol. 40, 2005. DOI: 10.1007/ s10853-005-2020-x.
- K. S. Fancey, "A latch-based weibull model for polymeric creep and recovery," [30]Journal of Polymer Engineering, vol. 21, 2001. DOI: 10.1515/POLYENG.2001.21. 6.489.
- [31] P. P. Provenzano, R. S. Lakes, D. Corr, and R. V. Jr., "Application of nonlinear viscoelastic models to describe ligament behavior," Biomechanics and Modeling in Mechanobiology, vol. 1, no. 1, 2002. DOI: 10.1007/s10237-002-0004-1.
- S. E. Duenwald, R. V. Jr., and R. S. Lakes, "Stress relaxation and recovery in [32]tendon and ligament: Experiment and modeling," Biorheology, vol. 47, no. 1, 2010. DOI: 10.3233/BIR-2010-0559.
- S. E. Duenwald, R. V. Jr., and R. S. Lakes, "Viscoelastic relaxation and recovery [33]of tendon," Annals of Biomedical Engineering, vol. 37, no. 6, 2009. DOI: 10.1007/ s10439-009-9687-0.
- G. Youssef, "Chapter 6 creep behavior of polymers," in Applied Mechanics of [34]Polymers, G. Youssef, Ed. Elsevier, 2022, pp. 145–164, ISBN: 9780128210789.
- G. Youssef, "Chapter 7 viscoelastic behavior of polymers," in Applied Mechanics [35]of Polymers, G. Youssef, Ed. Elsevier, 2022, pp. 165–192, ISBN: 9780128210789.
- [36]R. Gehwolf, G. Spitzer, A. Wagner, et al., "3d-embedded cell cultures to study tendon biology," Stem Cells and Aging. Methods in Molecular Biology, vol. 2045, 2019. DOI: https://doi.org/10.1007/7651 2019 208.
- [37]E. P. Brass, W. B. Forman, R. V. Edwards, and O. Lindan, "Fibrin formation: Effect of calcium ions," Blood, vol. 52, 4 1978. DOI: https://doi.org/10.1182/ blood. V52.4.654.654.

- J. Tomasch, B. Maleiner, P. Heher, et al., "Changes in elastic moduli of fibrin hydrogels within the myogenic range alter behavior of murine c2c12 and human c25 myoblasts differently," Front Bioeng. Biotechnol., 2022. DOI: 10.3389/fbioe. 2022.836520...
- A. Gugerell, K. Schlossleitner, S. Wolbank, et al., "High thrombin concentrations [39] in fibrin sealants induce apoptosis in human keratinocytes," Journal of Biomedical Materials Research, 2012. DOI: https://doi.org/10.1002/jbm.a.34007.
- C. L. Cummings, D. Gawlitta, R. M. Nerrem, and J. P. Stegemann, "Properties [40]of engineering vascular constructs made from collagen, fibrin, and collagen-fibrin mixtures," Biomaterials, vol. 25, 17 2004. DOI: https://doi.org/10.1016/j. biomaterials.2003.10.073.
- C. M. Schuh, A. G. Day, H. Redl, and J. Philips, "An optimized collagen-fibrin blend [41]engineering neural tissue promotes peripheral nerve repair," Tissue Engineering Part A, vol. 24, 17-18 2018. DOI: https://doi.org/10.1089/ten.tea.2017.0457.
- [42]V. K. Lai, S. P. Lake, C. R. Frey, R. T. Tranquillo, and V. H. Barocas, "Mechanical behavior of collagen-fibrin co-gels reflects transition from series to parallel interactions with increasing collagen content," Journal of Biomechanical Engineering, vol. 134, 1 2012. DOI: https://doi.org/10.1115/1.4005544.
- J. M. Jimenez, T. Tuttle, Y. Guo, D. Miles, A. Bunganza-Tepole, and S. Calve, [43]"Multiscale mechanical characterization and computational modeling of fibrin gels," Acta Biomaterialia, 2023. DOI: https://doi.org/10.1016/j.actbio.2023.03. 026.
- [44]W. Liu, L. M. Jawerth, E. Sparks, et al., "Fibrin fibers have extraordinary extensibility and elasticity," Science, 2006. DOI: https://doi.org/10.1126/science. 112731.
- W. Liu, C. Carlise, E. Sparks, and M. Guthold, "The mechanical properties of [45]single fibrin fibers," Journal of Thrombosis and Haemostasis, 2010. DOI: https: //doi.org/10.1111/j.1538-7836.2010.03745.x.